# New Baseband Architectures Using Machine Learning and Deep Learning in the Presence of Nonlinearities and Dynamic Environment

Ana Flávia Dos Reis

École Doctorale Informatique, Télécommunications et Électronique

Laboratoire d'Informatique, Signal et Image, Électronique et Télécommunications

# THÈSE

*Présentée par:* ***Ana Flávia dos Reis***

*Soutenue le:* ***13 Mars 2024***

## *New Baseband Architectures Using Machine Learning and Deep Learning in the Presence of Nonlinearities and Dynamic Environment*

Thèse en co-tutelle avec Universidade Tecnológica Federal do Paraná (UTFPR) – Brésil

*Thèse dirigée par:*

M. Jérémie Sublime — Professeur, Institut Supérieur d'Électronique de Paris

*Thèse co-dirigée par:*

M. Glauber Brante — Professeur, UTFPR

*Thèse co-encadrée par:*

M. Yahia Medjahdi — Maître de Conférences, IMT Nord-Europe

M. Bruno Sens Chang — Professeur, UTFPR

M. Faouzi Bader — Directeur de Telecommunication, Technology Innovation Institute (TII)

*Rapporteurs:*

M. Laurent Clavier — Professeur, IMT Nord-Europe

M. Cristiano Panazio — Professeur, Universidade de São Paulo (USP)

---

*Membres du jury:*

Mme. Anelise Munaretto — Professeur, UTFPR

M. Marios Kountouris — Professeur, EURECOM

**Ministério da Educação**
**Universidade Tecnológica Federal do Paraná**
**Campus Curitiba**

ANA FLAVIA DOS REIS

**NOVAS ARQUITETURAS DE BANDA DE BASE UTILIZANDO APRENDIZADO DE MÁQUINA E APRENDIZADO PROFUNDO NA PRESENÇA DE NÃO-LINEARIDADES E AMBIENTE DINÂMICO**

Trabalho de pesquisa de doutorado apresentado como requisito para obtenção do título de Doutor Em Ciências da Universidade Tecnológica Federal do Paraná (UTFPR). Área de concentração: Telecomunicações E Redes.

Data de aprovação: 13 de Março de 2024

Dra. Anelise Munaretto Fonseca, Doutorado - Universidade Tecnológica Federal do Paraná

Dr. Cristiano Magalhaes Panazio, Doutorado - Universidade de São Paulo (Usp)

Dr. Jeremie Sublime, Doutorado - Institut Superieur D Electronique de Paris - Isep

Dr. Laurent Clavier, Doutorado - École Nationale Supérieure Des Télécommunications

Dr. Marios Kountouris, Doutorado - Ecole Nationale Superieure Des Mines de Paris

Documento gerado pelo Sistema Acadêmico da UTFPR a partir dos dados da Ata de Defesa em 13/03/2024.

## ACKNOWLEDGEMENTS

First and foremost, I express my gratitude to God for all the blessings I have been given.

I would also like to dedicate a special thanks and love to my husband, Gabriel, for accepting the challenge of being a foreigner with me. His support and encouragement during this journey have been essential.

Estendo meu agradecimento aos meus pais, Décio e Deusana, por todas as renúncias feitas em nome da minha formação. Essas conquistas só têm sentido pois tenho vocês para comemorar comigo.

I am immensely grateful to Prof. Glauber Brante for his guidance and mentorship since my Master's degree. His generosity, friendship, and advice have shaped my academic path significantly. I also express my gratitude to Prof. Bruno Sens Chang for his kindness and for allowing me to work under his co-supervision.

To Profs. Yahia Medjahdi and Carlos Faouzi Bader, I extend my sincere thanks for their warm welcome and all the knowledge shared in our discussions. I am also thankful to Prof. Jérémie Sublime, who accepted me as his student and was always welcoming and kind.

To my colleagues and friends at ISEP, thank you for the time we spent together in France, whether over coffee, lunch, or funny moments in the lab. To the friends made at Maison du Brésil, for making my and Gabriel's journey lighter and giving us a family atmosphere far away from Brazil.

I would like to thank the professors on the jury for accepting the invitation and for all their suggestions. Finally, I gratefully acknowledge the financial support of INESC P&D Brasil and the Coordination for the Improvement of Higher Education Personnel (CAPES).

## ABSTRACT

The forthcoming sixth generation (6G) of wireless communication systems is expected to enable a wide range of new applications in vehicular communication, which is accompanied by a diverse set of challenges and opportunities resulting from the demands of this cutting-edge technology. In particular, these challenges arise from dynamic channel conditions, including time-varying channels and nonlinearities induced by high-power amplifiers. In this complex context, wireless channel estimation emerges as an essential element in establishing reliable communication. Furthermore, the potential of machine learning and deep learning in the design of receiver architectures adapted to vehicular communication networks is evident, given their capabilities to harness vast datasets, model complex channel conditions, and optimize receiver performance. Throughout the course of this research, we leveraged these potential tools to advance the state-of-the-art in receiver design for vehicular communication networks. In this manner, we delved into the characteristics of wireless channel estimation and the mitigation of nonlinear distortions, recognizing these as significant factors in the communication system performance. To this end, we propose new methods and flexible receivers, based on hybrid approaches that combine mathematical models and machine learning techniques, taking advantage of the unique characteristics of the vehicular channel to favor accurate estimation. Our analysis covers both conventional wireless communications waveform and a promising 6G waveform, targeting the comprehensiveness of our approach. The results of the proposed approaches are promising, characterized by substantial enhancements in performance and noteworthy reductions in system complexity. These findings hold the potential for real-world applications, marking a step toward the future in the domain of vehicular communication networks.



**Keywords:** Vehicular communication. Nonlinear Distortions. Channel Estimation. Machine Learning.

# RÉSUMÉ

La futur sixième génération (6G) de systèmes de communication sans fil devrait permettre un large éventail de nouvelles applications dans le domaine de la communication véhiculaire, ce qui s'accompagne d'un ensemble varié de défis et d'opportunités résultant des exigences de cette technologie de pointe. En particulier, ces défis découlent des conditions dynamiques des canaux, y compris les canaux variables dans le temps et les non-linéarités induites par les amplificateurs de puissance. Dans ce contexte complexe, l'estimation des canaux sans fil apparaît comme un élément essentiel pour établir une communication fiable. En outre, le potentiel de l'apprentissage automatique et de l'apprentissage profond dans la conception d'architectures de récepteurs adaptées aux réseaux de communication véhiculaires est évident, étant donné leurs capacités à exploiter de vastes ensembles de données, à modéliser des conditions de canal complexes et à optimiser la performance des récepteurs. Au long de cette recherche, nous avons tiré parti de ces outils potentiels pour faire progresser l'état de l'art en matière de conception de récepteurs pour les réseaux de communication véhiculaires. Ainsi, nous avons exploré les caractéristiques de l'estimation des canaux sans fil et de l'atténuation des distorsions non linéaires, en reconnaissant qu'il s'agit de facteurs importants pour la performance des systèmes de communication. À cette fin, nous proposons de nouvelles méthodes et des récepteurs flexibles, basés sur des approches hybrides qui combinent des modèles mathématiques et des techniques de l'apprentissage automatique, en tirant parti des caractéristiques uniques du canal véhiculaire pour promouvoir une estimation précise. Notre analyse couvre à la fois la forme d'onde des communications sans fil conventionnelles et une forme d'onde prometteuse de la 6G, ce qui démontre la complétude de notre approche. Les résultats des approches proposées sont prometteurs, caractérisés par des améliorations substantielles de la performance et des réductions notables de la complexité du système. Ces résultats offrent un potentiel pour des applications dans le monde réel, marquant un pas vers l'avenir dans le domaine des réseaux de communication véhiculaires.

**Mots clés:** Communication véhiculaire. Distorsions non linéaires. Estimation du canal. Apprentissage automatique.

## RESUMO

Espera-se que a futura sexta geração (6G) de sistemas de comunicação sem fio possibilite uma ampla gama de novas aplicações na comunicação veicular, o que deve ser acompanhado por um conjunto diversificado de desafios e oportunidades resultantes das demandas dessa tecnologia de ponta. Em particular, esses desafios decorrem das condições dinâmicas do canal, incluindo canais que variam no tempo e não linearidades induzidas por amplificadores de alta potência. Nesse complexo contexto, a estimativa de canal sem fio surge como um elemento essencial para estabelecer uma comunicação confiável. Além disso, o potencial do aprendizado de máquina e do aprendizado profundo no projeto de arquiteturas de receptores adaptadas às redes de comunicação veicular é evidente, dadas as capacidades desses métodos em aproveitar vastos conjuntos de dados, modelar condições complexas de canal e otimizar o desempenho do receptor. Ao longo desta pesquisa, aproveitamos essas ferramentas potenciais para avançar o estado da arte no projeto de receptores para redes de comunicação veicular. Dessa forma, aprofundamos as análises sobre as características da estimativa de canal sem fio e a atenuação de distorções não lineares, reconhecendo-as como fatores significativos no desempenho do sistema de comunicação. Para isso, propusemos novos métodos e receptores flexíveis, com base em abordagens híbridas que combinam modelos matemáticos e técnicas de aprendizado de máquina, aproveitando as características do canal veicular para favorecer uma estimativa precisa. A nossa análise abrange tanto uma forma de onda padrão de comunicações sem fio como uma forma de onda promissora ao 6G, visando a compreensão da nossa abordagem. Os resultados das abordagens propostas são promissores, caracterizados por melhorias substanciais no desempenho e reduções notáveis na complexidade do sistema. Essas descobertas têm potencial para aplicações no mundo real, marcando um passo em direção ao futuro no domínio das redes de comunicação veicular.



**Palavras-chave:** Comunicação Veicular. Distorções Não-lineares. Estimação de Canal. Aprendizado de Máquina.

## RÉSUMÉ DES TRAVAUX DE THÈSE

# Chapitre 1 - Introduction

En réponse à la demande croissante de débits de données plus élevés, de fiabilité et de connectivité, le domaine dynamique des systèmes modernes de communication sans fil présente des défis importants pour les applications attendues dans les prochaines générations de télécommunications. En particulier, la communication véhicule-à-tout (V2X) est un sujet majeur pour le développement de solutions dans le cadre des futures applications 6G et présente des défis en ce qui concerne la complexité des solutions et leur applicabilité à ces scénarios hautement variables et dynamiques [1].

Dans ce contexte, il est extrêmement important d'estimer le canal sans fil avec une qualité suffisante pour garantir une communication fiable, car cela affecte considérablement les performances globales du système et permet d'en exploiter tout le potentiel. En outre, pour répondre aux demandes futures, l'intégration d'outils d'intelligence artificielle est apparue comme un nouveau paradigme pour l'évolution des réseaux du futur [2]. En ce sens, ce travail est motivé par le potentiel des outils de l'apprentissage automatique et en particulier de l'apprentissage profond pour concevoir de nouvelles architectures de récepteurs capables de s'adapter aux conditions dynamiques du canal, en particulier dans le contexte des réseaux V2X, qui sont caractérisés par des canaux variant dans le temps et des non-linéarités dues à la présence d'amplificateurs de puissance.

Dans cette thèse, nous proposons d'explorer la combinaison de stratégies classiques avec des techniques d'apprentissage profond pour concevoir des récepteurs. L'analyse commence par l'OFDM, une forme d'onde largement utilisée dans les normes de communication sans fil et montre que cette combinaison permet une amélioration significative des performances, ainsi qu'une réduction de la complexité, pour différents scénarios et aspects pris en compte dans l'analyse. Cette étude est ensuite étendue à l'application de la méthode proposée à une forme d'onde candidate pour lesréseaux V2X à forte mobilité, montrant son potentiel en tant que technique prometteuse pour de futures applications dans le monde réel.

### Objectifs de la thèse

L'objectif principal de cette thèse est d'explorer l'application des techniques de l'apprentissage profond dans la conception de nouvelles architectures de récepteurs pour les communications V2X, en tenant compte de leur nature variable dans le temps et des effets non linéaires induits par les amplificateurs de puissance. Les objectifs de cette recherche sont donc les suivants:

- Étudier les exigences et les défis spécifiques présentés par les futurs scénarios de communication sans fil, en particulier dans le domaine des communications V2X;
- Proposer des algorithmes robustes basés sur l'aprendissage profond capables de suivre les canaux véhiculaires, en tenant compte de leur nature dynamique;
- Explorer des approches permettant de réduire la complexité des architectures proposées.

## Chapitre 2 - Principes fondamentaux

### Communication véhiculaire multiporteuse

Dans les systèmes de communication sans fil, le signal reçu est : le résultat de superposition de plusieurs versions retardées et atténuées du signal émis. Ce phénomène, appelé évanouissement, est influencé par l'effet des multitrajets du canal ainsi que l'effet Doppler. Le phénomène de multitrajet entraîne un évanouissement sélectif en la fréquence. D'autre part, l'effet Doppler est causé par la vitesse relative entre l'émetteur et le récepteur, entraînant une sélectivité dans le domaine temporel.

En raison de ces deux effets, le canal de communication sans fil présente une double sélectivité, variant à la fois en temps et en fréquence. Un canal doublement sélectif peut être présenté dans le domaine dit délai-Doppler (*delay*-Doppler - DD), par une réponse parcimonieuse quasi-statique avec des impulsions associées à des retards-Doppler différents.

La transmission multiporteuse est largement utilisée pour déployer des systèmes de communication sans fil afin d'éviter les problèmes liés à la propagation par trajets multiples. Ces schémas de modulation divisent la transmission en un format structuré dans lequel plusieurs symboles sont envoyés simultanément sur plusieurs fréquences dites sous-porteuses..

La modulation OFDM (*Orthogonal Frequency Division Multiplexing*) est l'un des schémas de modulation multiporteuse les plus importants, largement utilisé dans diverses normes de systèmes de communication sans fil. D'autres formes d'onde multiporteuses ont été proposées pour répondre à des défis et à des exigences spécifiques dans les systèmes de communication sans fil. Une forme d'onde notable est la modulation *Orthogonal Time Frequency Space Modulation* (OTFS), introduite dans [3], qui se distingue comme une forme d'onde prometteuse pour les futurs systèmes de communication véhiculaire.

Bien que les systèmes de modulation multiporteuse offrent des avantages tels qu'une efficacité spectrale élevée et une réduction des interférences inter-symboles, ils présentent des inconvénients liés au facteur de crête (*Peak-to-Average Power Ratio* - PAPR) élevé du signal transmis [4], qui est dû à l'utilisation d'un grand nombre de sous-porteuses pour la transmission du signal. Par conséquent, la transmission multiporteuse peut nuire considérablement à l'efficacité des amplificateurs de puissance fonctionnant dans des régions non linéaires, ce qui peut entraîner une dégradation de l'information. Dans les systèmes de communication sans fil, un PAPR élevé peut avoir une incidence négative sur l'efficacité de l'amplificateur de puissance.

**Techniques d'apprentissage automatique**

Les réseaux de neurones profonds (*Deep Neural Networks* - DNNs) représentent une partie fondamentale des techniques d'apprentissage automatique [5]. Ce type de réseau neuronal artificiel se caractérise par plusieurs couches interconnectées, dans lesquelles chaque couche est constituée d'un ensemble de noeuds, généralement appelés neurones ou unités, qui effectuent des calculs et des transformations spécifiques sur les données d'entrée.

Les LSTMs sont des blocs/unités neuronales qui conviennent pour traiter et faire des prédictions basées sur des séquences de données [6]. Contrairement aux DNN traditionnels, les réseaux LSTM ont la capacité de capturer les dépendances à long terme. Cela est possible grâce à des unités passerelles internes capables de maintenir le contenu de la mémoire de données et, en même temps, d'employer des structures capables de décider quand conserver ou remplacer l'information dans ces cellules. Par conséquent, ces caractéristiques de traitement avancées des réseaux LSTM leur permettent d'apprendre la corrélation du canal au fil du temps et de s'adapter aux estimations du canal.

Comme pour les DNN, l'entraînement des réseaux LSTM implique l'ajustement de ses paramètres internes à l'aide de techniques visant à minimiser la fonction de perte. Une fois entraînés, les réseaux LSTM peuvent être utilisés pour la prédiction et la génération

de séquences, ainsi que pour d'autres tâches nécessitant une compréhension des modèles temporels.

## Chapitre 3 - Modèle du système

Cette thèse est basée sur la norme IEEE 802.11p, qui est un sous-ensemble du protocole Wi-Fi et prend en charge la transmission de données pour la communication véhiculaire. Ainsi, cette étude prend en compte deux modèles différents de HPA ainsi que le scénario de mobilité. Dans un premier temps, nous examinons le modèle HPA sans mémoire, en désignant le signal d'entrée par $\mathbf{x}(t)$ et la sortie est donnée, selon le théorème de Bussgang [7], par

$$\mathbf{u}_{\text{mless}}(t) = \mathbf{x}(t) + \delta(t),$$

où $\tilde{\delta}(t)$ présente la distorsion non linéaire et $\gamma_0$ décrit un gain complexe et $\delta(t) = \tilde{\delta}(t)/\gamma_0$ est la distorsion non linéaire restante de l'amplificateur de puissance.

Les HPA sans mémoire modélisent efficacement le comportement à bande large des amplificateurs. Cependant, en règle générale, une augmentation de la largeur de bande devrait introduire un effet de mémoire plus important dans le signal amplifié [8]. Il existe différentes représentations connues des amplificateurs de puissance dans les communications à large bande pour approximer le comportement non linéaire avec des structures de mémoire. En particulier, le modèle Hammerstein [9] considère un HPA non linéaire sans mémoire en cascade avec un filtre à réponse impulsionnelle finie (*Finite Impulse Response* - FIR) pour modéliser les effets de la mémoire [10].

Enfin, le canal sans fil considéré suit le modèle de canal véhiculaire décrit dans [11], où les caractéristiques de retard du canal sont fournies pour différents environnements. La caractérisation est basée sur des mesures réelles avec un ou deux véhicules se déplaçant à des vitesses différentes, où les profils d'intensité du canal sont présentés en tant que fonction des retards de trajet et des gains de puissance moyens, étant donné le profil de retard de puissance du canal (*Power Delay Profile* - PDP), statistiquement décrit par une distribution d'évanouissement de Rayleigh avec une densité spectrale de puissance Doppler. Les scénarios modélisés comprennent la communication entre les véhicules (*Vehicle to Vehicle* - V2V) et entre les véhicules et l'infrastructure (*Roadside to Vehicle* - R2V) dans des environnements présentant différentes caractéristiques de trafic et de vitesse.

## Chapitre 4 - État de l'art sur l'estimation du canal véhiculaire

Ce chapitre présente l'état de l'art des méthodes d'estimation des canaux V2X considérées comme une référence dans ce travail. Il convient de noter que nous nous intéressons à une approche dite symbole par symbole, où l'estimation l'estimation du canal est effectuée pour chaque symbole reçu séparément en utilisant uniquement les pilotes précédents et actuels reçus, sans augmenter la latence de l'application [12].

La méthode de base considérée pour fournir une estimation du canal dans la norme IEEE 802.11p est l'estimateur LS, qui utilise des symboles d'apprentissage prédéfinis pour obtenir une estimation dans le domaine des fréquences pour chaque sous-porteuse. La méthode *Data Pilot-Aided* (DPA) utilise quant à elle le symbole reçu précédemment comme préambule pour estimer le canal du symbole actuel. Cette méthode démarre avec une estimation LS du premier symbole reçu. L'amélioration consiste à exploiter les caractéristiques de corrélation entre les symboles adjacents dans la transmission OFDM. Toutefois, la performance de ce système est fortement influencée par la fiabilité des pilotes de données, qui tend à se dégrader en raison de la dynamique sévère des canaux véhiculaires [13]. La méthode *Spectral Temporal Averaging* (STA) est présentée dans [14], dans laquelle une moyenne des canaux estimés dans les domaines temporel et fréquentiel est réalisée après l'estimation DPA.

Pour améliorer les performances des estimateurs conventionnels, les auteurs dans [15] et [16] ont envisagé un DNN pour le post-traitement des estimateurs DPA et STA, respectivement. L'objectif du DNN utilisé est de minimiser l'erreur quadratique moyenne (*Mean Squared Error* - MSE) entre l'information parfaite sur l'état du canal (*Channel State Information* - CSI) et l'estimation conventionnelle.

Afin de procéder à une analyse préliminaire des performances des estimateurs de canal lorsqu'ils sont appliqués à la norme IEEE 802.11p en présence de distorsions dues à des non-linéarités HPA sans mémoire, cette section présente des comparaisons de performance des estimateurs DPA et STA [14], ainsi que des estimateurs basés sur les DNN tels que DPA-DNN [15] et STA-DNN [16].

Les résultats obtenus montrent la supériorité des méthodes basées sur les DNN pour l'estimation du canal, de sorte que l'utilisation des DNN en tant que processus non linéaire améliore considérablement les performances des estimateurs conventionnels, en ajoutant la capacité d'apprendre des caractéristiques sur le canal et en réduisant l'erreur entre son estimation et le canal idéal, même lorsqu'il est affecté par des non-linéarités. En outre, quand les distorsions HPA sont prises en compte lors de l'apprentissage des DNNs, ces estimateurs surpassent le taux d'erreur binaire (*Bit Error Rate* - BER) fourni par

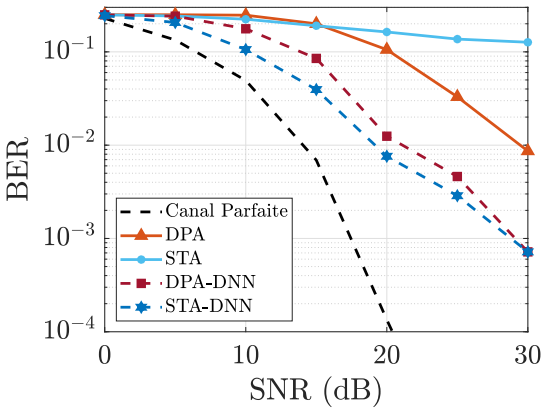


Absence des distorsions de HPA.

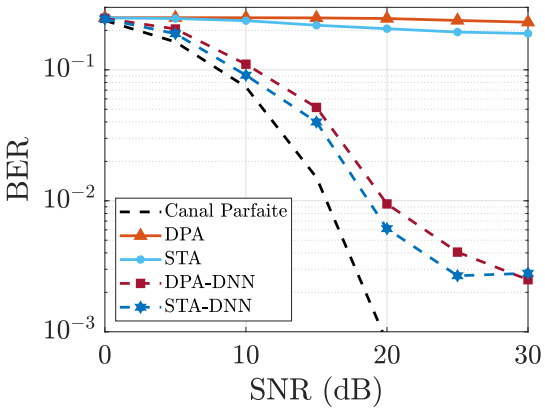


Avec des distorsions de HPA.

– **Performance des estimateurs conventionnels et des estimateurs basés sur les DNN.**

les estimateurs conventionnels dans les différents scénarios considérés, pouvant atteindre $10^{-2}$ à $\xi = 20$ dB, alors que les estimateurs conventionnels souffrent d'une dégradation significative de performance.

Selon la littérature existante, les méthodes basées sur les réseaux LSTM sont plus performantes que les réseaux de neurones profonds classiques lorsqu'il s'agit d'estimer des canaux V2X [12, 17]. Toutefois, ce gain de performance se fait au prix d'une complexité accrue. Reconnaissant à la fois les avantages et les limites, cette thèse propose une nouvelle approche qui est également basée sur les réseaux LSTM. Cependant, une méthode est envisagée pour réduire considérablement la complexité de l'estimateur, atténuant ainsi ce compromis. Une analyse complète des performances est effectuée, comparant les performances des méthodes de référence employant des DNN, des réseaux LSTM et notre propre proposition d'architecture.

## Chapitre 5 - Proposition d'estimation du canal basée sur les réseaux LSTM

Ce chapitre présente une nouvelle architecture de récepteur basée sur l'apprentissage proposée pour estimer le canal V2X. La méthode DPA-LSTM-NN comporte trois structures principales qui sont fondamentales pour ses performances. En outre, cette méthode prend en compte un processus d'échantillonnage de sous-porteuses à l'entrée de les réseaux LSTM, ce qui réduit le nombre de sous-porteuses actives prises en compte pour l'estimation du canal afin d'interpoler les informations manquantes sur les sous-porteuses et de réduire la complexité de la solution.

Parmi les caractéristiques de la méthode, il y a la prise en compte d'une estimation initiale plus fiable au moyen de l'estimation DPA. La DPA est capable d'apprendre les caractéristiques temporelles et fréquentielles du canal et de reconstruire l'estimation aussi proche que possible de la réponse idéale du canal. Ensuite, l'étage LSTM est conçu pour traiter des données séquentielles, en étant capable d'apprendre la corrélation du canal dans le temps et de prédire avec efficacité les réalisations futures du canal sur la base des observations précédentes. Il s'agit d'un élément clé pour traiter les effets non linéaires de le HPA. En complément, un NN est utilisé comme étape supplémentaire de compensation du bruit.

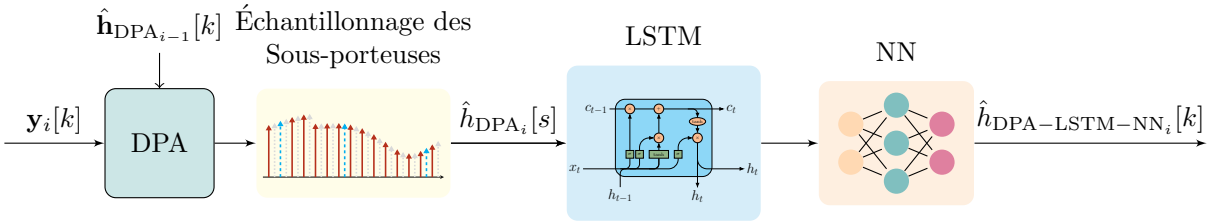


– **Méthode DPA-LSTM-NN proposée.**

Dans un premier temps, nous avons considéré un modèle de HPA non linéaire sans mémoire. Les performances du schéma DPA-LSTM-NN proposé sont évaluées et comparées aux performances des schémas DPA-DNN [15], LSTM-NN-DPA [17] et LSTM-DPA-TA [18] dans des scénarios avec différentes vitesses, ordres de modulation et niveaux de non-linéarité.

À titre d'exemple, les performances en termes de BER des schémas d'estimation utilisant la modulation 16-QAM pour les scénarios de mobilité élevée sont analysées, où il est possible d'obtenir un gain de performance significatif pour l'estimateur DPA-LSTM-NN proposé, surpassant les autres solutions quel que soit le niveau de bruit. Il est également important de souligner que le DPA-LSTM-NN proposé est le seul estimateur capable d'atteindre un BER de l'ordre de $10^{-4}$ dans les différents scénarios, ce qui est nécessaire pour de nombreuses applications pratiques attendues pour les futures communications véhiculaires.

Nous avons ensuite étendu l'analyse en considérant un modèle non linéaire de HPA avec effet mémoire. L'analyse des performances compare les estimateurs LSTM-NN-DPA [17], LSTM-DPA-TA [18] et DPA-LSTM-NN dans des scénarios avec des modèles HPA avec des effets de mémoire ayant un impact sur la communication entre une infrastructure installée sur une route et un véhicule récepteur l'approchant à une vitesse de $v = 50$ km/h. La comparaison, avec le cas de l'amplificateur sans mémoire, révèle une forte

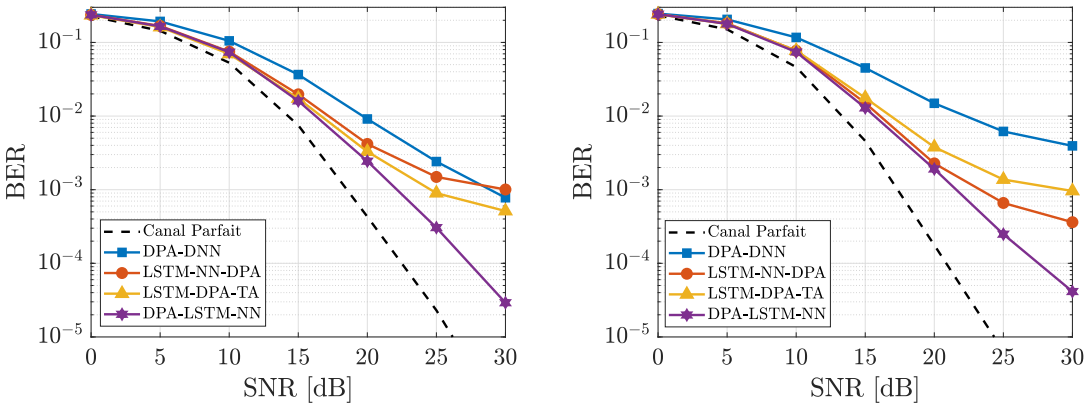


$v = 100$ km/h. $v = 200$ km/h.

**– Performance des estimateurs DPA-DNN [15], LSTM-NN-DPA [17], LSTM-DPA-TA [18] et DPA-LSTM-NN (proposée) pour une modulation 16-QAM dans le cas d'un HPA sans mémoire.**

dégradation en termes de BER due à la non compensation de la sélectivité fréquentielle causée par l'effet mémoire du HPA. Nous avons montré ensuite qu'il est possible de pallier à ce problème en appliquant une pré-compensation de cette sélectivité en fréquence. En outre, le DPA-LSTM-NN présente un avantage par rapport aux autres solutions dans le cas d'un HPA non-linéaire avec effet mémoire.

Nous avons ensuite analysé la complexité de de chacun de ses schémas d'estimation de canal. Celle-ci est exprimée en nombre d'opérations requises en fonction du nombre de sous-porteuses. Il convient de noter que le schéma DPA-LSTM-NN proposé présente les coefficients les plus faibles pour les facteurs les plus importants associés au nombre de sous-porteuses actives $K_{\text{on}}$ dans les opérations de multiplication et de division, ce qui a la plus grande incidence sur la complexité des estimateurs considérés. En outre, on peut constater que l'estimateur DPA-LSTM-NN proposé avec échantillonnage de sous-porteuse nécessite $49,9\%$ de moins d'opérations en valeur réelle en moins que les autres solutions basées sur les LSTM et $16,7\%$ de moins d'opérations en valeur réelle que le schéma DPA-DNN, et qu'il présente une amélioration significative des performances en matière de réduction des erreurs d'estimation.

***Ensemble learning* pour la généralisation de l'estimation des canaux véhiculaires**

Comme d'autres récepteurs dans la littérature [16–18], le schéma DPA-LSTM-NN considère l'entraînement sur un modèle de canal spécifique, bien que les caractéristiques du canal soient sujettes à variation et dépendent de l'environnement dans lequel les véhicules opèrent.

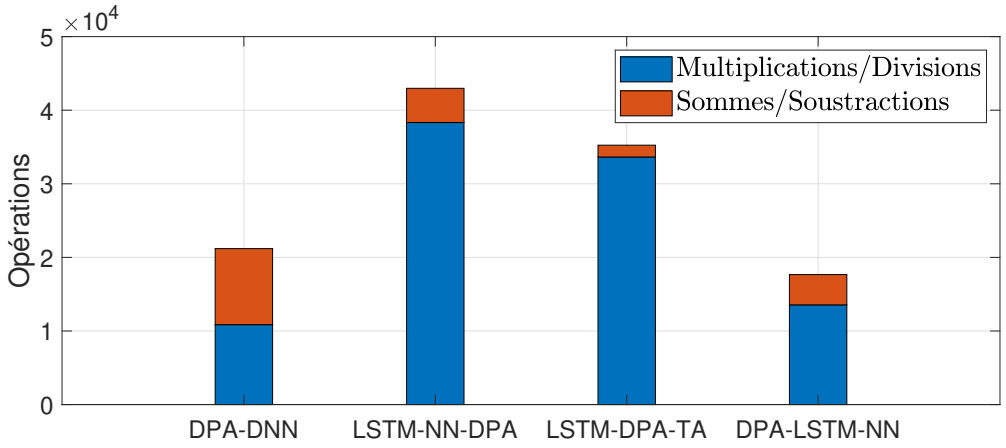


**– Complexité en termes d'opérations avec $K_{on} = 52$ sous-porteuses et $K_p = 4$ pilotes.**

À fin de généraliser les connaissances de l'estimateur DPA-LSTM-NN, nous avons proposé d'utiliser la technique *Ensemble Learning* (EL) pour améliorer les performances en combinant les prédictions de plusieurs modèles entraînes sur des ensembles de données qui prennent en compte différentes vitesses, des décalages Doppler maximaux et des retards de trajectoire.

Pour analyser l'impact de l'utilisation de la technique EL sur la généralisation de l'estimateur DPA-LSTM-NN, l'estimateur résultant de la combinaison de modèles entraînés sur des scénarios de vitesses et de PDP différents est comparé à des modèles entraînés spécifiquement pour un PDP/vitesse donné. Les résultats, tels que le scénario testé avec la communication V2V et la vitesse $v = 200$ km/h, montrent que le modèle EL présente une perte presque négligeable par rapport au cas le plus performant, dans lequel le modèle a été entraîné avec le même PDP/vitesse. D'autre part, une forte dégradation de performance peut être observée lorsque l'on teste les modèles formés avec le PDP et une vitesse fixe. De cette manière, le modèle EL constitue une alternative intéressante en offrant une estimation avec des pertes négligeables pour différents canaux. En outre, il est important de souligner que ces gains sont obtenus sans ajouter de complexité de calcul à l'estimation du canal, puisque le processus d'obtention du modèle EL combiné est effectué hors ligne.

## Chapitre 6 - Estimation de canal basée sur les réseaux LSTM pour les systemes OTFS

À mesure que les scénarios de communication entre véhicules continuent d'évoluer, la demande de systèmes de communication sans fil robustes et efficaces devient de plus en

plus critique. Dans ce contexte, bien que largement adoptés, les schémas de transmission multiporteuse conventionnels, tels que la modulation OFDM, présentent des limites inhérentes qui pourraient compromettre leur efficacité dans les futurs environnements véhiculaires [19]. En réponse à cela, l'OTFS [3, 20] est apparu comme un schéma de modulation prometteur, présentant une nouvelle approche de la communication sans fil. Dans ce contexte, ce chapitre présente l'étude sur la proposition d'un nouveau récepteur pour la forme d'onde OTFS, à comparer avec deux techniques de référence dans un scénario d'estimation de canal dans la transmission OTFS soumise à des distorsions non-linéaires induites par un HPA sans mémoire. Enfin, nous présentons l'évaluation de ce récepteur par le biais d'une analyse détaillée de ses performances.

### OTFS basée sur la SFFT

Une des applications les plus populaires des systèmes OTFS que l'on trouve dans la littérature est basée sur la transformée de Fourier rapide symétrique (*Symplectic Finite Fourier Transform* - SFFT) et la SFFT inverse (ISFFT), combinées à une modulation multiporteuse. Ces transformations sont utilisées pour convertir les canaux variables dans le temps en canaux invariants dans le domaine DD et vice versa. Cela permet de voir le système OTFS comme une technique multiporteuse avec des blocs de pré- et de post-traitement. En outre, pour une caractérisation plus réaliste des scénarios de communication sans fil, notre analyse considère que le signal émis est affecté par des non-linéarités induites par le HPA.

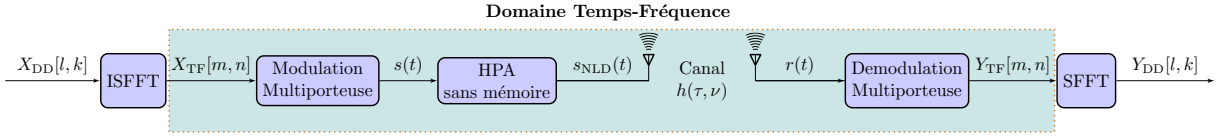


– **Architecture de l'OTFS basée sur la SFFT.**

### Méthodes de référence pour l'estimation du canal OTFS

L'état de l'art relatif à l'estimation du canal OTFS implique généralement l'estimation des caractéristiques du canal dans le domaine DD. Deux techniques établies, que nous appellerons *Threshold Channel Estimation* (TCE) [21] et *Correlation Channel Estimation* (CCE) [22], seront utilisées comme références de performance pour l'estimateur de canal basé sur les réseaux LSTM proposé.

Le travail de [21] a été le premier à présenter une solution pour l'estimation du canal dans les systèmes OTFS. Les auteurs ont introduit un schéma de pilote intégré, dans lequel un intervalle de garde suffisamment grand est appliqué autour d'un pilote exclusif

pour améliorer l'acquisition des réponses de retard et Doppler.

Dans [22] un estimateur est proposé pour OTFS dans lesquels la matrice d'autocorrélation du canal est acquise par estimation dans le domaine DD. Les auteurs supposent que le canal est invariant pendant au moins la durée d'un symbole OTFS, de sorte que le pilote et l'information sont envoyés dans des trames différentes.

Les propositions présentées dans [21, 22] nécessitent un intervalle de garde important pour atténuer l'interférence entre les symboles de données et les pilotes utilisés pour l'estimation du canal. En outre, les systèmes proposés nécessitent une puissance élevée pour les sous-porteuses pilotes. En conclusion, ces aspects peuvent avoir une incidence négative sur le rapport PAPR du signal transmis, comme le souligne [23], ce qui peut compromettre son application pratique.

**Méthode basée sur les réseaux LSTM proposée pour l'estimation du canal OTFS**

Un nouveau schéma d'estimation du canal est proposé pour les systèmes OTFS soumis aux non-linéarités causées par le HPA. La méthode commence par une estimation initiale du canal utilisant le préambule et les pilotes dans le domaine des fréquences. Cette estimation est injectée dans les réseaux LSTM, qui suit efficacement le comportement du canal. Ensuite, un NN est appliqué pour augmenter la capacité de réduction du bruit et affiner la précision de l'estimation. Grâce à ces étapes, nous pouvons maintenir un faible nombre de pilotes et obtenir une estimation fiable du canal, en particulier lorsqu'il s'agit de canaux hautement sélectifs. Il convient de noter ici que, contrairement aux propositions de [21, 22], les pilotes ont la même puissance que le signal transmis. Par conséquent, les échantillons du signal émis dans le domaine temps-fréquence servent de base au réseau LSTM-NN pour interpoler les informations sur le canal pour les porteuses de données et obtenir l'estimation finale.

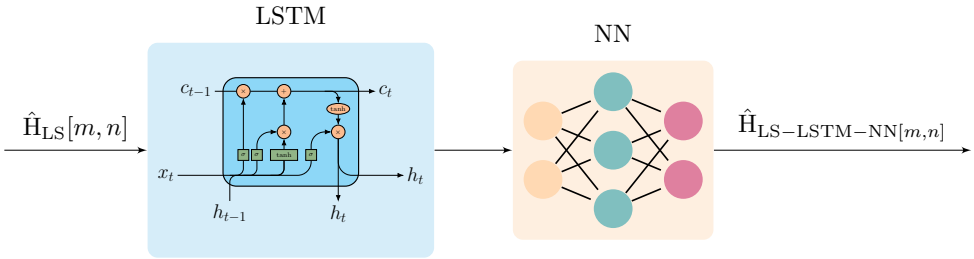


– **Méthode LS-LSTM-NN proposée.**

**Analyse des performances**

La performance du récepteur LS-LSTM-NN dans un scénario affecté par des distorsions résultant de non-linéarités HPA est analysée en termes de BER, débit de transmission et de PAPR. Nous comparons notre proposition aux méthodes de référence TCE [21] et CCE [22], dans lesquelles l'estimation du canal est réalisée à l'aide de la réponse pilote dans le domaine DD. Les résultats montrent les performances dans un scénario avec des véhicules se déplaçant à une vitesse de $v = 300$ km/h et pour les deux méthodes de référence, le SNR des pilotes est supposé être $\mathrm{SNR_p} = 40$ dB, conformément à leur conception.

L'évaluation du BER en considérant, par exemple, une modulation 16-QAM, montre les estimateurs de canal considérés présentent des performances comparables quand le SNR est relativement faible. Cependant, un gain notable est observé pour la méthode proposée quand le SNR est élevé. En revanche, les deux estimateurs présentés dans [21] et [22] ouffrent d'un BER trop élevé même dans les scénarios où le bruit devient négligeable devant le signal utile. Par conséquent, ces estimateurs ne parviennent pas à réduire le BER en dessous de $10^{-2}$ pendant la détection.

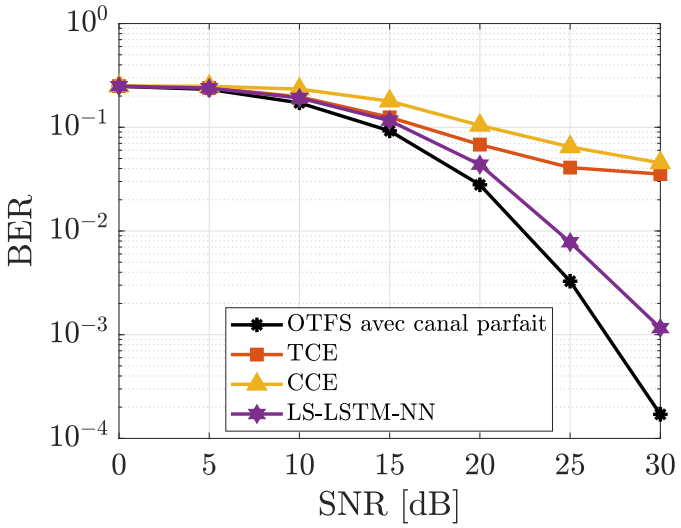


**– BER pour $v = 300$ km/h, modulation 16-QAM et IBO = 4 dB.**

L'analyse du PAPR est d'une importance fondamentale dans les scénarios de communication du monde réel. En comparant les techniques d'estimation du canal en termes d'impact sur le CCDF, il est possible de mettre en évidence le problème de l'attribution de pilotes avec une puissance très élevée pour faciliter l'estimation du canal dans le domaine DD. Plus précisément, l'estimateur LS-LSTM-NN proposé produit un gain de seuil de PAPR d'au moins 10 dB par rapport à la méthode proposée dans [21]. En

outre, cet avantage est encore plus prononcé par rapport à l'estimateur présenté dans [22]. En ce sens, nous notons que la meilleure performance du LS-LSTM-NN proposé est évidente, car il est le seul capable d'atteindre un taux d'erreur de $10^{-3}$ et est donc le seul à fournir des estimations fiables des canaux dans de tels scénarios.

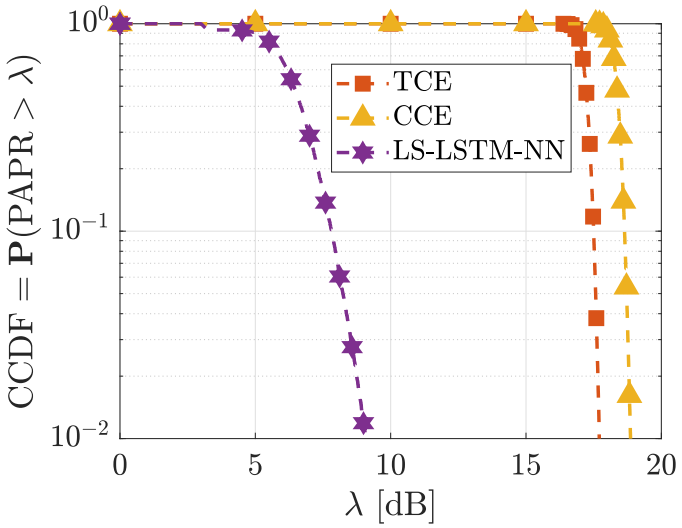


– **Analyse du PAPR.**

Il est important de souligner que la limitation du PAPR due à des pilotes de forte puissance dans le domaine DD est un facteur déjà étudié dans la littérature existante [23]. Toutefois, le maintien d'un PAPR plus faible est d'une importance capitale pour atténuer la distorsion induite par les HPA. Cette importance provient du fait que l'efficacité du HPA diminue à mesure que le PAPR du signal d'entrée augmente. En fait, il convient de noter que des valeurs de PAPR plus élevées peuvent compromettre considérablement la qualité de la communication et sont généralement impraticables dans des scénarios réels [24]. En revanche, notre système offre une voie pratique pour la communication OTFS. Enfin, nous soulignons que le calcul de l'ordre de complexité de calcul des différentes méthodes met en évidence la réduction de la complexité obtenue par l'estimateur de canal LS-LSTM-NN proposé, quelle que soit la taille de trame choisie.

## Chapitre 7 - Conclusions

Cette thèse s'est intéressée à la problématique de l'estimation des canaux des véhicules, notamment en tenant compte des effets des non-linéarités dues aux HPA. Tout d'abord, la recherche a permis de comprendre les limites des méthodes conventionnelles, qui souffrent généralement d'une dégradation significative des performances en présence de distorsions induites par les HPA. En conséquence, les résultats préliminaires de la recherche ont mis en évidence que les techniques DL présentent une robustesse inhérente

face à ces effets non linéaires. Cette analyse a encouragé la poursuite de l'exploration et de l'application de méthodes avancées basées sur la DL pour une estimation plus précise du canal véhiculaire.

Dans ce contexte, la contribution de cette recherche réside dans l'introduction de nouvelles architectures de récepteur basées sur l'apprentissage automatique, explicitement adaptées à l'estimation précise des canaux véhiculaires non-linéaires. En considérant le modèle HPA sans mémoire de la norme IEEE 802.11p, l'estimateur DPA-LSTM-NN proposé s'est révélé résistant aux effets induits par le HPA. En étendant cette analyse à des scénarios plus complexes impliquant des effets HPA non linéaires. Ainsi, la recherche montre qu'à partir d'une nouvelle technique de compensation peu complexe, l'efficacité du récepteur proposé est validée dans les scénarios présentés par les HPA à mémoire. Enfin, en prévision de la prochaine génération de communications sans fil 6G, une architecture pour l'estimation du canal OTFS a également été proposée, dans laquelle la supériorité de la proposition par rapport aux estimateurs conventionnels dans les scénarios de véhicules à haute mobilité, qui sont attendus pour les futures communications véhiculaires, ainsi que la réduction de la complexité lors de la détection du signal.

**RESUMO DOS TRABALHOS DE TESE**

## Capítulo 1 - Introdução

Em resposta à crescente demanda por taxas de dados, confiabilidade e conectividade mais altas, o cenário dinâmico dos modernos sistemas de comunicação sem fio apresenta desafios significativos para as aplicações esperadas nas próximas gerações de telecomunicações. Em particular, a comunicação veicular é uma das áreas de maior interesse para o desenvolvimento de soluções dentro das futuras aplicações 6G e apresentará desafios com relação à complexidade das soluções e sua aplicabilidade a esses cenários altamente variáveis e dinâmicos [1].

Nesse contexto, a estimativa do canal sem fio com qualidade suficiente para garantir uma comunicação confiável é extremamente importante, pois afeta significativamente o desempenho geral do sistema e libera todo o seu potencial. Além disso, para superar as futuras demandas, a integração de ferramentas de inteligência artificial surgiu como um novo paradigma para a evolução das futuras redes de comunicação sem fio [2]. Nesse sentido, o presente trabalho é motivado pelo potencial das ferramentas de aprendizado de máquina e aprendizado profundo para projetar novas arquiteturas de receptores capazes de se adaptar às condições dinâmicas do canal, especialmente no contexto de redes de comunicação veicular caracterizadas por canais variáveis no tempo e não linearidades devido à presença de amplificadores de alta potência (*High Power Amplifier* - HPA).

Propõe-se explorar a combinação de estratégias que utilizam modelos matemáticos e técnicas de aprendizado de máquina para projetar receptores. A análise inicia com uma forma de onda convencionalmente usada em padrões de comunicação sem fio, apresentando que essa combinação implica uma melhoria significativa no desempenho, bem como uma redução na complexidade, para diferentes cenários e aspectos considerados. Posteriormente, esse estudo é estendido para aplicar o método proposto a uma forma de onda candidata a futuras redes veiculares, apresentando seu potencial como uma técnica promissora para futuras aplicações no mundo real.

### Objetivos da tese

O principal objetivo desse trabalho é explorar a aplicação de técnicas de aprendizado de máquina no projeto de novas arquiteturas de receptores para comunicações veiculares, levando em conta sua natureza variável no tempo e os efeitos não lineares induzidos por HPA. Portanto, a presente pesquisa tem as seguintes finalidades:

- Investigar os requisitos e desafios específicos apresentados pelos futuros cenários de comunicação sem fio, especialmente na comunicação veicular.
- Propor algoritmos robustos baseados em aprendizado de máquina que possam rastrear dinamicamente os canais veiculares, considerando a sua natureza dinâmica;
- Explorar abordagens para reduzir a complexidade das arquiteturas propostas.

## Capítulo 2 - Princípios fundamentais

### Comunicação veicular multiportadora

Em sistemas de comunicação sem fio, o sinal recebido é uma composição de vários componentes que chegam de diferentes caminhos, cada um com diferentes atrasos e intensidades de sinal. Esse fenômeno é chamado de desvanecimento e é influenciado por fatores como a propagação por múltiplos percursos e o deslocamento Doppler. A propagação por múltiplos percursos ocorre devido às recepções de sinal que chegam em momentos diferentes de vários caminhos, levando ao desvanecimento seletivo em frequência. Por outro lado, o deslocamento Doppler é causado pelo movimento entre o transmissor e o receptor, resultando em seletividade no domínio do tempo.

Devido a ambos os efeitos, o canal de comunicação sem fio apresenta dupla seletividade, variando tanto no tempo quanto na frequência. Os canais duplamente seletivos podem ser representados com eficiência no chamado domínio delay-Doppler (DD), em que a resposta ao impulso do canal variável no tempo se apresenta como uma derivação de canal quase estática e esparsa, com um local determinado pelo atraso do caminho e pelo efeito Doppler.

A transmissão com multiportadoras é amplamente usada para implantar sistemas de comunicação sem fio com o objetivo de evitar os problemas decorrentes do efeito de propagação por múltiplos caminhos. Esses esquemas de modulação dividem a transmissão em um formato estruturado em que vários símbolos são enviados simultaneamente, cada um ocupando sub-bandas diferentes.

A modulação por divisão ortogonal de frequência (*Orthogonal Frequency Division Multiplexing* - OFDM) é um dos mais proeminentes esquemas de modulação de multiportadoras, amplamente utilizado em vários padrões de sistemas de comunicação sem fio. Outras formas de onda de multiportadoras foram propostas para atender a desafios e requisitos específicos em sistemas de comunicação sem fio. Uma forma de onda notável é a modulação *Orthogonal Time Frequency Space Modulation* (OTFS), introduzida em [3], que se destaca como uma forma de onda promissora para futuros sistemas de comunicação veicular.

Embora os sistemas de modulação de multiportadoras ofereçam benefícios como alta eficiência espectral e interferência entre símbolos reduzida, eles apresentam desvantagens associadas à alta razão entre a potência de pico e a potência média (*Peak-to-Average Power Ratio* - PAPR) do sinal transmitido [4], que surge devido à utilização de um grande número de subportadoras para a transmissão do sinal. Consequentemente, a transmissão por multiportadoras pode prejudicar significativamente a eficiência dos HPAs que operam em regiões não lineares, o que pode levar à degradação das informações.

**Técnicas de aprendizado de máquina**

As redes neurais profundas (*Deep Neural Networks* - DNNs) são fundamentais entre as técnicas de aprendizado produndo [5]. Esse tipo de rede neural artificial é caracterizado por várias camadas interconectadas, em que cada camada consiste em um conjunto de nós, geralmente chamados de neurônios ou unidades, que realizam cálculos e transformações específicos nos dados de entrada.

A LSTM é um tipo de arquitetura de rede neural recorrente adequada para processar e fazer previsões com base em sequências de dados [6]. Diferentemente do caso das DNNs tradicionais, as redes baseadas em LSTM têm a capacidade de capturar dependências de longo prazo. Isso é feito por unidades de porta interna capazes de armazenar o conteúdo da memória dos dados e, ao mesmo tempo, empregar estruturas capazes de decidir quando manter ou substituir as informações dessas unidades. Portanto, essas características avançadas de processamento das redes LSTM permitem que elas aprendam a correlação do canal ao longo do tempo e se adaptem às estimativas do canal.

Semelhante às DNNs, o treinamento da rede LSTM envolve o ajuste de seus parâmetros internos por meio de técnicas para minimizar a função de perda. Depois de treinado, um LSTM pode ser usado para previsão de sequências, geração e outras tarefas que exijam uma compreensão dos padrões temporais.

## Capítulo 3 - Modelo do sistema

A presente tese baseia-se no padrão IEEE 802.11p, um subconjunto do protocolo Wi-Fi que oferece suporte à transmissão de dados para comunicação veicular. Assim, o estudo considera dois modelos diferentes de HPA juntamente com o cenário de mobilidade. Inicialmente, o modelo HPA sem memória é examinado, denotando o sinal de entrada como $\mathbf{x}(t)$ e, seguindo o teorema de Bussgang [7], tem-se a saída dada por

$$\mathbf{u}_{\text{mless}}(t) = \mathbf{x}(t) + \delta(t),$$

em que $\tilde{\delta}(t)$ apresenta a distorção não linear e $\gamma_0$ descreve um ganho complexo e $\delta(t) = \tilde{\delta}(t)/\gamma_0$ é a distorção não-linear restante do HPA,

Os HPAs sem memória modelam com eficácia o comportamento de banda estreita dos amplificadores. No entanto, como uma tendência geral, espera-se que um aumento na largura de banda introduza um efeito de memória mais forte no sinal amplificado [8]. Há diferentes representações conhecidas de HPAs em comunicações de banda larga para aproximar o comportamento não linear com estruturas de memória. Em particular, o modelo Hammerstein [9] considera um HPA não linear sem memória em cascata com um filtro de resposta ao impulso finito (*Finite Impulse Response* - FIR) para modelar os efeitos de memória [10].

Por fim, o canal sem fio considerado segue o modelo de canal veicular descrito em [11], em que as características de atraso do canal são fornecidas para diferentes ambientes. A caracterização é baseada em medições reais com um ou dois veículos se movendo em velocidades diferentes, onde são apresentados perfis de intensidade do canal em função de atrasos de caminho e ganhos médios de potência, dado o perfil de atraso de potência do canal (*Power Delay Profile* - PDP), descritos estatisticamente por uma distribuição de desvanecimento de Rayleigh com uma densidade espectral de potência Doppler. Os cenários modelados incluem comunicação entre veículos (*Vehicle to Vehicle* - V2V) e entre veículo e infraestrutura (*Roadside to Vehicle* - R2V) em ambientes com diferentes características de tráfego e velocidade.

## Capítulo 4 - Estado da arte sobre estimação de canal veicular

Esse capítulo apresenta o estado da arte para os métodos de estimação de canal veicular considerados como referência nesse trabalho. Destaca-se que o foco desse trabalho está nos estimadores de canal símbolo a símbolo, *i.e.*, nos quais a estimativa de canal é

realizada para cada símbolo recebido separadamente usando apenas os pilotos recebidos anterior e atual, sem aumentar a latência da aplicação [12].

O método básico considerado para fornecer estimativa de canal no padrão IEEE 802.11p é o estimador LS, o qual utiliza símbolos predefinidos de treinamento para obter uma estimativa no domínio da frequência para cada subportadora. Por sua vez, o método *Data Pilot-Aided* (DPA) emprega o símbolo recebido anteriormente como preâmbulo para estimar o canal do símbolo atual. Como ponto de partida, o primeiro símbolo recebido utiliza o método LS. Dessa forma, o método DPA melhora o desempenho explorando as características de correlação entre os símbolos adjacentes na transmissão OFDM. No entanto, o desempenho desse esquema é fortemente influenciado pela confiabilidade dos pilotos de dados, que tende a se degradar devido à dinâmica severa dos canais veiculares [13]. Por sua vez, o método *Spectral Temporal Averaging* (STA) é apresentado em [14], em que uma média dos canais estimados nos domínios de tempo e frequência é realizada após a estimativa DPA.

Para melhorar o desempenho dos estimadores convencionais, os autores em [15] e [16] consideraram uma DNN para o pós-processamentos dos estimadores DPA e STA, respectivamente. O objetivo da DNN empregada é minimizar o erro quadrático médio (*Mean Squared Error* - MSE) entre as informações perfeitas sobre o estado do canal (*Channel State Information* - CSI) e a estimativa convencional.

Para fins de uma análise preliminar do desempenho dos estimadores de canal quando aplicados ao padrão IEEE 802.11p na presença de distorções devido a não linearidades HPA sem memória, essa seção apresenta as comparações de desempenho dos estimadores DPA e STA [14], bem como estimadores baseados em DNN, como o DPA-DNN [15] e o STA-DNN [16].

Os resultados obtidos evidenciam a superioridade dos métodos baseados em DNN na estimativa do canal, de modo que o uso de DNN como um processo não linear melhora consideravelmente o desempenho dos estimadores convencionais, acrescentando a capacidade de aprender recursos sobre o canal e reduzindo o erro entre sua estimativa e o canal ideal, mesmo quando afetado por não-linearidades. Além disso, quando as distorções HPA são consideradas, os estimadores baseados em DNN melhoram a taxa de erro de bit (*Bit Error Rate* - BER) fornecida pelos estimadores convencionais em diferentes cenários considerados, sendo capazes de atingir uma taxa de erro de bit de $10^{-2}$ a $SNR = 20$ dB, enquanto os estimadores convencionais sofrem uma grave degradação de desempenho.

Conforme a literatura existente, destaca-se que os métodos LSTM apresentam

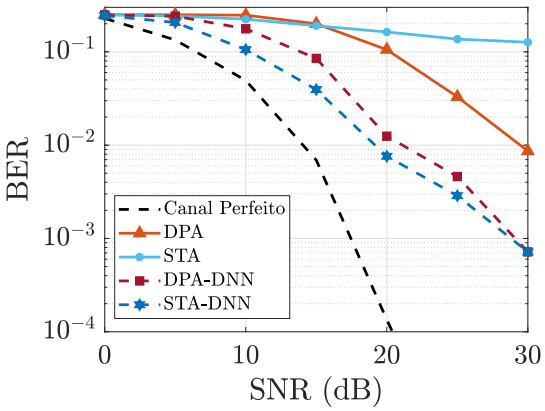


Sem distorções de HPA.

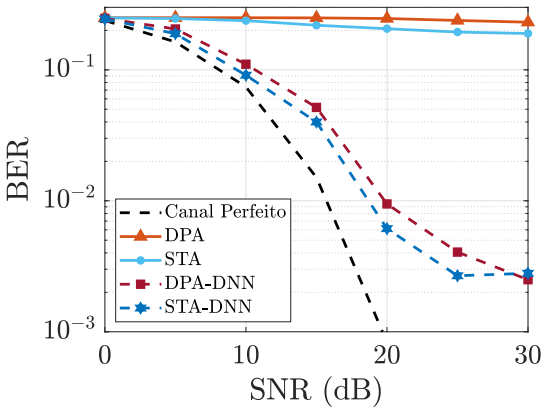


Com distorções de HPA.

– **Desempenho dos estimadores convencionais e baseados em DNN.**

desempenho superior em comparação com os métodos DNN ao estimar o canal veicular [12, 17]. No entanto, esse ganho de desempenho ocorre às custas do aumento da complexidade. Reconhecendo tanto as vantagens quanto as limitações, a presente tese propõe uma nova abordagem que também se baseia em redes LSTM. No entanto, é considerado um método para reduzir substancialmente a complexidade do estimador, atenuando esse aumento de complexidade. Uma análise completa do desempenho é realizada, comparando o desempenho de métodos de referência que empregam DNN, LSTM e a nova proposta.

## Capítulo 5 - Proposta para estimação de canal baseada em LSTM

Essa seção apresenta uma nova arquitetura de receptor baseada em aprendizado proposta para estimar o canal veicular. O método DPA-LSTM-NN apresenta três estruturas principais que são fundamentais para seu desempenho. Além disso, o esse método considera um processo de amostragem de subportadora na entrada do LSTM, reduzindo o número de subportadoras ativas consideradas para a estimativa do canal, de modo a interpolar as informações das subportadoras faltantes e reduzir a complexidade da solução.

Dentre os recursos do método, está primeiro a consideração de uma estimativa inicial mais confiável, por meio da estimativa DPA. O DPA é capaz de aprender as características de tempo e frequência do canal e reconstruir a estimativa o mais próximo possível da resposta ideal do canal. Em seguida, a estrutura LSTM é projetada para lidar com dados sequenciais, sendo capaz de aprender a correlação do canal ao longo do tempo e prever com eficiência as realizações futuras do canal com base em observações

anteriores. Isso é fundamental para lidar com os efeitos não-lineares do HPA. Além disso, uma NN é empregada como uma etapa adicional de compensação de ruído.

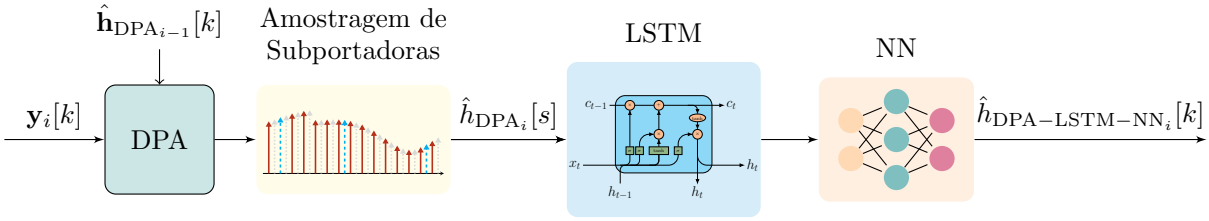


– **Método DPA-LSTM-NN proposto.**

Iniciamos nossa análise com foco no HPA sem memória. A avaliação de desempenho do esquema DPA-LSTM-NN proposto é comparando com os esquemas DPA-DNN [15], LSTM-NN-DPA [17] e LSTM-DPA-TA [18] em cenários com diferentes velocidades, ordens de modulação e impactos de não-linearidade.

Como exemplo, o desempenho em BER dos esquemas de estimativa usando modulação 16-QAM para cenários de alta mobilidade é analisado, onde é possível obter um ganho de desempenho significativo para o estimador DPA-LSTM-NN proposto, superando as outras soluções independentemente do nível de ruído. Também é importante destacar que o método proposto é o único estimador a atingir BER da ordem de $10^{-4}$ nos diferentes cenários, o que é exigido por muitas aplicações práticas esperadas para futuras comunicações veiculares.

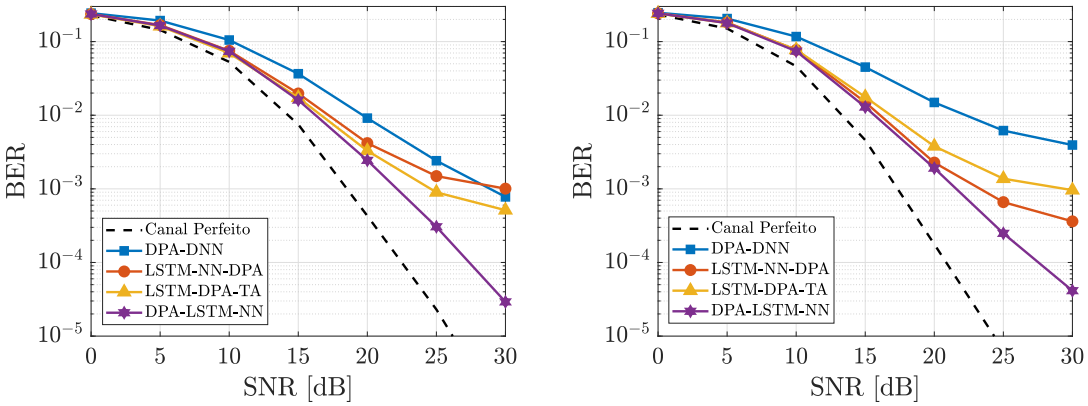


$v = 100$ km/h. $v = 200$ km/h.

– **Desempenho dos estimadores DPA-DNN [15], LSTM-NN-DPA [17], LSTM-DPA-TA [18] and DPA-LSTM-NN (proposto) para modulação 16-QAM no caso com HPA sem memória.**

Utilizamos a análise anterior para expandir a discussão sobre cenários práticos com não-linearidades, com os efeitos de memória do modelo HPA sendo considerados como

uma etapa adicional na avaliação de desempenho. A análise de desempenho compara os estimadores LSTM-NN-DPA [17], LSTM-DPA-TA [18] e o DPA-LSTM-NN em cenários com modelos HPA com efeitos de memória impactando a comunicação entre uma antena transmissora montada em uma estrada e um veículo receptor que se aproxima com uma velocidade de $v = 50$ km/h. A comparação entre os casos com HPA sem memória e HPA com memória sem compensação revela um aumento significativo de BER devido aos efeitos de memória. Apesar disso, a compensação de memória HPA é efetiva contra essa perda, sendo responsável por um desempenho mais próximo do cenário sem memória para todos os estimadores considerados. Além disso, o DPA-LSTM-NN mostra uma vantagem sobre outras soluções em cenários com efeitos de memória HPA.

O resumo das operações de valor real exigidas pelos esquemas de estimativa de canal, como uma função do número de subportadoras ativas é apresentado. Destaca-se que o esquema DPA-LSTM-NN proposto tem os menores coeficientes para os fatores mais significativos associados ao número de subportadoras ativas $K_{\text{on}}$ nas operações de multiplicações e divisões, o que resulta na redução da complexidade em comparação aos demais estimadores considerados. Além disso, observa-se que o estimador DPA-LSTM-NN proposto com amostragem de subportadoras necessita $49,9\%$ menos operações do que outras soluções baseadas em LSTM e $16,7\%$ menos operações do que o esquema DPA-DNN, além de apresentar uma melhoria significativa no desempenho.

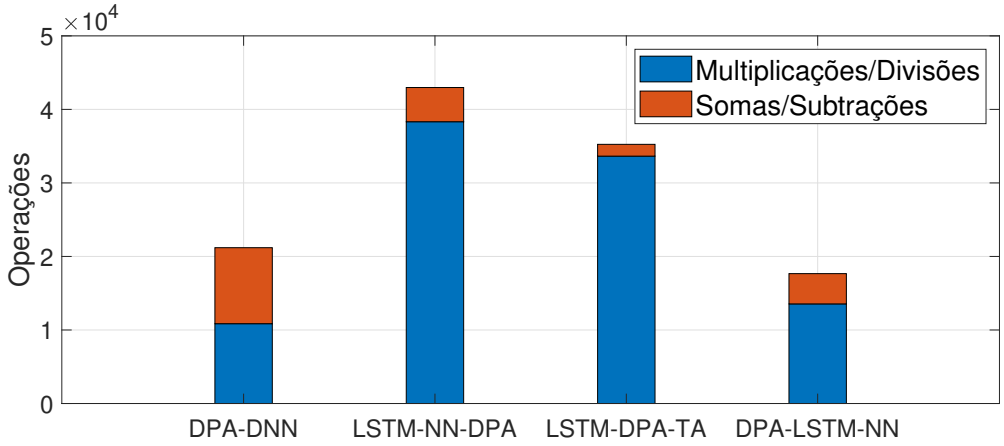


– **Complexidade computacional em termos de operações com $K_{\text{on}} = 52$ subportadoras e $K_{\text{p}} = 4$ pilotos.**

### *Ensemble learning* para generalização da estimação do canal veicular

Assim como outros receptores presentes na literatura [16–18], o esquema DPA-LSTM-NN considera o treinamento em um modelo de canal específico, embora as características do canal estejam sujeitas a variações e dependam do ambiente em que os

veículos estão operando. Para estender a análise do estimador DPA-LSTM-NN proposto, de forma a generalizar a solução proposta, empregamos a técnica *Ensemble Learning* (EL) para melhorar o desempenho combinando as previsões de vários modelos treinados com conjuntos de dados que consideram diferentes velocidades, deslocamentos máximos de Doppler e atrasos de caminho.

Para analisar o impacto do uso da técnica EL na generalização do estimador DPA-LSTM-NN, o estimador resultante da combinação de modelos treinados em cenários de diferentes velocidades e perfis de atraso de potência (*Power Delay Profile* - PDP) é comparado com modelos treinados especificamente para um determinado PDP/velocidade. Os resultados mostram que o modelo EL tem uma perda quase insignificante em comparação com o caso de melhor desempenho, em que o modelo foi treinado com o mesmo PDP/velocidade. Por outro lado, uma perda significativa de desempenho pode ser observada ao testar os modelos treinados com PDP e velocidade fixa. Dessa forma, o modelo EL apresenta uma alternativa interessante ao oferecer uma estimativa com perdas consideravelmente menores para diferentes canais. Além disso, é importante ressaltar que esses ganhos são obtidos sem acrescentar complexidade computacional à estimativa do canal, pois o processo de obtenção do modelo EL combinado é feito off-line.

## Capítulo 6 - Estimação de canal baseada em LSTM para sistemas OTFS

Como os cenários de comunicação veicular continuam a evoluir, a demanda por sistemas de comunicação sem fio robustos e eficientes torna-se cada vez mais crítica. Nesse contexto, embora amplamente adotados, os esquemas de transmissão multiportadora convencionais, como a modulação OFDM, revelam limitações inerentes que podem prejudicar sua eficácia em futuros ambientes veiculares [19]. Em resposta a isso, o OTFS [3, 20] surgiu como um esquema de modulação promissor, apresentando uma nova abordagem para a comunicação sem fio. Nesse contexto, esse capítulo apresenta o estudo sobre a proposta de um novo receptor para a forma de onda OTFS, a ser comparado com duas técnicas referência em um cenário estimativa de canal na transmissão OTFS sujeita a distorções induzidas por HPA sem memória. Por fim, apresentamos a avaliação desse receptor por meio de uma análise detalhada de seu desempenho.

### OTFS baseado em SFFT

Uma das implementações mais populares para sistemas OTFS encontradas na literatura é baseada na transformada rápida de Fourier simétrica (*Symplectic Finite Fourier Transform* - SFFT) e na SFFT inversa (ISFFT), combinada com uma modulação de várias portadoras. Essas tranformações são usadas para converter canais variantes no tempo em canais invariantes no domínio DD e vice-versa, o que permite interpretar o sistema OTFS como blocos de pré e pós-processamento aplicados a um esquema de sinalização multiportadora. Além disso, para uma caracterização mais realista dos cenários de comunicação sem fio, nossa análise considera que esse sinal no domínio do tempo é afetado por não linearidades induzidas por HPA, o que segue o modelo HPA sem memória.

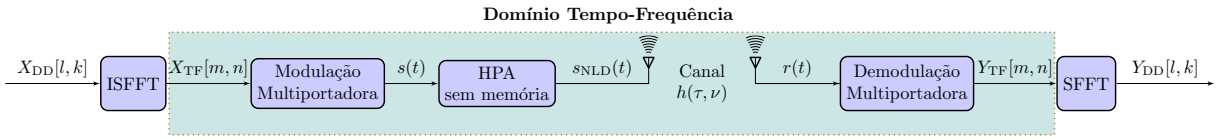


– **Arquitetura para o OTFS baseado em SFFT.**

### Métodos referência para estimativa de canal OTFS

A literatura relacionada à estimativa de canais OTFS geralmente envolve a estimativa das características do canal no domínio DD. Duas técnicas estabelecidas, que denotaremos como *Threshold Channel Estimation* (TCE) [21] e *Correlation Channel Estimation* (CCE) [22], serão usadas como referências de desempenho para o estimador de canal baseado em LSTM proposto.

O trabalho em [21] foi o primeiro a apresentar uma solução para a estimativa de canal em sistemas OTFS. Os autores introduziram um esquema de piloto incorporado, no qual um intervalo de guarda suficientemente grande é aplicado em torno de um piloto exclusivo para melhorar a aquisição de respostas de atraso e Doppler.

Em [22], é proposto um estimador para sistemas OTFS em que a matriz de canal de correlação é adquirida por meio de estimativa no domínio DD. Os autores assumem que o canal é invariável por mais de um símbolo de duração, de modo que o piloto e as informações são enviados em quadros diferentes.

As propostas apresentadas em [21,22] exigem um intervalo de guarda substancial para atenuar a interferência de símbolos de dados desconhecidos nos pilotos usados para estimativa de canal. Além disso, os esquemas propostos requerem uma potência de piloto elevada. Como uma conclusão importante, esses aspectos podem afetar negativamente

a PAPR do sinal transmitido, conforme destacado em [23], o que pode prejudicar sua aplicação prática.

**Método baseado em LSTM proposto para estimativa de canal OTFS**

É proposto um novo esquema de estimativa de canal para sistemas OTFS sujeitos a distorções induzidas por HPA. O método começa com uma estimativa inicial de canal derivada do preâmbulo e dos pilotos no domínio da frequência. Essa estimativa serve como entrada para uma camada LSTM, rastreando efetivamente o comportamento do canal. Posteriormente, uma NN é aplicada para aumentar a capacidade de redução de ruído e refinar a precisão da estimativa. Por meio dessas etapas, podemos manter uma baixa sobrecarga de piloto e obter uma estimativa de canal confiável, especialmente ao lidar com canais altamente seletivos. Deve-se observar aqui que, ao contrário das propostas em [21, 22], os pilotos têm a mesma potência que o sinal transmitido. Consequentemente, as informações piloto são usadas como base para a rede LSTM-NN interpolar as informações do canal para as portadoras de dados e obter a estimativa final.

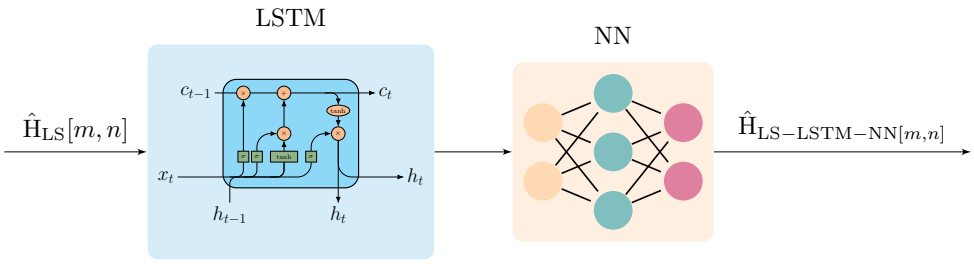


– **Diagrama de blocos para o estimador LS-LSTM-NN proposto.**

**Análise de desempenho**

A análise do desempenho do receptor LS-LSTM-NN em um cenário afetado por distorções resultantes de não linearidades HPA é feita em termos de BER, taxa de transferência e PAPR. Comparamos nossa proposta com os métodos de referência TCE [21] e CCE [22], nos quais a estimativa de canal é feita usando a resposta piloto no domínio DD. Os resultados mostram os desempenhos em um cenário com os veículos se movendo a uma velocidade de $v = 300$ km/h e para ambos os métodos de referência, supõe-se que a SNR dos pilotos seja $\mathrm{SNR_p} = 40$ dB, de acordo com seu projeto.

A avaliação da BER considerando, por exemplo, uma modulação 16-QAM, mostra que para cenários com alto nível de ruído os estimadores de canal considerados apresentam desempenhos comparáveis. Entretanto, um ganho notável é observado para o método proposto na região de baixo ruído do sinal. Além disso, ambos os estimadores apresentados em [21] e [22] mostram um patamar de erro ainda mais expressivo em cenários com alta

qualidade do sinal. Consequentemente, esses estimadores não conseguem reduzir a BER a um nível inferior a $10^{-2}$ durante a detecção.

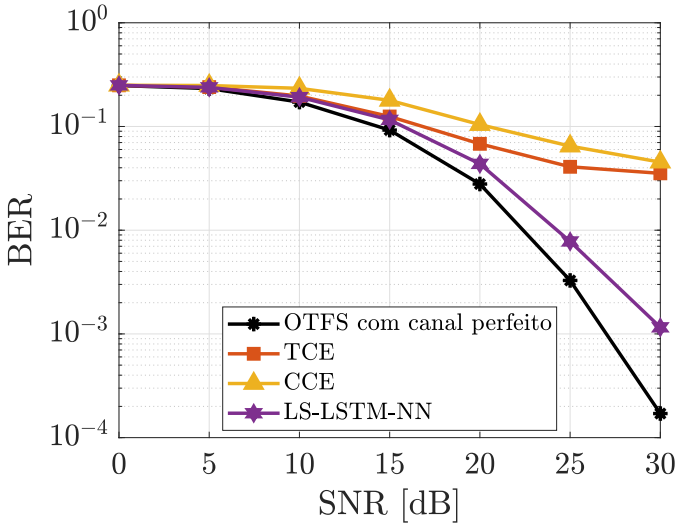


– **BER para $v = 300$ km/h, modulação 16-QAM e IBO = 4 dB.**

A análise da PAPR tem importância fundamental nos cenários de comunicação do mundo real. Ao comparar as técnicas de estimativa de canal em termos de seu impacto na CCDF, é possível destacar o problema de alocar pilotos com potência muito alta para facilitar a estimativa de canal no domínio DD. Especificamente, o estimador LS-LSTM-NN proposto produz um ganho de limiar de PAPR de pelo menos 10 dB quando comparado com o método proposto em [21]. Além disso, essa vantagem é ainda mais acentuada quando comparada ao estimador apresentado em [22]. Nesse sentido, observamos que o melhor desempenho do LS-LSTM-NN proposto é evidente, pois é o único capaz de atingir uma taxa de erro de $10^{-3}$ e, portanto, é o único a fornecer estimativas de canal confiáveis em tais cenários.

É importante destacar que a limitação de PAPR devido a pilotos de alta potência no domínio DD é um fator já investigado na literatura existente [23]. No entanto, manter uma PAPR mais baixa é de suma importância para atenuar a distorção induzida por HPAs. Essa importância decorre da indicação de que a eficiência do HPA diminui com o aumento da PAPR do sinal de entrada. De fato, vale observar que valores mais altos de PAPR podem prejudicar significativamente a qualidade da comunicação e, em geral, são impraticáveis em cenários do mundo real [24]. Em contrapartida, nosso esquema oferece um caminho prático para a comunicação OTFS. Por fim, destacamos que o cálculo da ordem da complexidade computacional dos diferentes métodos enfatiza a redução na complexidade obtida pelo estimador de canal LS-LSTM-NN proposto, independentemente

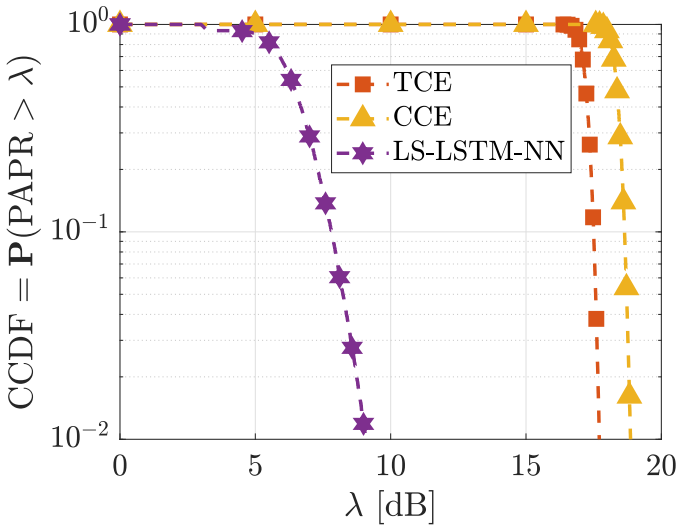


– **Análise da PAPR.**

do tamanho do quadro escolhido.

## Capítulo 7 - Conclusões

A presente tese abordou alguns dos desafios na estimativa de canais de veículos, especialmente considerando os efeitos de não linearidades devido a HPAs. Em primeiro lugar, a investigação apresentou perspectivas sobre as limitações dos métodos convencionais, que geralmente sofrem uma degradação significativa do desempenho na presença de distorções induzidas por HPAs. Além disso, os resultados preliminares da pesquisa destacaram que as técnicas de DL, especialmente as DNNs, apresentam robustez inerente contra esses efeitos não-lineares. Consequentemente, essa análise incentivou uma maior exploração e aplicação de métodos avançados baseados em DL para uma estimativa mais precisa do canal veicular.

Nesse contexto, a contribuição dessa pesquisa está na introdução de novas arquiteturas de receptor baseadas em aprendizado de máquina, explicitamente adaptadas à estimativa precisa de canais veiculares não lineares. Ao considerar o modelo HPA sem memória dentro do padrão IEEE 802.11p, o estimador DPA-LSTM-NN proposto demonstrou ser altamente resistente aos efeitos induzidos pelo HPA. Assim, a pesquisa mostra que a partir de uma nova técnica de compensação de baixa complexidade, a eficácia do receptor proposto é validada nos cenários apresentados pelos HPAs com memória. Por fim, em antecipação à próxima era da comunicação sem fio 6G, também foi proposta uma arquitetura para estimativa de canal OTFS, na qual foi apresentada a superioridade da proposta em relação aos estimadores convencionais em cenários veiculares de alta

mobilidade, que são esperados para as futuras comunicações veiculares, bem como a redução da complexidade computacional durante a detecção de sinais.

## LIST OF FIGURES

## LIST OF TABLES

## ACRONYMS

| | |
|---|---|
| AE | Auto-Encoder |
| AI | Artificial Intelligence |
| AM/AM | Amplitude-to-Amplitude |
| AM/PM | Amplitude-to-Phase |
| AWGN | Additive White Gaussian Noise |
| BER | Bit Error Rate |
| CCDF | Complementary Cumulative Distribution Function |
| CCE | Correlation Channel Estimation |
| CNNs | Convolutional Neural Networks |
| CP | Cyclic Prefix |
| CSI | Channel State Information |
| DD | Delay-Doppler |
| DL | Deep Learning |
| DNN | Deep Neural Network |
| DPD | Digital Pre-Distortion |
| DPA | Data-Pilot Aided |
| EL | Ensemble Learning |
| EX | Expressway |
| FBF | Frame-by-Frame |
| FFT | Fast Fourier Transform |
| FIR | Finite Impulse Response |
| HPA | High Power Amplifier |
| IBO | Input Back-off |
| ICI | Inter-Carrier Interference |
| IFFT | Inverse Fast Fourier Transform |
| ISFFT | Inverse SFFT |
| ISI | Inter-Symbol-Interference |
| LSTM | Long Short-Term Memory |
| LS | Least Square |
| MIMO | Multiple-Input Multiple-Output |
| ML | Machine Learning |
| MSE | Mean Squared Error |
| NLD | Nonlinear Distortion |
| NN | Neural Network |
| NMSE | Normalized Mean Squared Error |
| OFDM | Orthogonal Frequency Division Multiplexing |
| OTFS | Orthogonal Time Frequency Space |
| PAPR | Peak-to-Average Power Ratio |
| PDP | Power Delay Profile |
| QAM | Quadrature Amplitude Modulation |
| RF | Radio Frequency |

| | |
|---|---|
| R2V | Roadside-to-Vehicle |
| ReLU | Rectified Linear Unit |
| SBS | Symbol-by-Symbol |
| SDWW | Expressway Same Direction with Wall |
| SFFT | Symplectic Fast Fourier Transform |
| SNR | Signal-to-Noise Ratio |
| SISO | Single-Input Single-Output |
| SS | Suburban Street |
| STA | Spectral Temporal Averaging |
| TCE | Threshold Channel Estimation |
| TDL | Tapped Delay Line |
| TF | Time-Frequency |
| UC | Urban Canyon |
| V2V | Vehicle-to-Vehicle |

## SUMMARY

# 1 INTRODUCTION

## 1.1 Motivation

In response to the growing demand for higher data rates, reliability, and connectivity, the dynamic scenario of modern wireless communication systems poses significant challenges to the applications expected in the next generations of telecommunications [28]. In particular, vehicular communication is one of the areas of greatest interest for the development of solutions within future 6G applications, being crucial to enable connected vehicles and road infrastructure, which will improve road safety and promote greater traffic efficiency and comfort for drivers [1]. Transportation systems and smart cities are expected to have a profound impact on modern society by making everyday transport more efficient and comfortable, but also entail challenges related to the high level of connectivity required between network nodes, combined with the respective user requirements [29]. On this road, along with the increase in the number of devices and user demands, vehicular communications will introduce challenges regarding the complexity of the solutions and their applicability to these highly variable and dynamic scenarios.

In this context, estimating the wireless channel with sufficient quality in order to ensure reliable communication is critically important, as it significantly affects the overall system performance and unlocks its full potential. The existing literature presents several mathematical tools for channel estimation in vehicular channels [14, 30, 31]. However, these solutions often rely on simplifications that diverge from the complexities of modern wireless communication systems [12], such as assuming a linear channel behavior or using simplified mathematical models. In this regard, data availability is crucial to meet the requirements of future wireless networks and the approaches for estimating the channel in modern wireless network scenarios will require more robust and flexible solutions to exploit the data generated by the network and make real-time decisions [32].

Contrary to the assumption made by the above-mentioned works, which consider a linear communication environment assuming an ideal radio frequency (RF) interface, the reality of vehicular communications involves multicarrier modulation techniques, which introduces intricate challenges associated with high peak-to-average power ratio (PAPR) [33], leading to nonlinear distortions (NLD) in the output signal of the high power amplifier (HPA) at the transmitter. These NLDs can impair the channel estimation and

detection capability of the receivers, leading to a considerable degradation in the overall system performance. This highlights the importance of considering these often neglected effects in the development of vehicular communication solutions tailored for practical scenarios. At the transmitter side, a digital pre-distortion (DPD) block is commonly adopted in order to linearize the output signal [34], where the nonlinear HPA is linearized from its inverse function before transmission. However, such a linearization task is not trivial to be optimally performed, while occurring at a complexity cost. As an alternative, the HPA nonlinearity can also be compensated at the receiver side, where it may be possible to reduce the power consumption [35].

To overcome these demands in a more realistic scenario, the integration of artificial intelligence (AI) tools has emerged as a new paradigm for the evolution of future wireless communication networks. Machine learning (ML) and deep learning (DL) algorithms, well recognized for their ability to analyze huge amounts of data and learn from them, stand out as solutions capable of improving network performance and reducing inefficient energy consumption through the acquisition and processing of available data [36]. Furthermore, recent advancements in data processing, security measures, and accuracy enhancements have further elevated the applicability and effectiveness of AI-based solutions in wireless communications [2].

In this context, this work is driven by the potential of ML and DL tools to design novel receiver architectures capable of adapting to dynamic channel conditions, particularly in the context of vehicular communication networks characterized by time-varying channels and nonlinearities due to the presence of HPAs. The ML techniques are leveraged to enhance flexibility by concurrently performing two critical tasks: channel estimation and nonlinear distortion reduction, considering the effects of nonlinearities as an additional source of noise and mitigating them on the receiver side. To this end, it is proposed to explore the combination of strategies that use mathematical models and ML techniques to design receivers, using the characteristics of the vehicle channel in order to favor estimation. We started the analysis with a waveform conventionally used in wireless communication standards, presenting that this combination implies a significant improvement in performance, as well as a reduction in complexity, for different scenarios and aspects considered in the analysis. Subsequently, we extend this analysis to apply the proposed method to a waveform candidate for future vehicular networks, showcasing its potential as a promising technique for future real-world applications.

## 1.2 Objectives

Future communication scenarios are expected to progress in terms of connectivity, user requirements, and consequently, challenges. From this perspective, recently, there has been a growing interest in ML and DL solutions as tools to meet these demands. In this context, the primary objective of this work is to explore the application of these techniques in designing novel receiver architectures for multicarrier vehicular communications, taking into account its time-varying nature and the nonlinear effects induced by HPAs. Thus, this research presents the following goals:

- Investigate the specific requirements and challenges posed by future wireless communication scenarios, particularly in vehicular communication. This involves a comprehensive analysis of the distortions caused by HPAs and a thorough review of existing solutions in the literature, with a focus on exploring ML and DL techniques.
- Propose robust algorithms based on ML and DL that can dynamically track vehicular channels, considering the dynamic nature of vehicular communication.
- Explore methods to reduce the complexity of the proposed receivers. This reduction will be achieved by combining ML and DL approaches with mathematical methods and utilizing techniques that explore wireless channel information through statistical analysis.

## 1.3 Thesis outline

The organization of this work and the chapter's content are presented as follows.

**Chapter 2** gives a summary of some fundamentals about the time-varying wireless channel, introducing some basic concepts on vehicular communication, and presenting the background related to multicarrier systems. Additionally, it outlines the DL techniques that will be further considered in our investigation.

**Chapter 3** presents the characteristics of the communication system model, focusing on essential aspects of vehicular communication, particularly when considering orthogonal frequency division multiplexing (OFDM) transmission scheme, that will be the focus of the first part of the thesis content. The details on the HPA nonlinear distortions models are presented and the vehicular channel modeling is also covered.

**Chapter 4** introduces the state-of-the-art channel estimators proposed in the literature, which serve as benchmarks for the novel proposals presented in this manuscript. In this chapter, we present the preliminary analysis of the impact of HPA nonlinearities on the performance of conventional and deep neural network (DNN)-based estimators. We emphasize the advantages of hybrid schemes in estimating the vehicular channel, motivating the study on advanced DL techniques to effectively track the vehicular channel.

**Chapter 5** presents detailed information about the novel long short-term memory (LSTM)-based channel estimation method designed for vehicular communication scenarios. Extensive comparative analyses are conducted against benchmark methods, considering different effects of nonlinearities. The simulation results, which encompass different vehicular channel models, reveal the performance superiority of the proposed estimator compared to the conventional methods, also recording a significant decrease in computational complexity. This chapter further delves into two extensions of the investigation. Firstly, it explores the impact of nonlinear HPA memory effects on channel estimation, acknowledging their importance in realistic communication scenarios. Secondly, a proposal for generalized learning architecture for vehicular channel estimation is proposed using the ensemble learning (EL) technique applied to the LSTM-based method.

**Chapter 6** presents the broadening of the work to the orthogonal time frequency space (OTFS) waveform, recently proposed as a potential waveform for mobility channel deployment. Here, the analysis is based on the advantages presented for OTFS over the OFDM transmission. The results of the proposed channel estimation solutions for OTFS, including an analysis of computational complexity and performance, are presented and compared to the existing state-of-the-art solutions.

**Chapter 7** concludes the thesis, presenting the final considerations and perspectives for future work.

## 1.4 Publications

This work investigates the challenges inherent to vehicular communications and opportunities in proposing new estimation algorithms designed for these scenarios. The main contributions of this thesis are summarized as follows.

- We provided a preliminary analysis of the impact of HPA nonlinearities on the performance of conventional and DNN-based channel estimation schemes employed

in vehicular scenarios. The results show that the DNN-based estimation schemes outperform conventional estimators, evidencing their superiority in providing reliable estimation in mobility scenarios in the presence of HPA nonlinear distortions. This study was published in

**A. F. dos Reis,** Y. Medjahdi, G. Brante, B. Sens Chang, F. Bader. "*Deep learning based receivers for IEEE 802.11p standard with high power amplifiers distortions*". In: Proceedings of the IEEE 95th Vehicular Technology Conference, 2022, Helsinki, Finland (VTC2022-Spring).

- We proposed a novel low-complexity receiver based on LSTM network. This receiver presents robust performance in the presence of HPA-induced nonlinearities and is adapted to estimate the doubly selective channel deployed by the IEEE 802.11p standard for vehicular communications. In addition, we propose a new technique to exploit the characteristics of the vehicular channel, by sampling the subcarriers used at the input of the LSTM. The results show the superiority of the proposal in comparison with other state-of-the-art schemes. Furthermore, this scheme significantly reduces the computational complexity due to the subcarrier sampling procedure. This proposal was published in

  **A. F. dos Reis,** Y. Medjahdi, B. Sens Chang, J. Sublime, G. Brante, F. Bader. "*Low Complex LSTM-NN-Based Receiver for Vehicular Communications in the Presence of High-Power Amplifier Distortions*", in IEEE Access, vol. 10, pp. 121985-122000, 2022, doi: 10.1109/ACCESS.2022.3223113.

- We proposed a generalized learning architecture to combine the predictions of multiple models of vehicular channels using the EL technique applied to the method based on LSTM. We show that using a model trained for a specific dataset in a new scenario can lead to poor performance and reduced reliability in vehicular communication. However, our proposed method overcomes these limitations and provides robustness to variations in channel conditions. This proposal was published in

  **A. F. dos Reis,** G. Brante, B. Sens Chang, Y. Medjahdi, F. Bader, J. Sublime. "*Ensemble Learning for LSTM-based Vehicle Channel Estimation Generalization*". In: XLI BRAZILIAN SYMPOSIUM ON TELECOMMUNICATIONS AND SIGNAL PROCESSING - SBrT 2023, OCTOBER 08–11, 2023, SÃO JOSÉ DOS CAMPOS, SP.

- We extended the analysis of the impact of HPAs' nonlinearities on vehicular channel

estimation performance by investigating the use of LSTM-based receivers in models that consider the memory effects inherent in nonlinear HPAs. In addition, we present a low-complexity method to compensate part of the memory NLD effects on the transmitter side, while handling the remaining distortions along with the channel estimation. The results present that considering more realistic NLD models significantly affects receiver performance, being an important aspect in developing estimators for future vehicular communication applications. Furthermore, the importance of compensating the signal at the transmitter side when the memory effects of the HPA are considered is highlighted. This study was published in

**A. F. dos Reis,** Y. Medjahdi, B. Sens Chang, G. Brante, F. Bader. "*Memory Effects of High-Power Amplifiers in LSTM-based Vehicular Channel Estimation*", in IEEE Access, vol. 11, pp. 79994-80002, 2023, doi: 10.1109/ACCESS.2023.3299871.

- Presenting a broadening analysis of future waveforms designed for vehicular communication, we address channel estimation in nonlinear OTFS systems. Our contribution involves proposing a novel channel estimation method within the time-frequency domain, aiming to reduce the PAPR impact and improve the detection capacity of OTFS signals. This estimator is effectively applied to a model that includes nonlinear effects induced by HPAs in an OTFS transmission system. The results show that it is possible to obtain a robust channel estimate without the need for signal linearization at the transmitter and to effectively compensate for nonlinearities together with the channel estimate. To validate the effectiveness of our proposed estimator, we carried out a comparative analysis with classical OTFS estimation methods, with the proposed method presenting greater accuracy in tracking the channel and a substantial reduction in the computational complexity required to detect the received signals. This study is currently undergoing peer review.

  **A. F. dos Reis,** B. Sens Chang, Y. Medjahdi, G. Brante, F. Bader. "*LSTM-Based Time-Frequency Domain Channel Estimation for OTFS Modulation*". Submitted to the IEEE Transactions on Vehicular Technology.

# 2 FUNDAMENTALS AND BACKGROUND

This chapter explores the fundamental concepts of wireless communication. First, the concepts of propagation and fading are presented. Following that, the chapter delves into the concept of multicarrier transmission, highlighting its advantages in wireless communication and exposing the challenges related to the PAPR problem during power amplification. Lastly, we introduce the fundamental concepts of the DL techniques that will be used in this thesis.

## 2.1 Multipath propagation and fading

In typical wireless communication systems, the setup consists of one or more transmitters and receivers, each equipped with at least one antenna for the purpose of transmitting and receiving information. As signals are transmitted through the wireless channel, they may experience attenuation, which is the reduction in signal strength as it propagates through space.

At the receiver, the received signal is a composition of various components arriving from different paths, each with different delays and signal strengths. These components can either combine constructively or destructively. This phenomenon is referred to as fading and is influenced by factors such as propagation and Doppler shift. The propagation occurs due to signal receptions arriving at different times from various paths, leading to frequency-selective fading. On the other hand, Doppler shift is caused by motion between the transmitter and receiver, resulting in time domain selectivity.

Due to both effects, the wireless communication channel exhibits double selectivity, varying both in time and frequency [25]. This doubly selective characteristic is illustrated in Figure 1, where the influences of both time-varying and frequency-selective channels are integrated during signal transmission. A doubly selective channel is frequently encountered in highly dynamic communication environments, such as vehicular communication. In scenarios like vehicular communication, the temporal variations arise from vehicle movement, while frequency variations result from reflections off buildings, other vehicles, or changing terrain. Moreover, doubly selective channels can be effectively represented in the so-called delay-Doppler (DD) domain [37], where the impulse response of the time-varying channel presents as a quasi-static and sparse channel derivation, with a location determined by the path delay and the Doppler effect. As described in [38],

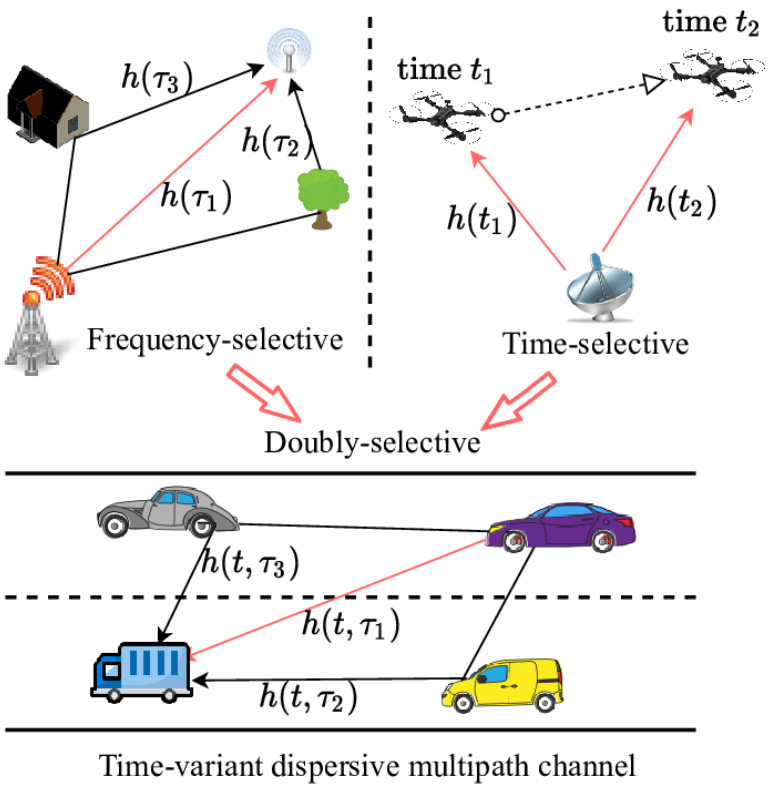


**Figure 1 – Doubly selective channels [19].**

assuming $\kappa$ paths with delays $\tau_k$, Doppler frequencies $\nu_k$ and complex gains $S_k$, the received signal is given by a weighted superposition of Time-Frequency (TF) shifts of the transmitted signal $x(t)$ as

$$y(t) = \sum_{k=1}^{\kappa} S_k x(t-\tau_k) e^{j2\pi\nu_k t}. \tag{1}$$

## 2.2 Multicarrier systems

Multicarrier modulation is widely used to deploy wireless communication systems aiming to avoid the problems given the multipath effect. These modulation schemes split the transmission into a structured format in which the data stream is parallelized into low-rate streams transmitted on adjacent subcarriers, enabling modulation without causing interference between subcarriers. The number of streams is designed to match the bandwidth of each subchannel but remains smaller than the coherence bandwidth of the channel. Also, the maximum delay spread of the channel is lower than the symbol duration and, consequently, each subchannel experiences a flat fading and the inter-symbol-interference (ISI) in each subchannel becomes very small [25].

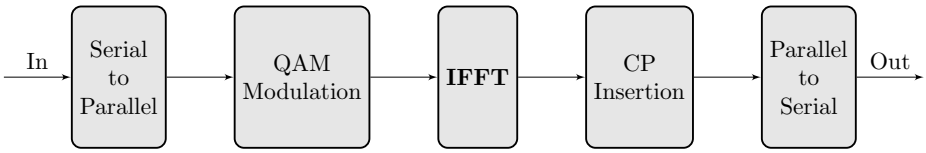


**Figure 2 – OFDM transmitter block diagram [25].**

The OFDM is one of the most prominent multicarrier modulation schemes, widely utilized in several standards for wireless communications systems. This modulation technique efficiently spaces orthogonal subcarriers, a key characteristic that significantly mitigates the impact of frequency-selective fading in the channel by reducing the interference between adjacent subcarriers. As depicted in Figure 2, the OFDM modulation process is comprised of a serial-to-parallel conversion, the quadrature amplitude modulation (QAM), the inverse fast Fourier transform (IFFT), the cyclic prefix (CP) insertion, and a parallel-to-serial conversion before transmission. Thus, it is characterized by a distinct implementation at both the transmission and reception levels, where for the transmission, the IFFT operation is performed on the subcarriers to transform the data from the frequency domain to the time domain. The IFFT operation to obtain the transmitted OFDM signal is expressed by

$$x(t) = \mathrm{IFFT}\left(X[k]\right) = \frac{1}{\sqrt{K}} \sum_{k=0}^{K-1} X[k] \cdot e^{\frac{j2\pi}{K} kt}, \quad k = 0, 1, \ldots, K-1, \tag{2}$$

where $K$ is the total number of subcarriers, $X[k]$ represents the modulated symbol on the $k$-th subcarrier and $t$ denotes the time index. The CP is strategically inserted to achieve circular convolution with a linear and time-invariant channel, thereby enhancing the robustness of the transmitted signal against ISI. The process involves appending each symbol with a replica of the last symbols within the duration $T - T_{\mathrm{CP}}$. Thus, the cyclically-extended symbol appears periodic when convoluted with the channel. Mathematically, this can be expressed as:

$$x_{\mathrm{CP}}(t) = x(t) \text{ for } T - T_{\mathrm{CP}} \leq t < T. \tag{3}$$

Here, $T_{\mathrm{CP}}$ is the duration of the CP, and $T$ is the total duration of the OFDM symbol. Consequently, the transmitted OFDM signal with the cyclic prefix is given by

$$x_{\mathrm{TX}}(t) = \begin{cases} x_{\mathrm{CP}}(t), & 0 \leq t < T_{\mathrm{CP}} \\ x(t), & T_{\mathrm{CP}} \leq t < T + T_{\mathrm{CP}} \end{cases}. \tag{4}$$

The received signal can be expressed as

$$y(t) = h(t) * x_{\mathrm{TX}}(t) + n(t), \tag{5}$$

where $h(t)$ is the time-varying channel impulse response, $*$ denotes convolution, and $n(t)$ is the additive white Gaussian noise (AWGN). The received OFDM signal can be efficiently demodulated using the fast Fourier transform (FFT). The received signal in the frequency domain is given by

$$\mathbf{y}_i[k] = \mathbf{h}_i[k]\mathbf{x}_i[k] + \mathbf{n}_i[k], \tag{6}$$

where for all $k$ subcarriers within the $i$-th OFDM symbol, $\mathbf{h}_i[k]$ is the frequency response of the channel, $\mathbf{x}_i[k]$ is the frequency-domain representation of the transmitted signal, and $\mathbf{n}_i[k]$ is the frequency-domain representation of the AWGN. The diagonalization of the channel ensures flat fading in each subchannel and, under this condition, one-tap equalizers are sufficient to compensate for the effects of the channel. Finally, the equalized signal is given by

$$\hat{\mathbf{x}}_i[k] = \frac{\mathbf{h}_i[k]}{\mathbf{y}_i[k]}. \tag{7}$$

Although widely adopted in wireless communication systems due to its ability to mitigate the effects of frequency-selective fading and provide efficient spectrum utilization, OFDM modulation is sensitive to inter-carrier interference (ICI) and can struggle in scenarios with time-varying channels, since the assumption of a quasi-static channel may not hold, especially in highly dynamic environments such as vehicular communication [39]. To address these drawbacks, recent proposals in the field of wireless communications aim to develop innovative modulation schemes and receiver architectures.

Several other multicarrier waveforms have been proposed to address specific challenges and requirements in wireless communication systems. One notable waveform is OTFS modulation, first introduced in [3]. This waveform extends the principles of OFDM to the DD domain, providing enhanced performance in highly dispersive environments. The OTFS stands out as a promising waveform for future vehicular communication systems, offering improved resilience against time-varying channels and highly dispersive environments.

Besides OFDM and OTFS, which are the primary focus of this thesis, various multicarrier modulation schemes have gained attention in recent wireless communication literature [40, 41], positioning them as candidates for 6G communication. Each of these schemes offers unique advantages and is tailored to specific communication scenarios. Research and development in multicarrier modulation continue to evolve,

focusing on designing waveforms that can efficiently utilize the spectrum, accommodate diverse communication requirements, and improve the overall performance of wireless communication systems. These advancements are vital for addressing the challenges and meeting the demands of future wireless networks.

## 2.3 Radio frequency (RF) high-power amplifier (HPA)

While multicarrier modulation systems offer benefits such as high spectral efficiency and reduced ISI, they usually come with drawbacks associated with the high PAPR of the transmitted signal [4]. The elevated PAPR arises due to the utilization of a large number of subcarriers for signal transmission. Consequently, multicarrier transmission can significantly impair the efficiency of power amplifiers that operate within nonlinear regions, potentially leading to information degradation.

Figure 3 presents the characteristic curve of a typical HPA, illustrating the relationship between the input power and the resulting output power of the amplifier. At lower input power levels, the HPA operates in the linear zone, where output power $P_{out}$ proportional to input power $P_{in}$ with a constant amplifier gain. In general, this zone is free of nonlinear distortions and provides amplification in a linear and predictable manner. However, as the input power increases, the output power gradually saturates, reaching the compression zone. Within this zone, even though the input power continues to rise, the rate of increase in output power diminishes. This is the region where the amplification is nonlinear, and the amplifier begins to saturate. Notably, this zone is characterized by a particular point, known as the 1 dB compression point, where the actual gain of the HPA deviates from the ideal linear gain by 1 dB. With further increases in $P_{in}$, the saturation zone is reached. At this zone, the amplifier reaches minimal or no increase in output power. As a result, the amplifier is unable to further amplify the input signal, resulting in a flat portion of the characteristic curve, with very high NLD.

These nonlinear signal characteristics can lead to unnecessarily high power consumption at the HPA, often resulting in a high PAPR. The PAPR is a crucial parameter that represents the ratio between the peak power of the signal and its average power. In wireless communication systems, a high PAPR can adversely affect power efficiency by demanding excessive power to handle the peaks in the signal. This can have a significant impact on the overall system performance, making it a critical consideration in system design and operation. The maximum PAPR for the transmitted signal $x(t)$ is

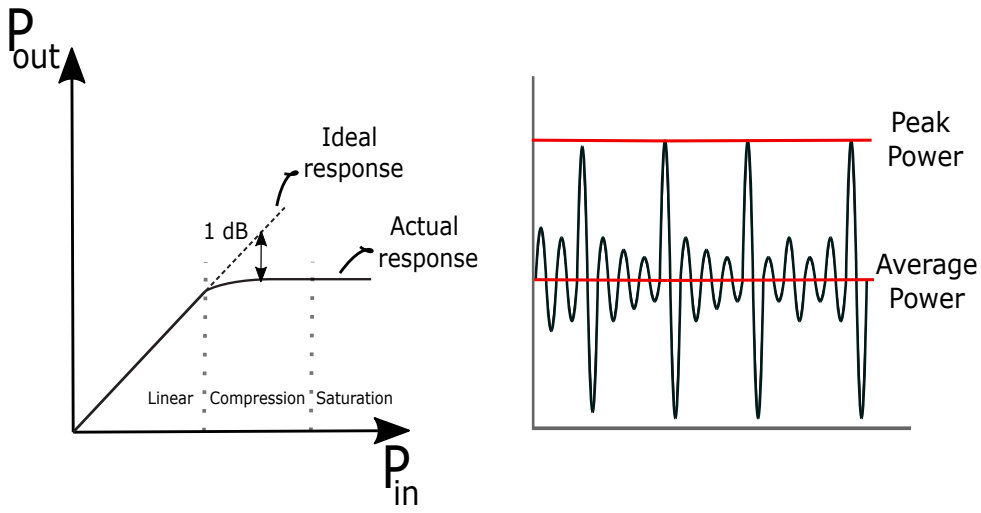


**Figure 3 – Characteristic curve of the HPA [26].**

given by [4, 42]

$$\text{PAPR} = \max_{\forall t} \frac{|x(t)|^2}{P_{\text{avg}}}, \tag{8}$$

where $P_{\text{avg}}$ is average power of the signal over its entire duration $T$, given as

$$P_{\text{avg}} = \frac{1}{T}\int_0^T |x(t)|^2 \, dt. \tag{9}$$

The complementary cumulative distribution function (CCDF) is used to characterize a signal's PAPR performance by analyzing the statistical behavior of its fluctuations. Specifically, the CCDF quantifies the probability that the PAPR of the signal exceeds a given threshold, offering a comprehensive understanding of its power characteristics. The CCDF is mathematically expressed as

$$\text{CCDF} = \mathbb{P}(\text{PAPR} > \gamma) = 1 - \mathbb{P}(\text{PAPR} \leq \gamma), \tag{10}$$

where $\gamma$ is a constant and defines the threshold for the CCDF.

It is also important to emphasize that the efficiency of the HPA is inversely related to the PAPR of the input signal, being given as [43]

$$\eta_{\text{HPA}} = \left(\frac{1}{\text{PAPR}}\right)^{\epsilon} \eta_{\text{HPA}_{\max}}, \tag{11}$$

where $\eta_{\text{HPA}_{\max}}$ is the maximal HPA efficiency and $\epsilon \in [0, 1]$ is the efficiency exponent, which depends on the class of the HPA.

Several techniques have been developed to mitigate the PAPR problem in OFDM

systems [44], such as amplitude peak clipping and filtering [45], coding schemes [46] and selective mapping [47]. However, these techniques can be often related to the impact on the overall system performance, introducing transmit signal power increase, data rate loss and higher computational complexity.

## 2.4 Deep learning (DL) techniques

In recent years, the advent of DL techniques has emerged in various domains, revolutionizing the way complex problems are approached and solved. In the field of wireless communications, DL techniques have gained substantial attraction due to their ability to learn complex patterns and representations directly from data. Many solutions can be found in the context of channel estimation and signal detection [48, 49], resource allocation and optimization [50], modulation and demodulation [51], and more. This section covers the fundamentals related to DL-based methods that will be applied to the receivers under consideration in our research.

### 2.4.1 Deep neural networks (DNN)

DNNs are fundamental among the DL techniques [5, 52]. This type of artificial neural network (NN) is characterized by multiple interconnected layers, hence the term *deep* indicating the depth of layers. Each layer consists of a set of nodes, often referred to as neurons or units, which perform specific computations and transformations on the input data.

As presented in Figure 5, a typical DNN consists of three main types of layers: the Input Layer, Hidden Layers, and the Output Layer. In this architecture, each neuron applies an activation function to process its input, performing mathematical operations to the model, and enabling it to learn complex patterns within the data. This iterative process continues through the layers until the final output is produced, making DNNs powerful tools for complex pattern recognition and representation. The mathematical expression for a neuron operation in a DNN is given as

$$a_j^{(l)} = \sigma\left(\sum_{i=1}^{n^{(l-1)}} w_{ji}^{(l)} a_i^{(l-1)} + b_j^{(l)}\right), \tag{12}$$

where $\sigma$ presents the activation function, $w_{ji}^{(l)}$ is the weight of the connection between

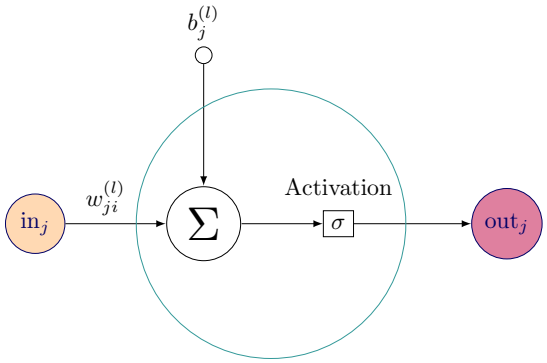


**Figure 4 – Neuron structure.**

neuron $i$ in layer $l-1$ and neuron $j$ in layer $l$, $a_i^{(l-1)}$ is the activation of neuron $i$ in layer $l-1$ and $b_j^{(l)}$ is the bias associated with neuron $j$ in layer $l$.

After defining the DNN architecture, the next step is to estimate the weights ($w_{ji}^{(l)}$) and biases ($b_j^{(l)}$) through the learning procedure during the training phase. Initially, these weights and biases are initialized, often with random values, to start the training process. During the training, the input data are passed through the network, and computations involving the initialized weights and biases are performed. As presented in the basic neuron structure in Figure 4, the activation function is applied in each layer to obtain the network's output. To assess the performance of the DNN, the generated output is compared to the actual target values using a suitable loss function, which quantifies the error or difference between predicted and actual values. The error information is then back-propagated through the network using an optimization algorithm, typically based on gradient descent. This backward propagation calculates the loss with respect to the weights and biases, allowing for adjustments that minimize the loss. Through several iterations, also called epochs, the weights and biases are updated in a way that minimizes the error, guided by the learning algorithm and its learning rate. In this iterative process, the objective is to achieve the convergence of the training. Finally, once the model is trained and validated, it can be used to make predictions on new data during the testing phase.

### 2.4.2 Long short-term memory (LSTM)

The LSTM is a type of recurrent unit that is well-suited for processing and making predictions based on sequences of data [6]. Unlike in traditional DNN, LSTM-

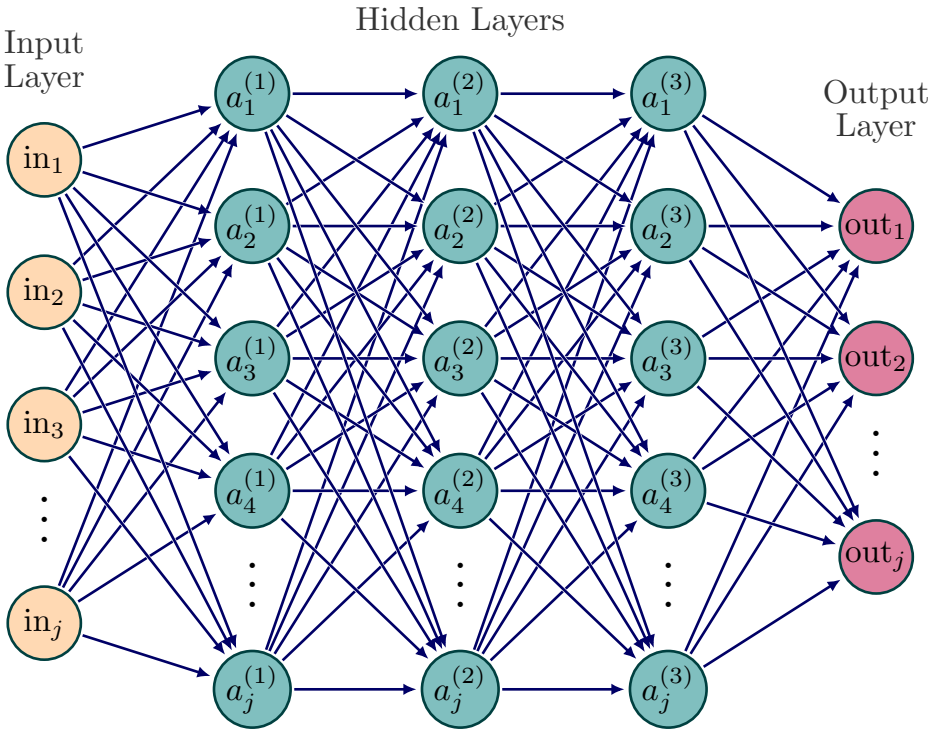


**Figure 5 – DNN architecture.**

based networks have the ability to capture long-term dependencies. This is done by internal gate units capable of storing the memory content of the data while employing structures capable of deciding when to keep, or override, information of these memory cells. Therefore, such advanced processing characteristics of the LSTM make it able to learn the channel correlation over time and adapt the channel estimates accordingly [17, 18].

Figure 6 presents the structure of the classical LSTM unit. Following [6], the operations with the inputs are illustrated by the activation function $\sigma$ and the hyperbolic tangent. These operations regulate the information flow and define which information is overridden and which is kept memorized in the current cell state. As outputs, the LSTM unit produces $c_t$, the memory cell state at the time step $t$, and the output $h_t$. The loop continues until the end of the sequential information so that $h_t$ of the last unit is the output of the LSTM network. Similar to DNNs, LSTM training involves adjusting its internal parameters through techniques like backpropagation and gradient descent to minimize the loss function. Once trained, an LSTM can be used for sequence prediction, generation, and other tasks that require an understanding of temporal patterns. Internally, the gates of the LSTM cell are calculated as:

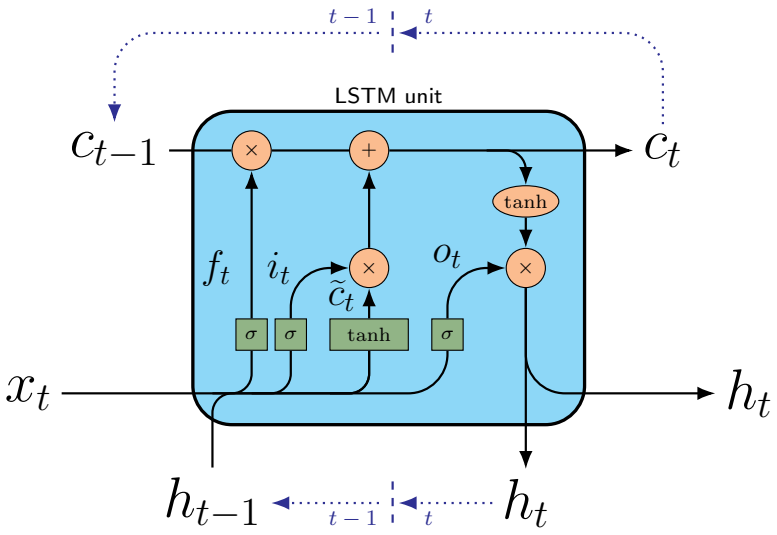


**Figure 6 – Structure of the LSTM unit.**

- Forget Gate: $f_t = \sigma(x_t U_f + h_{t-1} W_f + b_f)$
- Input Gate: $i_t = \sigma(x_t U_i + h_{t-1} W_i + b_i)$
- Output Gate: $o_t = \sigma(x_t U_o + h_{t-1} W_o + b_o)$

Recalling that $\sigma$ represents the activation function. The weight matrices $U_q$, $W_q$ correspond to the input and recurrent connections, where the subscript $q$ can either be the input gate $(i)$, output gate $(o)$ or the forget gate $(f)$. The notation $h_{t-1}$ represents the previous hidden state and $x_t$ the current input, while $b_f$, $b_i$ and $b_o$ are bias terms. Thus, the behavior of an LSTM cell is guided by the following steps.

- Internal memory update

$$c_t = \sigma(f_t \odot c_{t-1} + i_t \odot \tilde{c}_t), \tag{13}$$

  where $\odot$ is the Hadamard product and $\tilde{c}_t$ is the candidate memory state at time step $t$, which is calculated based on the current input and previous hidden state as

$$\tilde{c}_t = \tanh(x_t U_c + h_{t-1} W_c + b_c), \tag{14}$$

  where $U_c$ and $W_c$ are the weight matrices to the input and recurrent connections and $b_c$ is the current bias for candidate memory information.

- Hidden state output update

$$h_t = o_t \odot \tanh(c_t), \tag{15}$$

which is used for predictions or passed to the next time step.

Such processing characteristics of the LSTM allow it to learn the channel correlation over time and adapt the channel estimates accordingly.

Building on these foundations, where we start by providing fundamental insights into wireless communication, identifying the advantages of multicarrier transmission as well as recognizing the challenges presented by these techniques, and beginning our exploration of DL techniques, the subsequent chapter delves into a detailed system model. These fundamental concepts interact in the context of our research, preparing the ground for a comprehensive understanding of the channel estimation methods proposed.

# 3 SYSTEM MODEL

In this chapter, a thorough description of the communication system model is presented. For the first part of this thesis, comprising chapters 3-5, the focus will be on the OFDM modulation, as the transmission scheme is founded on the IEEE 802.11p standard [27]. In addition, the models for the HPAs that are under consideration in our analysis are described. Finally, the characteristics of the vehicular communication models are provided.

## 3.1 IEEE 802.11p standard

The IEEE 802.11p standard [27] is a subset of the Wi-Fi protocol that uses 10 MHz frequency bandwidth and supports data transmission for roadside-to-vehicle (R2V) and vehicle-to-vehicle (V2V) communication. As illustrated by Figure 7, this standard specifies that every packet transmission consists of a preamble, a signal field, which carries the physical layer information, and a data field. The preamble has short and long training symbols, known at the receiver in order to conduct the channel synchronization, and the long training symbols are split into two predefined sequences $\mathbf{t}_{p,1}$ and $\mathbf{t}_{p,2}$, used for channel estimation. Moreover, a CP is used to absorb the ISI caused by the multipath propagation.

Each OFDM symbol utilizes a total of $K = 64$ subcarriers in the data field, with $K_{\text{on}} = 52$ subcarriers being active and the remaining 12 serving as a guard band. Out of the $K_{\text{on}}$ subcarriers, $K_{\text{p}} = 4$ are allocated as pilots, and the remaining 48 carry the actual data. For each active subcarrier $k \in \mathcal{K}_{\text{on}}$, with $\mathcal{K}_{\text{on}}$ being the set containing the $K_{\text{on}}$ active subcarriers, the received OFDM symbols are expressed as

$$\mathbf{y}_i[k] = \mathbf{h}_i[k]\mathbf{u}_i[k] + \mathbf{n}_i[k], \tag{16}$$

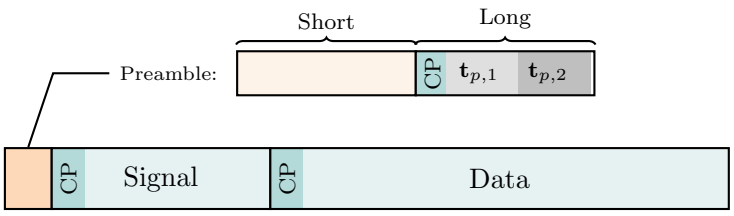


**Figure 7 – IEEE 802.11p packet structure [27].**

**Table 1 – IEEE 802.11p Standard.**

| Parameter | Values |
|---|---|
| Bandwidth | 10 MHz |
| Carrier Frequency ($f_c$) | 5.9 GHz |
| CP Duration | 1.6 $\mu$s |
| Symbol Duration | 8 $\mu$s |
| Short Training Symbols duration | 1.6 $\mu$s |
| Long Training Symbols duration | 6.4 $\mu$s |
| Total number of subcarriers ($K$) | 64 |
| Subcarrier spacing | 156.25 kHz |
| Modulation | QPSK, 16-QAM, 64-QAM |
| Coding rate | 1/2, 2/3, 3/4 |
| Data Rate | Up to 27 Mbps |

where for all $k$ subcarriers within the $i$-th OFDM symbol, $\mathbf{h}_i[k]$ denotes the time-variant frequency response of the subcarriers, $\mathbf{u}_i[k]$ is the $k$-th subcarrier in the $i$-th transmitted OFDM data symbol that is impacted by the HPA-induced distortions and $\mathbf{n}_i[k]$ represents the AWGN, with power

$$\eta_0 = \frac{\varepsilon_p}{\xi \cdot K}, \tag{17}$$

where $\varepsilon_p$ is the preamble power per sample, $\xi$ the average signal-to-noise ratio (SNR) at the receiver and $K$ is the total number of subcarriers employed within each OFDM symbol.

The channel coefficients $\mathbf{h}_i[k]$ are modeled over a Rayleigh fading channel with Jakes' Doppler spectrum, with the Doppler frequency given by

$$f_{\mathrm{D}} = \frac{v}{c} f_{\mathrm{c}}, \tag{18}$$

where $v$ is the speed of the vehicle, $c$ is the speed of light and $f_{\mathrm{c}}$ is the carrier frequency. Table 1 summarizes the IEEE 802.11p standard physical layer specifications.

## 3.2 Memoryless HPA

Our analysis considers two different HPA models along with the mobility scenario. We start by examining the memoryless HPA model, denoting the input signal as $\mathbf{x}(t)$, which is assumed to be a zero mean complex Gaussian random process so that, following [53], we have the output given by

$$\tilde{\mathbf{u}}_{\mathrm{mless}}(t) = \gamma_0 \mathbf{x}(t) + \tilde{\delta}(t), \tag{19}$$

where $\tilde{\delta}(t)$ is a NLD with zero mean and variance $\sigma_{\tilde{\delta}}{}^2$, that is uncorrelated with $\mathbf{x}(t)$, while $\gamma_0$ describes a complex gain. Then, according to the Bussgang theorem [7] $\gamma_0$ is compensated at the transmitter and we can write the output of the HPA as

$$\mathbf{u}_{\text{mless}}(t) = \mathbf{x}(t) + \delta(t), \tag{20}$$

where $\delta(t) = \tilde{\delta}(t)/\gamma_0$ is the remaining NLD of the HPA.

The memoryless polynomial model considered here follows [53], which exhibits both amplitude-to-amplitude (AM/AM) and amplitude-to-phase (AM/PM) distortions by approximating its characterizations with a polynomial. Thus, for a given input signal $\mathbf{x}(t)$, the amplified output signal $\tilde{\mathbf{u}}_{\text{mless}}(t)$ can be expressed as

$$\begin{aligned} \tilde{\mathbf{u}}_{\text{mless}}(t) &= \phi_a\Big(\rho(t)\Big) \exp\left(j\Big(\phi_p\Big(\rho(t)\Big) + \varphi(t)\Big)\right) \\ &= \varsigma\Big(\rho(t)\Big) \exp\Big(j\varphi(t)\Big), \end{aligned} \tag{21}$$

in which $\rho(t)$ is the input signal modulus, $\varphi(t)$ is the input signal phase, $\phi_a\Big(\rho(t)\Big)$ and $\phi_p\Big(\rho(t)\Big)$ represent the AM/AM and AM/PM characteristics of the HPA respectively, while

$$\varsigma\Big(\rho(t)\Big) = \phi_a\Big(\rho(t)\Big) \exp\left(j\phi_p\Big(\rho(t)\Big)\right) \tag{22}$$

presents the complex soft envelope of the amplified output signal.

Moreover, the soft envelope of the amplified signal employed in our simulations is approximated by

$$\varsigma\Big(\rho(t)\Big) \approx \sum_{l=1}^{P} a_l \rho(t)^l, \tag{23}$$

where, according to the description of the polynomial model [53], $a_l$ denotes the coefficients of the polynomial with order $P = 9$, obtained by the least square (LS) method.

To mitigate the impact of nonlinearities, the HPA is configured to operate at a specific input back-off (IBO), which is relative to the 1 dB compression point. As detailed in Section 2.3, this allows the amplifier to operate in a range that minimizes nonlinear distortions [54]. In this matter, before amplifying the signal by the HPA, it is scaled by the gain $\varrho$ to ensure the desired IBO, given by

$$\varrho = \sqrt{\frac{\tau_{\text{1dB}}}{10^{\frac{\text{IBO}}{10}} \tau_{\mathbf{x}}}}, \tag{24}$$

where $\tau_{\text{1dB}}$ is the input power at 1 dB compression point and $\tau_{\mathbf{x}}$ is the mean power of the input signal.

## 3.3 Memory HPA

Usually, memoryless HPAs effectively model the narrowband behavior of the amplifiers. However, as a general trend, an increase in bandwidth is expected to introduce a stronger memory effect in the amplified signal. In addition, wideband HPAs usually provide higher power levels [8], while restricting amplifiers to the linear amplification range yields poor efficiency [55]. There are different well-known representations of HPAs in wideband communications to approximate the nonlinear behavior with memory structures. For instance, Volterra models have been widely employed to model HPAs [9]. Nevertheless, besides allowing for a detailed analysis of the HPAs' behavior, the literature [9,56] has recognized this model for its computational demands associated with higher-order kernels. This increasing complexity of these kernels can make the Volterra model less attractive from a theoretical perspective. Consequently, alternative models have been developed to provide simplifications and improve computational efficiency while still capturing essential aspects of HPA behavior [57]. In particular, we can refer to the Wiener and Hammerstein models, which consider a static nonlinear model used in series with a linear filter to model the memory effects [10].

Both Wiener and Hammerstein models are equivalent, with the Wiener model assuming a linear filter followed by a memoryless nonlinear block [58,59]. In contrast, the Hammerstein model accounts for the memory effects by incorporating a linear filter after the nonlinearities [9,60]. Figure 8 illustrates the transmitter side of the communication system modeled using a nonlinear HPA with memory, in which the Hammerstein model is constructed as a memoryless polynomial, described in Subsection 3.2, in cascade with a finite impulse response (FIR) filter with $F$-taps. We denote $\mathbf{X}_{i,k}$ as the QAM data symbols for all $k$ subcarriers within each $i$-th symbol and the output signal affected by the memory effects of the HPA as $\mathbf{u}(t)$, where $t$ stands for the time domain index. We employ the Hammerstein model [9], considering the memory effects in a cascade with the static nonlinearity of the HPA. Following [9], we consider a FIR filter with $F = 3$ whose coefficients are given by $\boldsymbol{\omega} = [0.7692, 0.1538, 0.0769]$, obtained by measurements. It is noteworthy that $\omega$ can be modeled in practice either at the constructions of the HPA, or at a setup stage of the communication equipment.

Figure 9 shows the normalized magnitude of the frequency response of the HPA output as a function of the index of the subcarriers. Notice that the frequency response is not flat for the $K_{\text{on}}$ subcarriers[1].

[1]Notice also that there are 12 inactive subcarriers, whose magnitudes are close to zero.

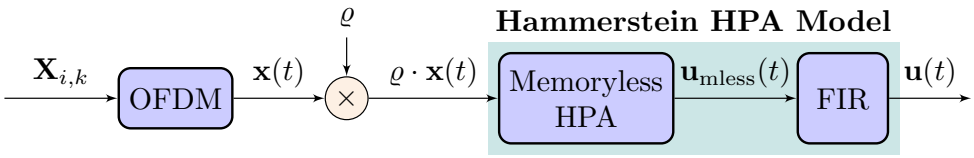


**Figure 8 – Transmission system model for the case with memory effect.**

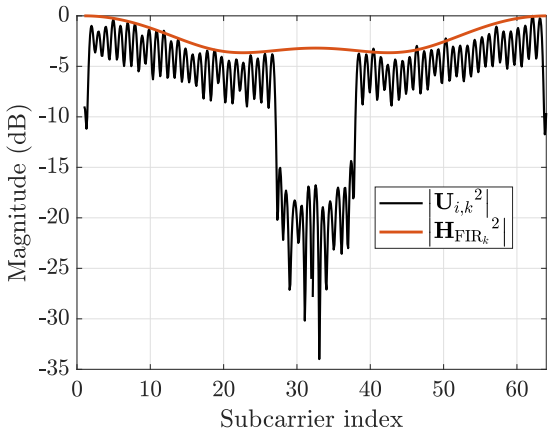


**Figure 9 – Frequency response of the memory HPA output.**

## 3.4 Vehicular channel model

The wireless channel considered in this work follows the vehicular channel model described in [11], where the tapped delay line (TDL) characteristics of the channel are provided for different environments. The characterization is based on real measurements with one or two vehicles moving under different velocities, which models R2V and V2V scenarios, respectively. The channel intensity profile for six vehicular channel models is given as taps as a function of path delays and average power gains, given the channel power delay profile (PDP), where each tap is statistically described by a Rayleigh fading distribution with a Doppler power spectral density. Table 2 describes the PDP of the different channel models, described as

- R2V Urban Canyon (R2V-UC): Communication between a transmitting antenna and a vehicle approaching at 32-48 km/h in an environment with urban canyon characteristics and dense traffic.
- R2V Suburban Street (R2V-SS): Communication between a transmitting antenna and a vehicle approaching at 32-48 km/h in a suburban environment.
- R2V Expressway (R2V-EX): Communication between a transmitting antenna and a vehicle approaching at 104 km/h on a highway.

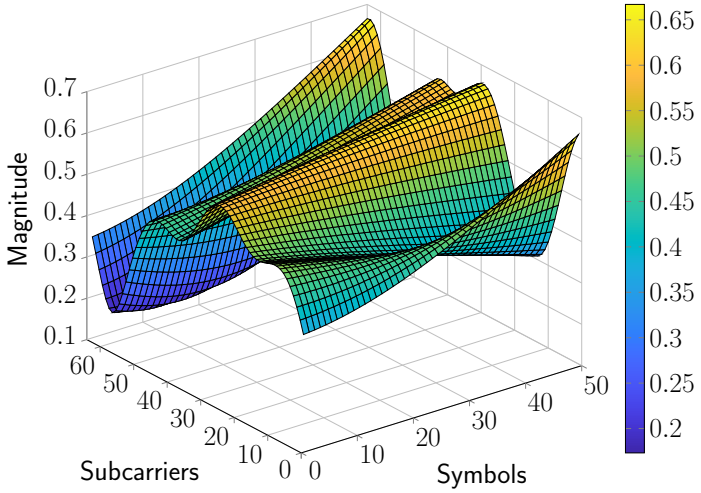


**Figure 10 – Channel frequency response.**

**Table 2 – Channel models power delay profiles.**

| | | |
|---|---|---|
| **R2V-UC** | **Path delays [ns]** | 0, 1, 2, 100, 101, 102, 200, 201, 300, 301, 500, 501 |
| | **Average path gains [dB]** | 0, 0, 0, -11.5, -11.5, -11.5, -19.0, -19.0, -25.6, -25.6, -28.1,-28.1 |
| **R2V-SS** | **Path delays [ns]** | 0, 1, 100, 101, 200, 201, 300, 301, 400, 500, 600, 700 |
| | **Average path gains [dB]** | 0, 0, -9.3, -9.3, -14, -14, -18, -18, -19.4, -24.9, -27.5, -29.8 |
| **R2V-EX** | **Path delays [ns]** | 0, 1, 2, 100, 101, 102, 200, 201, 300, 301, 500, 501 |
| | **Average path gains [dB]** | 0, 0, 0, -9.3, -9.3, -9.3, -20.3, -20.3, -21.3, -21.3, -28.8, -28.8 |
| **V2V-UC** | **Path delays [ns]** | 0, 1, 100, 101, 102, 200, 201, 202, 300, 301, 400, 401 |
| | **Average path gains [dB]** | 0, 0, -10, -10, -10, -17.8, -17.8, -17.8, -21.1, -21.1, -26.3, -26.3 |
| **V2V-EX** | **Path delays [ns]** | 0, 1, 2, 100, 101, 200, 201, 202, 300, 301, 302 |
| | **Average path gains [dB]** | 0, 0, 0, -6.3, -6.3, -25.1, -25.1, -25.1, -22.7, -22.7, -22.7 |
| **V2V-SDWW** | **Path delays [ns]** | 0, 1, 100, 101, 200, 300, 400, 401, 500, 600, 700, 701 |
| | **Average path gains [dB]** | 0, 0, -11.2, -11.2, -19, -21.9, -25.3, -25.3, -24.4, -28, -26.1, -26.1 |

- V2V Urban Canyon (V2V-UC): Communication between two vehicles where urban canyon characteristics exist. The vehicles move at 32-48 km/h in a dense traffic environment.

- V2V Expressway (V2V-EX): Communication between two vehicles entering the highway at the same time and accelerating to reach 104 km/h.

- V2V Expressway Same Direction with Wall (V2V-SDWW): Communication between two vehicles entering at the same time on a highway having a center wall. The vehicles were moving at 104 km/h.

As an illustrative example, Figure 10 showcases the channel frequency response for the V2V-UC model, given as the time-variant transfer function obtained by Fourier transforming the impulse response with respect to the delay. Notably, the channel exhibits

a smooth variation in the frequency domain, which is a crucial characteristic in practical vehicular communications scenarios.

Our analysis is based on a system model that encompasses several critical aspects of wireless vehicular communication systems. Thus, based on the main specifications of the IEEE 802.11p standard and their relevance in vehicular communication scenarios, we explore the characteristics of HPA with and without memory, recognizing their impact on signal distortions and overall system performance. In addition, we present the distinct characteristics that arise from the dynamic nature of the vehicular environment model. The combination of these components builds the basis for our subsequent exploration of advanced receiver architectures and channel estimation techniques in the context of wireless vehicular communication systems.

# 4 STATE-OF-THE-ART ON VEHICULAR CHANNEL ESTIMATION

This chapter introduces the methods that will serve as benchmarks for our subsequent analysis. We highlight that, in contrast to frame-by-frame (FBF) proposals [61, 62], our focus is on symbol-by-symbol (SBS) channel estimators, *i.e.*, in which the channel estimation is performed for each received symbol separately using only the previous and current received pilots, without increasing the latency of the application [12].

The IEEE 802.11p [27] standard defines the physical layer specifications for vehicular communication based on the OFDM scheme, with channel estimation supported by pilot subcarriers. In addition, this standard takes into account a preamble known at the receiver, which is used to synchronize the channel. Due to the limited number of data pilots, several methods in the literature have been proposed to improve channel estimation in vehicular networks. Most methods for IEEE 802.11p networks are based on the data-pilot aided (DPA) scheme, which exploits the demapped data symbols in order to improve the channel estimation, thus providing a low computational complexity solution [14, 30, 31].

In view of the challenges of vehicular communication networks, DNN-based schemes have been successfully employed recently to improve channel estimation for vehicular channels. For instance, an auto-encoder (AE)-DNN was proposed by [15] in order to improve the DPA method. Convolutional neural networks (CNNs) have also been considered as a solution for vehicular scenarios [61, 62]. The TS-ChannelNet estimator introduced by [61] suffers from high computational complexity, since it considers integrating both LSTM and CNN to achieve the final channel estimates. The authors in [62] present an estimator based on weighted adaptive interpolation, which is able to reduce the complexity and at the same time outperforms TS-ChannelNet, given a modification considered in the IEEE 802.11p standard to allocate the pilots within each transmitted frame, adapting the scheme according to the mobility condition. However, by considering FBF solutions, both CNN-based receivers require the reception of the whole frame before starting the channel estimation.

Moreover, other recent studies have considered more advanced DL-based algorithms to explore the correlation between OFDM symbols. As it was shown in [17] and [18], DL is able to capture more features of the vehicular channel and to improve the estimation performance compared to conventional methods. In this sense, a promising

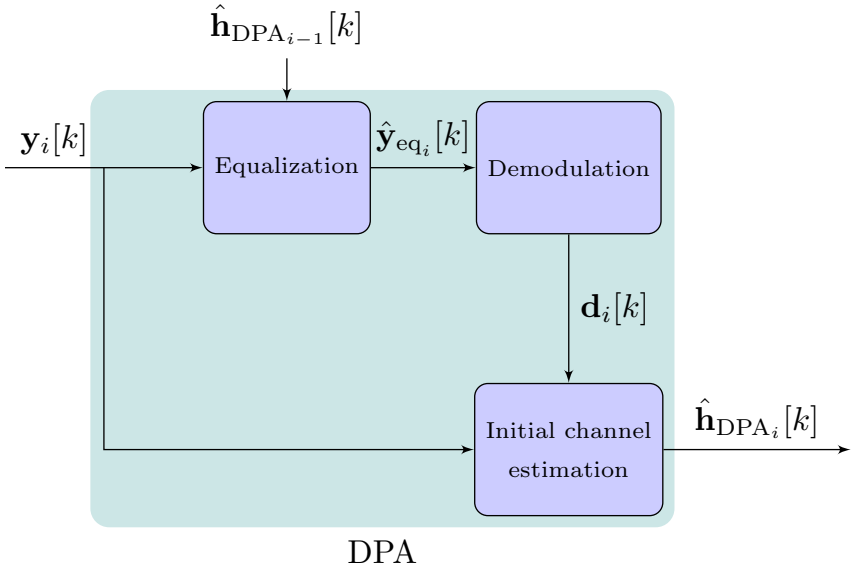


**Figure 11 – Block diagram of the DPA method.**

approach relies on the LSTM network, which can be a robust and efficient DL solution to track the vehicular channel, especially in high mobility scenarios. Nevertheless, the LSTM architecture still poses a significant challenge related to its high complexity.

## 4.1 Conventional estimators

### 4.1.1 LS

The basic method considered to provide channel estimation in the IEEE 802.11p standard is the LS estimator. Recalling Figure 7, the two long training predefined symbols $\mathbf{t}_{p,1}$ and $\mathbf{t}_{p,2}$, are demodulated to obtain the received frequency domain symbols for each $k$-th subcarrier, denoted by $\mathbf{y}_{p,1}[k]$ and $\mathbf{y}_{p,2}[k]$. Thus, the LS channel estimation is given by

$$\hat{\mathbf{h}}_{\mathrm{LS}}[k] = \frac{\mathbf{y}_{p,1}[k] + \mathbf{y}_{p,2}[k]}{2\mathbf{p}[k]}, \tag{25}$$

where $\mathbf{p}[k]$ is the predefined preamble sequence in frequency domain.

### 4.1.2 DPA

As illustrated by its block diagram in Figure 11, the DPA method employs the previously received symbol as a preamble to estimate the channel for the current symbol. Considering the estimate for the first symbol as $\hat{\mathbf{h}}_{\mathrm{DPA}_0}[k] = \hat{\mathbf{h}}_{\mathrm{LS}}[k]$, the equalization of the

current $i$-th symbol at the $k$-th subcarrier is given by

$$\hat{\mathbf{y}}_{\mathrm{eq}_i}[k] = \frac{\mathbf{y}_i[k]}{\hat{\mathbf{h}}_{\mathrm{DPA}_{i-1}}[k]}, \tag{26}$$

so that $\hat{\mathbf{y}}_{\mathrm{eq}_i}[k]$ is then demapped to the nearest constellation point to result in $\mathbf{d}_i[k]$. The DPA initial channel estimate is obtained as

$$\hat{\mathbf{h}}_{\mathrm{DPA}_i}[k] = \frac{\mathbf{y}_i[k]}{\mathbf{d}_i[k]}. \tag{27}$$

In contrast to the LS estimation, which exhibits significant degradation due to the time variation, the DPA method enhances the performance by exploiting the correlation characteristics between adjacent symbols in the OFDM transmission. However, the performance of this scheme is heavily influenced by the data pilots' reliability, which tends to degrade given the harsh dynamic of vehicular channels. In addition, classical DPA-based methods incur error propagation during the frames, a problem that is even more significant in high-order modulation schemes and high-mobility [13].

### 4.1.3 STA

Several channel estimation schemes based on DPA method are proposed in the literature to rapidly track time-varying channels. For instance, the spectral temporal averaging (STA) method is introduced in [14], where an average of the estimated channels in time and frequency domains is performed after the DPA estimation. As illustrated in its block diagram in Figure 12, the STA estimation is obtained by averaging (27) in the frequency domain to obtain

$$\hat{\mathbf{h}}_{\mathrm{update}_i}[k] = \sum_{\lambda=-\beta}^{\lambda=\beta} \omega_\lambda \hat{\mathbf{h}}_{\mathrm{DPA}_i}[k+\lambda], \tag{28}$$

where $\omega_\lambda = \frac{1}{2\beta+1}$, with $\beta$ being the frequency averaging coefficient. Next, the channel's final estimation is computed as

$$\hat{\mathbf{h}}_{\mathrm{STA}_i}[k] = \left(1 - \frac{1}{\alpha}\right) \hat{\mathbf{h}}_{\mathrm{STA}_{i-1}}[k] + \frac{1}{\alpha} \hat{\mathbf{h}}_{\mathrm{update}_i}[k], \tag{29}$$

where $\alpha$ is the time averaging coefficient that, as well as $\beta$, is an integer parameter inherent to the STA. To improve the performance, $\alpha$ and $\beta$ must be chosen experimentally depending on the channel variation, and fixing these parameters can increase the gradually accumulated demapping error from $\mathbf{d}_i[k]$ [14].

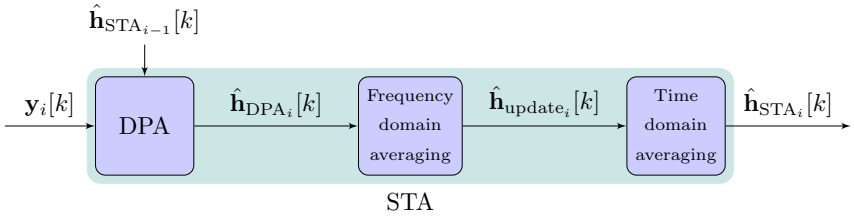


**Figure 12 – Block diagram of the STA estimator [14].**

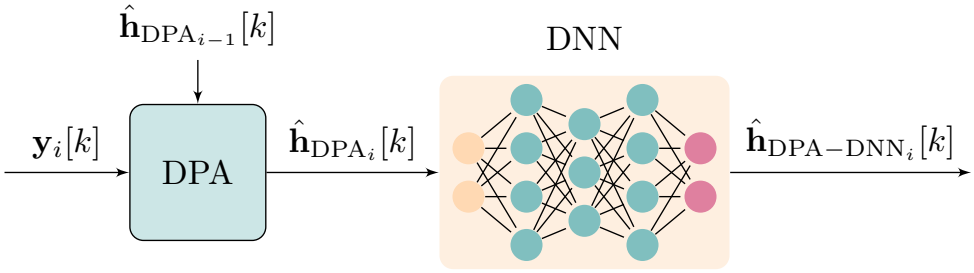


**Figure 13 – Block diagram of the DPA-DNN estimator [15].**

## 4.2 DNN-based estimators

### 4.2.1 DPA-DNN

The DPA-DNN scheme [15] considers an initial DPA estimation that is followed by an offline trained AE with three hidden layers, consisting respectively of 40, 20 and 40 neurons. Figure 13 illustrates the approach, in which the goal of the DNN is to update the estimation initially obtained with the DPA, by learning to correct the estimation errors between $\hat{\mathbf{h}}_{\mathrm{DPA}_i}[k]$ and the perfect channel. The output is denoted by $\hat{\mathbf{h}}_{\mathrm{DPA-DNN}_i}[k]$, which is the DPA-DNN channel estimation.

The authors in [15] show that the trained DNN is capable of learning the channel frequency domain characteristics, preventing the error propagation typical of the DPA method.

### 4.2.2 STA-DNN

In order to reduce complexity when compared to the scheme proposed in [15], the authors in [16] considered a three-layer DNN, with 15 neurons in each layer, which is used as a post-process to the conventional STA estimator. Figure 14 illustrates such approach, in which the STA estimation $\hat{\mathbf{h}}_{\mathrm{STA}_i}[k]$ is used as the input of the DNN in order to produce $\hat{\mathbf{h}}_{\mathrm{STA-DNN}_i}[k]$.

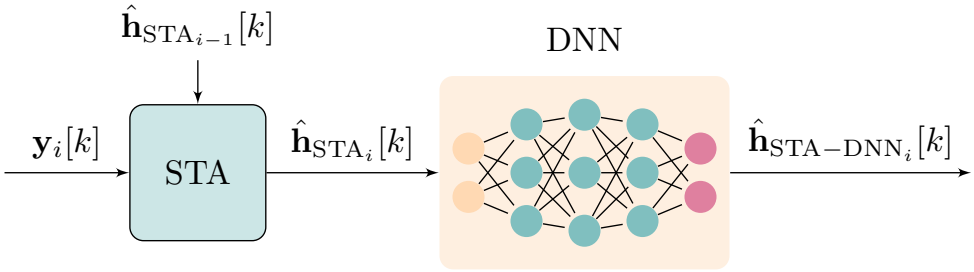


**Figure 14 – Block diagram of the STA-DNN estimator [16].**

The goal of the employed DNN is to minimize the mean squared error (MSE) between the perfect channel state information (CSI) and the STA estimate, so that

$$\mathrm{MSE}_{\mathrm{STA-DNN}} = \frac{1}{N_{\mathrm{T}}} \sum_{i=1}^{N_{\mathrm{T}}} \left( \mathbf{h}_{\mathrm{i}} - \hat{\mathbf{h}}_{\mathrm{STA}_i} \right)^2, \tag{30}$$

where $N_{\mathrm{T}}$ is the number of training samples. Unlike the proposal in [15], the nonlinear processing along with the STA allows the proposed estimator to capture more features of the time and frequency correlations of the channel. The results in [16] show that the proposed STA-DNN scheme provides a performance improvement while reducing the computational complexity of the solution.

## 4.3 Numerical results: conventional vs. DNN-based estimators

This section presents a preliminary analysis of the performances of the state-of-the-art channel estimators when applied to the IEEE 802.11p standard in the presence of distortions due to memoryless HPA nonlinearities based on the model as described in Section 3.2. The results are presented in terms of the normalized MSE (NMSE) and bit error rate (BER) of the DPA and STA [14] estimators, as well as DNN-based estimators such as the DPA-DNN [15] and the STA-DNN [16]. The V2V-UC vehicular channel model [11] is considered, deploying the communication channel between two vehicles moving at $v = 50$ km/h in a dense traffic environment. The estimations are performed for transmitted OFDM frame of size $L = 100$ symbols and 16-QAM modulation.

Figure 15a and Figure 15b present the NMSE result in the linear and nonlinear scenario with fixed IBO $= 4$ dB, respectively. It is worth noting that the objective of the DNN in both DL-based solutions is to minimize the NMSE between the ideal channel and the channel estimation from the chosen conventional method. However, this is done without any prior knowledge regarding the HPA nonlinearities effects. The superiority

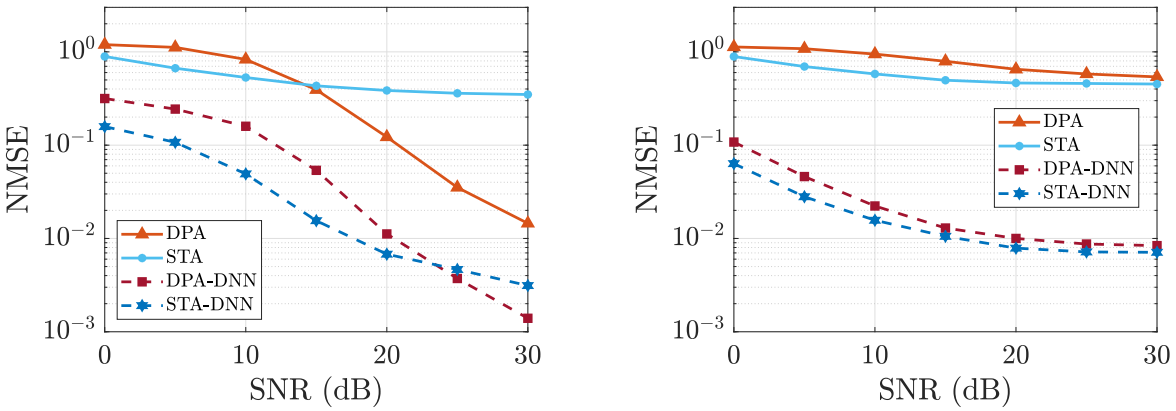


(a) Without HPA nonlinearities.

(b) With HPA nonlinearities.

**Figure 15 – NMSE performance for the conventional and DNN-based estimators.**

of the DNN-based methods in estimating the channel is evident, so that using DNN as a nonlinear process considerably enhances the conventional estimators' performance, adding the ability to learn features about the channel and reducing the error between its estimation and the ideal channel, even when impacted by NLDs.

Figure 15a shows that, starting from the SNR of $\xi = 25$ dB, the DPA-DNN presents less channel estimation error than the STA-DNN estimator, once the impact due to demapping error is small for high SNR region and the initial DPA estimation emerges over STA. Moreover, the results presented by Figure 15b show that, when the HPA distortions are considered, the STA-DNN hybrid solution slightly outperforms the DPA-DNN, proving to be more likely to capture the nonlinearities of the HPA while reducing also the computational complexity due to its DNN architecture. Figure 16a shows that the DNN-based estimators outperform the BER provided by the conventional estimators in all considered scenarios. In Figure 16b it is observed that the DNN-based estimators are still capable of providing a BER of around $10^{-2}$ at $\xi = 20$ dB, while the conventional estimators suffer from severe performance degradation.

It is worth pointing out that, in performing an average of the estimated channels in time and frequency domains, the classical STA takes more about the correlation of the channel gain over successive received OFDM symbols into account than the DPA estimation, providing a better entry for the DNN. As a consequence, the complexity of the STA-DNN in terms of the number of neurons of the DNN can be reduced when compared to the DPA-DNN, while still providing a slightly better BER performance.

In order to compare the estimators with different nonlinear distortion effects, Figure 17 presents the BER performance by employing different IBO values. Intuitively,

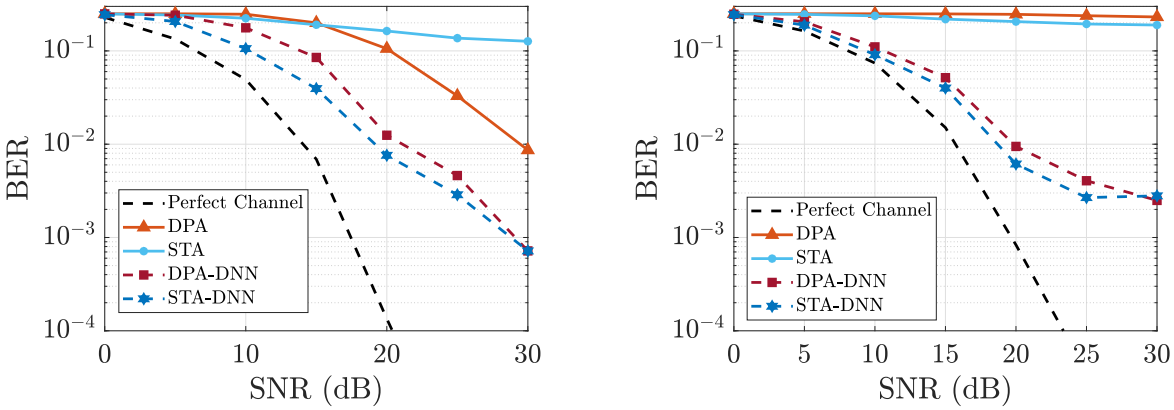


(a) Without HPA nonlinearities.

(b) With HPA nonlinearities.

**Figure 16 – BER performance for the conventional and DNN-based estimators.**

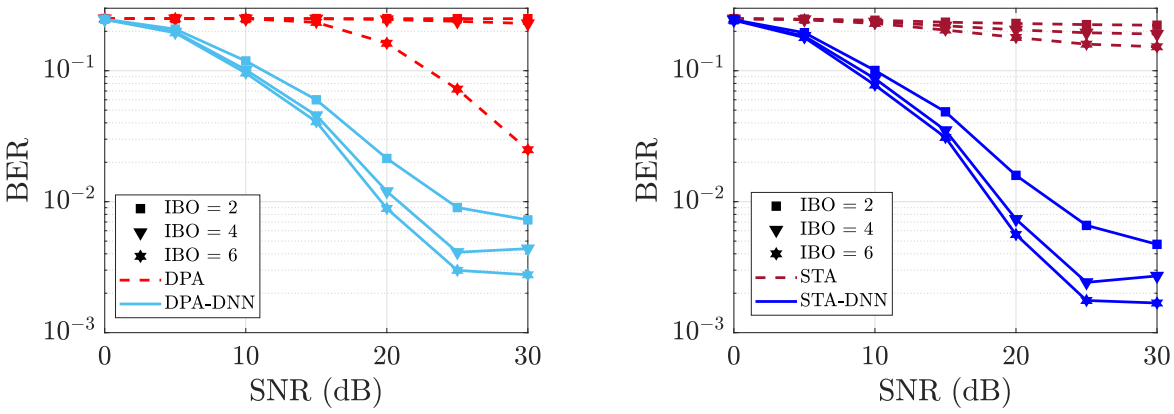


(a) Initial DPA and AE-DNN estimators

(b) STA and STA-DNN estimators.

**Figure 17 – BER performance for the conventional and DNN-based estimators for IBO $\in \{2, 4, 6\}$ dB.**

since increasing the IBO represents an approximation to the characteristics of the ideal HPA and its linear properties, a lower IBO implies a worse BER performance as an expected result. In accordance with that, it is possible to notice that both classical and DNN-based estimators show better performance with the increase of the IBO. Nevertheless, the DNN-based estimators are more robust to these nonlinear effects, since the variation in performance is smaller than the one from the conventional estimators. The results presented in Figures 17a and 17b show that, even for the scenario with IBO $= 2$ dB, both DPA-DNN and STA-DNN are capable to achieve BER lower than $10^{-2}$ at $\xi = 25$ dB, whereas the conventional initial DPA estimator and the STA estimator exhibit respectively high error rates of 0.25 and 0.22. As a key result, this study shows that DNN-based methods implicitly have some robustness against these nonlinearities. This stands in contrast to using only conventional channel estimators without DNNs, for which the performance is considerably degraded by the HPA distortions. This motivates the exploration of advanced DL-based methods for accurate vehicular channel estimation.

## 4.4 LSTM-based estimators

Although the DPA method improves performance compared to the LS estimator, a relevant performance loss is observed in communication scenarios with high mobility. In these cases, the demapping error increases since the correlation between symbols, explored by the DPA, decreases [16]. In order to deal with this issue, recently, more modern DL algorithms have been introduced to address the error propagation issue.

### 4.4.1 LSTM-NN-DPA

The LSTM-NN-DPA scheme has been proposed in [17], which employs an LSTM network allied with a NN in order to reconstruct the channel as close as possible to the ideal channel response. The authors consider that the input of the LSTM receives the LS of the $K_\mathrm{p}$ pilot subcarriers, in two consecutive OFDM symbols, denoted by $\hat{\mathbf{h}}_{\mathrm{LS}_{i,\mathrm{p}}}[k]$ and $\hat{\mathbf{h}}_{\mathrm{LS}_{i-1,\mathrm{p}}}[k]$, and the previously estimated channel $\hat{\mathbf{h}}_{\mathrm{LSTM-NN-DPA}_{i-1,d}}[k]$ for the $K_\mathrm{d}$ subcarriers. Then, the estimate after the NN is denoted by $\hat{\mathbf{h}}_{\mathrm{LSTM\text{-}NN}_i}[k]$, which is further used as the input of the DPA method, providing the final estimation $\hat{\mathbf{h}}_{\mathrm{LSTM\text{-}NN\text{-}DPA}_i}[k]$, $\forall k \in \mathcal{K}_\mathrm{on}$. The block diagram of the LSTM-NN-DPA scheme is shown in Figure 18, while numerical results in [17] show that this method is able to learn the time and frequency characteristics of the channel, tracking its variation and mitigating noise. Thus,

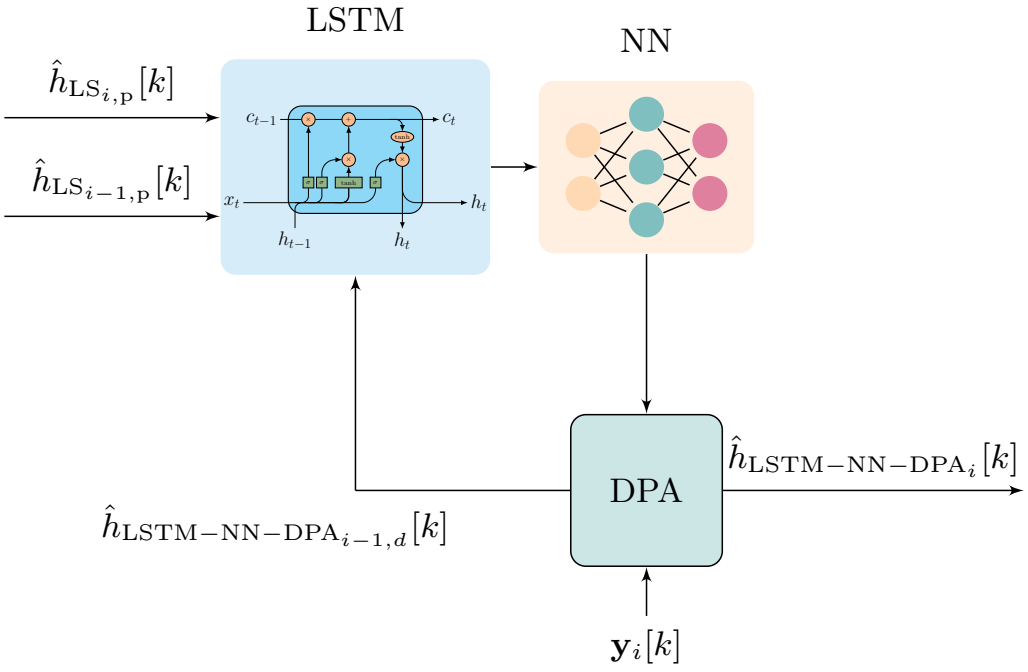


**Figure 18 – Block diagram of the LSTM-NN-DPA [17] scheme.**

significant performance improvement in comparison to previous DNN-based receivers has been achieved.

### 4.4.2 LSTM-DPA-TA

Another LSTM-based receiver has been proposed by [18], where the LSTM estimates are directly fed to the DPA method, producing $\hat{\mathbf{h}}_{\text{LSTM-DPA}_i}[k]$ as an output. Then, noise mitigation is achieved by means of a TA scheme, defined as

$$\begin{aligned}\hat{\mathbf{h}}_{\text{LSTM-DPA-TA}_i}[k] = &\left(1-\frac{1}{\alpha}\right)\hat{\mathbf{h}}_{\text{LSTM-DPA-TA}_i-1}[k] \\ &+\frac{1}{\alpha}\hat{\mathbf{h}}_{\text{LSTM-DPA}_i}[k],\end{aligned} \tag{31}$$

where $\alpha$ defines the fixed time averaging weight.

Figure 19 illustrates the block diagram of the LSTM-DPA-TA scheme. Furthermore, this estimator exhibits a lower computational complexity when compared to LSTM-NN-DPA, while achieving similar performance in different mobility scenarios. Nevertheless, both LSTM-NN-DPA and LSTM-DPA-TA still require a large number of neurons to perform the operations in the LSTM units, since all active subcarriers are used.

In line with existing literature, we underscore that LSTM methods exhibit

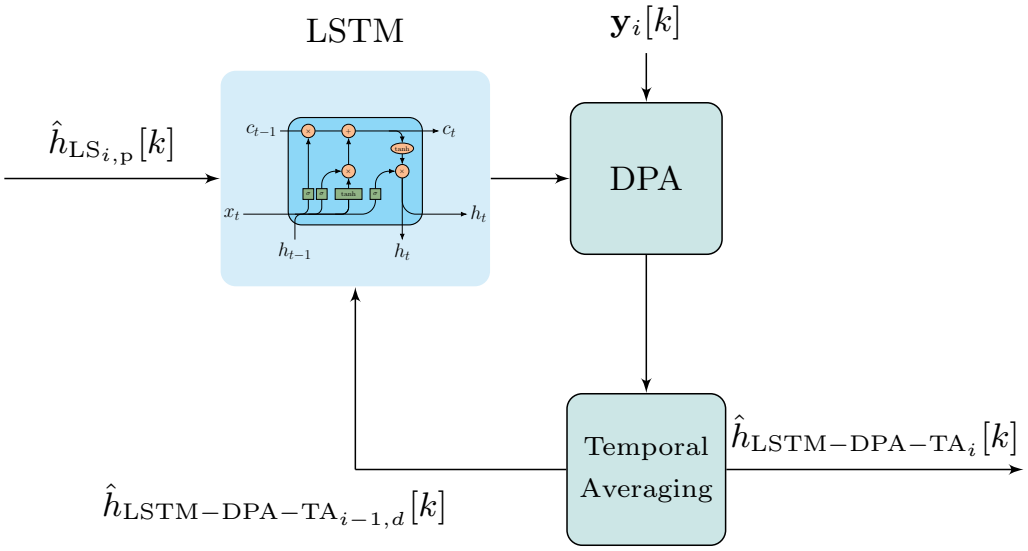


**Figure 19 – Block diagram of the LSTM-DPA-TA [18] scheme.**

superior performance compared to DNN methods when estimating the vehicular channel [12, 17]. However, this performance gain comes at the expense of increased complexity. Recognizing both the advantages and limitations, our proposed approach is also based on LSTM networks. Nevertheless, in this thesis we have developed a method to substantially reduce the complexity of the estimator, mitigating this trade-off. By introducing a new approach, we are able to balance the computational demands with the superior performance associated with LSTM methods, making it more suitable for real-world applications where computational resources are often limited.

# 5 PROPOSED LSTM-BASED CHANNEL ESTIMATION

This chapter presents a novel learning-based receiver architecture proposed to estimate the vehicular channel. Through a comprehensive analysis, we compare the performance of the proposed estimator with benchmark methods from the literature, validating its efficacy in scenarios characterized by dynamic conditions and nonlinearities inherent in vehicular communications. The results provide a perspective on the robustness and adaptability of the proposed learning-based receiver architecture, proving its potential to improve channel estimation in realistic vehicular communication environments.

## 5.1 DPA-LSTM-NN

This section introduces a novel learning-based receiver architecture proposed for estimating the vehicular channel. Using the DPA procedure detailed in Section 4.1.2 as initial estimation, the proposed DPA-LSTM-NN scheme performs first a coarse channel estimation that is used as the input of an LSTM layer. Since the LSTM is a powerful tool to track the channel variation and learn the channel correlation in the time domain, we favored the use of the DPA method instead of more complex estimators, such as STA [14]. The LSTM is then followed by a NN in order to mitigate the remaining noise from the hybrid estimator, refining the channel estimation. Such a combination of the DPA, LSTM, and NN provides robustness with respect to the HPA distortions at the receiver.

### 5.1.1 Subcarrier sampling

The DPA-LSTM-NN considers a subcarrier sampling process at the input of the LSTM, so that it interpolates the subcarriers' information to reduce the complexity of the solution. The small maximum delay spread of the channel leads to a weak frequency selectivity, *i.e.*, $h[k] \approx h[k \pm 1]$. Thus, we define a subset $\mathcal{S} \subset \mathcal{K}_{\text{on}}$, so that only the DPA estimates $\hat{\mathbf{h}}_{\text{DPA}_i}[s]$, $\forall s \in \mathcal{S}$, are selected as inputs of the LSTM layer. Moreover, we also define $\mathcal{K}_{\text{p}}$ as the set containing the $K_{\text{p}}$ pilot subcarriers, while $\mathcal{K}_{\text{d}}$ is the set of the $K_{\text{d}}$ data subcarriers, so that $\mathcal{K}_{\text{on}} = \mathcal{K}_{\text{p}} \cup \mathcal{K}_{\text{d}}$. As an example, let us consider a slice of vehicular channel of Figure 10 for an arbitrary symbol index, plotting the magnitude as a function of the subcarrier index. Figure 20a shows all active subcarriers for a given symbol index, with pilot subcarriers illustrated with dashed lines and data subcarriers in solid lines. In this example, the scenario follows the IEEE 802.11p standard, where there are $K_{\text{on}} = 52$

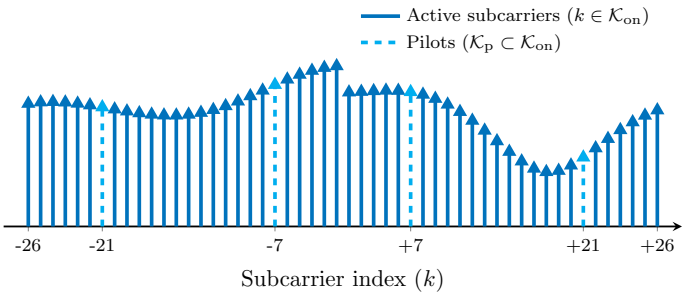


(a) Active subcarriers, including pilots.

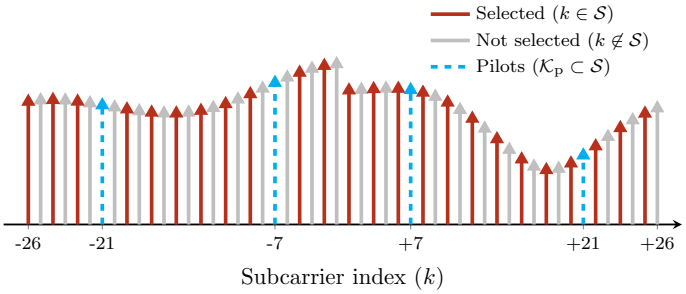


(b) Subcarriers with 1/2 sampling rate.

**Figure 20 – Subcarrier sampling procedure.**

active subcarriers, out of which $K_p = 4$ subcarriers are pilots and the remaining $K_d = 48$ subcarriers carry the data.

Notice that the inclusion of the set $\mathcal{K}_p$ in $\mathcal{S}$ is mandatory since it carries the OFDM pilots, so that $\mathcal{K}_p \subset \mathcal{S}$. Therefore, we sample only among the subcarriers in $\mathcal{K}_d$. Figure 20b illustrates a 1/2 sampling rate, where the $K_p = 4$ pilot subcarriers are included, while 24 out of the $K_d = 48$ data subcarriers are chosen. The selected subcarriers are taken using a simple down-sampling pattern. In this manner, the size of the LSTM layer can be adjusted according to the cardinality of $\mathcal{S}$, denoted as $|\mathcal{S}|$, which allows to effectively manage the complexity of the channel estimation process.

Finally, it is worth noting that the input of the LSTM layer has size $2|\mathcal{S}|$, while its output has size $2|\mathcal{K}_{on}|$, related to the real and imaginary parts from the complex-valued channel estimations. The interpolation to produce the channel estimates for all active subcarriers is intrinsically performed by the LSTM, by means of training.

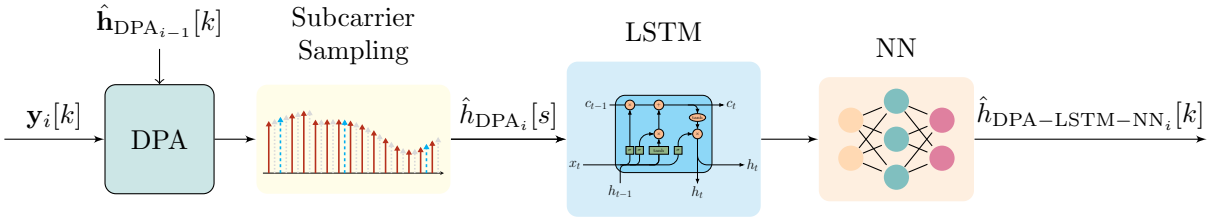


**Figure 21 – Proposed DPA-LSTM-NN channel estimator with subcarrier sampling.**

### 5.1.2 NN post-processing and training

The output from the LSTM layer is then processed by a shallow NN with $N_1$ neurons to reduce the noise and provide the final channel estimation, denoted as $\hat{\mathbf{h}}_{\mathrm{DPA-LSTM-NN}_i}[k]$. Furthermore, we follow [5] to define the parameters related to the training and testing stages of our method. The number of samples used for the training and testing phases is defined by splitting 10000 different realizations of the vehicular channel into sets with 80% and 20% of the total, respectively. The batch size is set to be sufficiently smaller than the size of the training dataset, thus speeding up its generalization and the training process, while the number of training epochs is set large enough to ensure the convergence of the model. For the optimizer, we favored the adaptive moment estimation (ADAM) with the rectified linear unit (ReLU) activation function to minimize the loss between the perfect channel and the estimates from the proposed DPA-LSTM-NN. This choice is motivated by its fast computing time, a small number of parameters to tune, and its well-known ability to solve optimization problems. As suggested in [5], the learning rate is set as 0.001, which is automatically adapted by the ADAM during its progress, until the method converges. Finally, following [63], the training for all the estimators is performed at the highest expected SNR value in order to reduce the impact of the noise and better learn the channel variations. Table 3 summarizes the DL architecture and parameters used in the training phase from our proposed scheme. The block diagram of the proposed DPA-LSTM-NN architecture is presented in Figure 21.

## 5.2 Performance in the presence of memoryless HPA

We start our analysis focusing on the memoryless HPA. For a transmitted OFDM frame consisting of $L = 50$ symbols, the performance evaluation of the proposed DPA-LSTM-NN scheme is done in terms of BER and NMSE, and compared with DPA-DNN [15], LSTM-NN-DPA [17] and LSTM-DPA-TA [18] schemes. For all schemes, a convolutional encoder with code rate 1/2 at the transmitter and a Viterbi decoder at the

**Table 3 – Parameters for training the proposed estimator.**

| Parameter | Values |
|---|---|
| Hidden size of the LSTM | $\|S\|$ |
| Hidden size of the NN | $N_1$ |
| Epochs | 500 |
| Training samples | 8000 |
| Testing samples | 2000 |
| Batch size | 128 |
| Optimizer | Adam |
| Learning rate | 0.001 |

receiver is taken into account, as defined by the IEEE 802.11p standard [27]. Furthermore, we consider the V2V-UC vehicular channel model, with two vehicles moving in opposite directions, modeling a single-input single-output (SISO) transmission with line-of-sight (LoS). The comparison is done in scenarios with speeds $v = 50$ km/h (low mobility scenario), $v = 100$ km/h (high mobility scenario) and $v = 200$ km/h (very high mobility scenario). Also, we considered 16-QAM and QPSK modulation techniques, aiming to cover both lower and higher modulation order aspects in the analysis, while the impact of the HPA nonlinearities has been considered for IBO = 4 dB for the higher modulation order and, since QPSK is considerably more robust with respect to the nonlinearities, we extend our analysis to higher effects of HPA-induced nonlinearities, employing IBO = 2 dB in this case.

We first investigate the impact of the subcarrier down-sampling factor on the BER performance of the proposed DPA-LSTM-NN scheme. Figure 22 plots the BER as a function of the SNR of the DPA-LSTM-NN estimator for the low mobility scenario ($v = 50$ km/h), 16-QAM modulation with an IBO = 4 dB. Notice that we indicate the size of the LSTM unit and the number of neurons of the NN in the legend. For instance, (52-15) indicates an LSTM unit with size $P = 52$ hidden states and $N_1 = 15$ neurons. Then, we have considered different sets of sampled subcarriers with $P = |\mathcal{S}| \in \{52, 36, 28, 20, 16\}$. Since the $K_{\mathrm{p}} = 4$ pilot subcarriers are always included in $\mathcal{S}$, we illustrate the cases of sampling the data subcarriers with rates 1/1, 2/3, 1/2, 1/3 and 1/4, respectively. We observe that it is possible to reduce the input size of the LSTM $U$ and the number of $P$ hidden states considerably with a slight degradation in the BER performance. Consequently, the LSTM demonstrated to be capable of interpolating the information of the missing subcarriers even with $P = 28$. Therefore, in the sequel we only consider the DPA-LSTM-NN scheme with $P = |S| = 28$ hidden states and an LSTM input

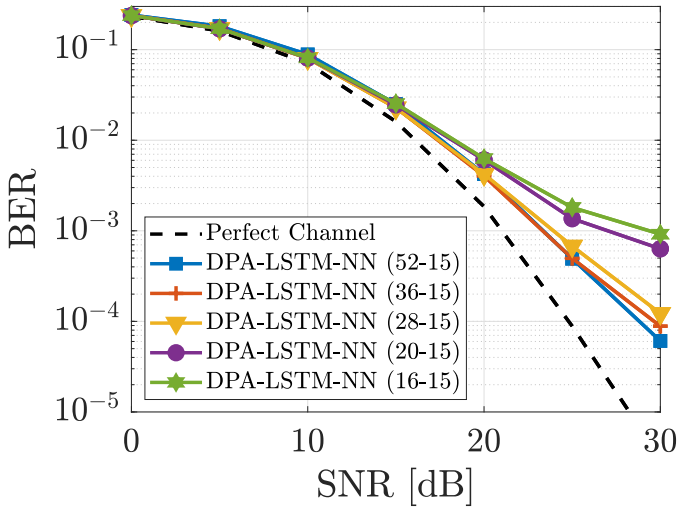


**Figure 22 – BER performance of the proposed DPA-LSTM-NN scheme for different sets of sampled subcarriers, with $|\mathcal{S}| \in \{52, 36, 28, 20, 16\}$, $v = 48$ km/h, 16-QAM modulation and IBO = 4 dB in the memoryless case.**

$U = 2|S| = 56$.

Figure 23 compares the BER performance of the estimation schemes using 16-QAM modulation and IBO = 4 dB. As illustrated in Figure 23a for the low mobility scenario, LSTM-NN-DPA [17] and LSTM-DPA-TA [18] perform better than our proposed scheme at low SNR. This is due to the demapping error of the DPA method, which increases in low SNR. Thus, since [17,18] use the LSTM layer before the DPA, they achieve increased performance. However, when the SNR increases the DPA method provides cleaner information to the LSTM layer, compared to LS used in [17,18]. Then, we observe that the DPA-LSTM-NN scheme outperforms all other benchmark methods when $\xi \geq$ 22 dB. Note also that such SNR level is crucial to achieve BER lower than $10^{-3}$, required by many practical applications. Furthermore, for high and very high mobility scenarios, respectively in Figures 23b and 23c, we observe a higher advantage for the proposed DPA-LSTM-NN estimator, outperforming the other solutions regardless of the SNR. It is also important to highlight that the proposed method is the sole estimator to achieve BER in the order of $10^{-4}$ for high and very high mobility. In addition, considering a BER of $10^{-3}$, the proposed scheme has 4 dB of SNR gain compared to the LSTM-DPA-TA method in Figure 23b, and 2 dB of SNR gain compared to the LSTM-NN-DPA method in Figure 23c.

The performance improvement of the proposed estimator with respect to LSTM-NN-DPA and LSTM-DPA-TA is illustrated in Figure 24 in terms of the NMSE gap. Here, let us highlight that the NMSE is calculated as the error between the channel estimated

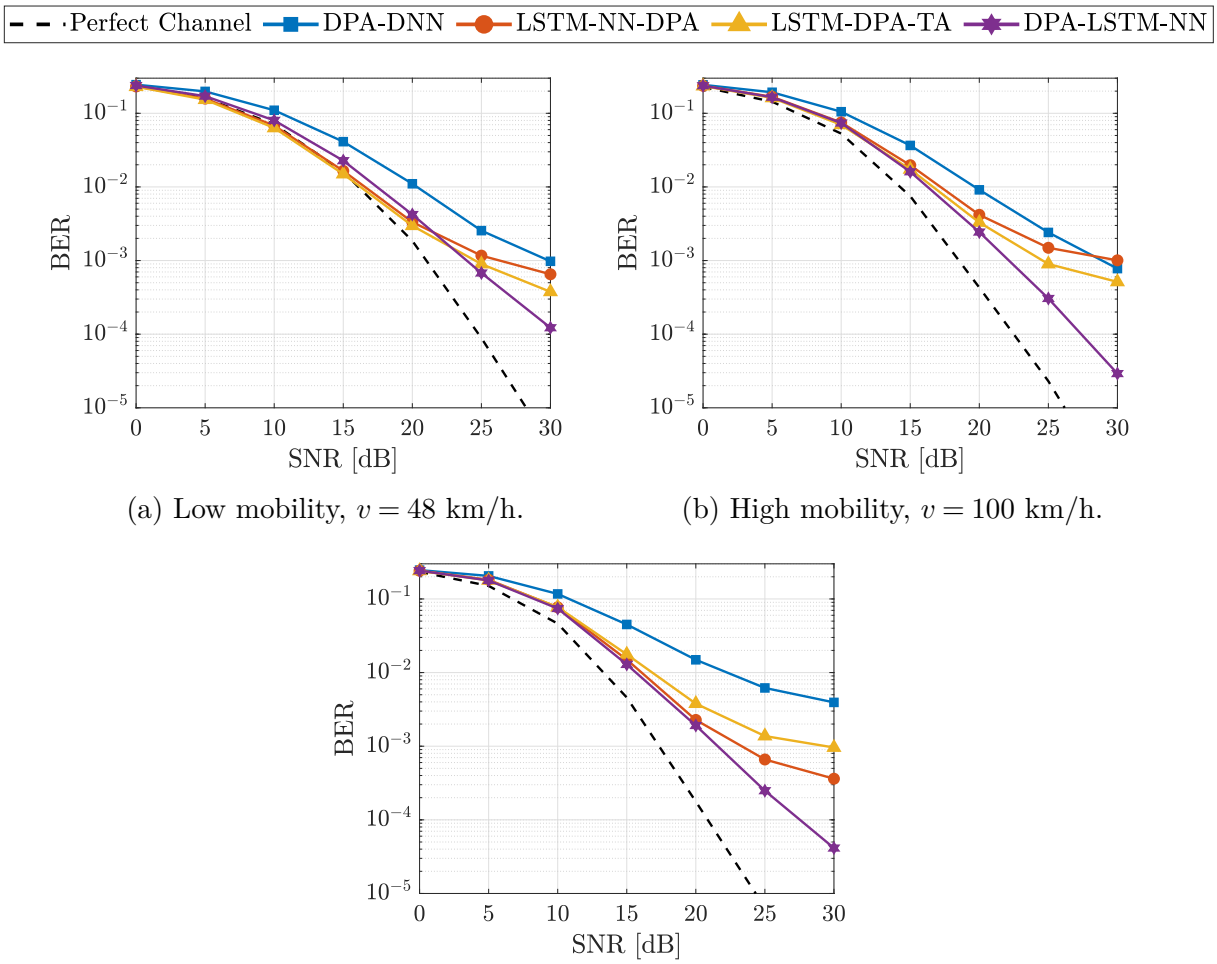


(a) Low mobility, $v = 48$ km/h.

(b) High mobility, $v = 100$ km/h.

(c) Very high mobility, $v = 200$ km/h.

**Figure 23 – BER performance of the DPA-DNN [15], LSTM-NN-DPA [17], LSTM-DPA-TA [18] and DPA-LSTM-NN (proposal) using 16-QAM modulation and IBO = 4 dB in the memoryless case.**

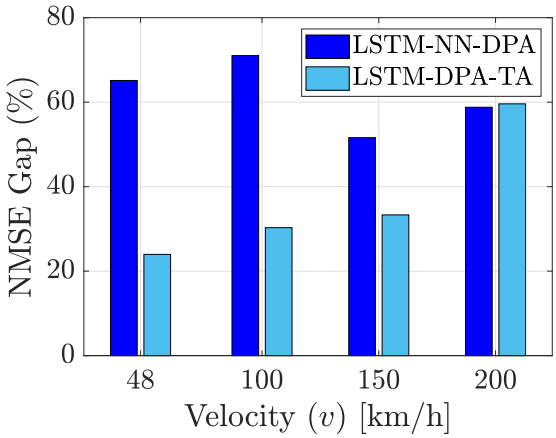


**Figure 24 – NMSE gap between the proposed DPA-LSTM-NN and LSTM-NN-DPA/LSTM-DPA-TA, with $\xi = 30$ dB, 16-QAM modulation, IBO = 4 dB in the memoryless case and $v \in \{48, 100, 150, 200\}$ km/h.**

for each receiver and the perfect channel, *i.e.* the channel where CSI is known. Thus, we calculate the NMSE for fixed SNR $\xi = 30$ dB, 16-QAM modulation, IBO = 4 dB, for different speeds and obtain the NMSE gain achieved by the proposed method compared to each benchmark. Comparing DPA-LSTM-NN and LSTM-NN-DPA, we observe that the NMSE gap is always higher than 40% regardless of $v$. Comparing DPA-LSTM-NN and LSTM-DPA-TA the NMSE gap is always higher than 20%, increasing with $v$. This result shows that the proposed DPA-LSTM-NN performs better in minimizing the error between the perfect channel and its channel estimates in high SNR, being a better choice for tracking the channel in the presence of nonlinear distortions.

In order to focus on the effects of the HPA-induced nonlinearities, the error rate performance is evaluated with IBO = 2 dB in Figure 25. Low, high and very high mobility scenarios are considered with QPSK modulation. Similarly to the results considering 16-QAM modulation, we observe that the proposed DPA-LSTM-NN scheme outperforms other methods, except in the low mobility scenario at low SNR. Nevertheless, we can notice here that both LSTM-NN-DPA and LSTM-DPA-TA estimators present an error floor at high SNR. This is mainly due to the low IBO, since the LS estimation used as the input of the LSTM layers in [17, 18] is highly degraded by the HPA nonlinear distortions. In addition, the performance gap between the LSTM-NN-DPA, LSTM-DPA-TA and our proposed method increases with the SNR, since the DPA method provides more reliable channel estimates in this case. Figure 26 corroborates such analysis, by showing the NMSE gap between ours and the benchmark LSTM-based estimators in the same scenario of Figure 25. Similar conclusions as in Figure 26 can be obtained, with the DPA-LSTM-NN method outperforming other schemes by at least 53%.

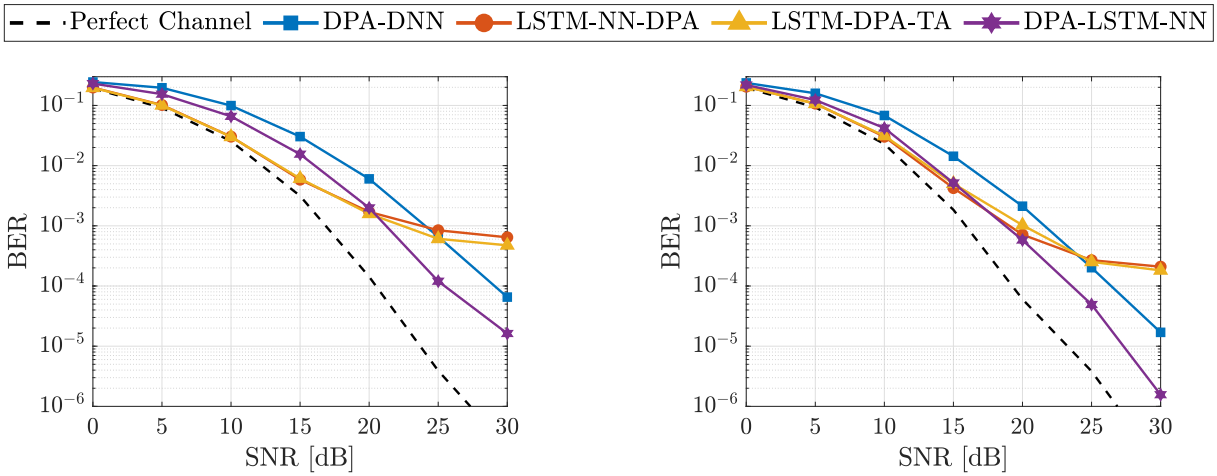


(a) Low mobility, $v = 48$ km/h.

(b) High mobility, $v = 100$ km/h.

(c) Very high mobility, $v = 200$ km/h.

**Figure 25 – BER performance of the DPA-DNN [15], LSTM-NN-DPA [17], LSTM-DPA-TA [18] and DPA-LSTM-NN (proposal) using QPSK modulation and IBO = 2 dB in the memoryless case.**

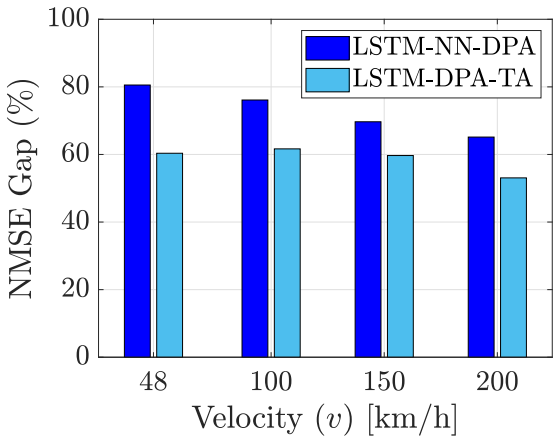


**Figure 26 – NMSE gap between the proposed DPA-LSTM-NN and LSTM-NN-DPA/LSTM-DPA-TA, with $\xi = 30$ dB, QPSK modulation, IBO = 2 dB in the memoryless case and $v \in \{48, 100, 150, 200\}$ km/h.**

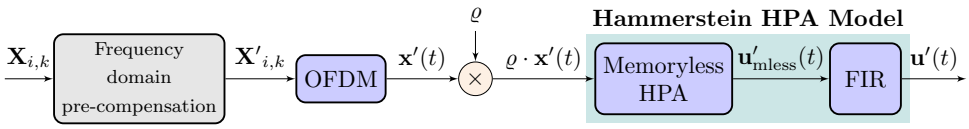


**Figure 27 – Transmission system model for the case with memory effect compensated.**

## 5.3 Performance in the presence of memory HPA

We take advantage of the previous analysis to extend the discussion regarding practical scenarios with NLDs. Thus, the effects of memory of the HPA model are now considered as an additional step to the analysis. It is important to note that a memoryless HPA model is an acceptable approximation for narrowband signals with nearly constant envelope modulations. However, the distortion cancellation performance in scenarios with higher bandwidth or higher data rates is degraded if the memory effects of the HPA are neglected [9, 59, 60].

### 5.3.1 Compensation at the transmitter

As presented in Figure 9, the frequency response of the HPA with memory is not flat for the active subcarriers, which can significantly affect the channel estimation. In order to mitigate this impact, we present a method to compensate part of the memory NLD effects at the transmitter side using only a priori known HPA information, while handling the remaining distortions together with the channel estimation. This low-complexity proposal considers a matched filter precoding as a compensation block, as presented in Figure 27, ensuring a flat spectrum for all data subcarriers in the transmitted signal. The precoded QAM data symbols can be written as

$$\mathbf{X}'_{i,k} = \frac{\mathbf{X}_{i,k}}{\mathbf{H}_{\text{FIR}k}}, \tag{32}$$

where $\mathbf{H}_{\text{FIR}k}$ is the frequency response of the FIR filter for the $k$-th subcarrier, *i.e.*, it corresponds to the FFT of $\boldsymbol{\omega}$, recalling that we consider $\boldsymbol{\omega} = [0.7692, 0.1538, 0.0769]$, which are obtained from measurements and modeled according to the HPA characteristics. This strategy assigns a compensation step with low complexity to the transmitter. The result is shown in Figure 28, where we can observe a flat spectrum except for the guard band, *i.e.* inactive, subcarriers. This alleviates the signal degradation.

According to [53], since $\mathbf{x}(t)$ is an OFDM signal with a large number of subcarriers, it can be approximated as a zero mean normal distribution, *i.e.*, $\mathbf{x}(t) \sim$

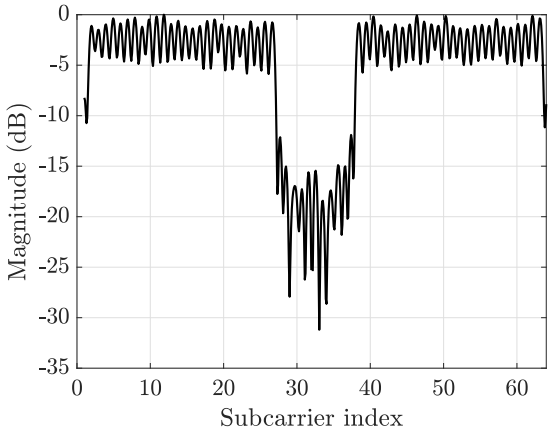


**Figure 28 – Frequency response of the HPA output compensated.**

$\mathcal{N}(0, \vartheta)$, with $\vartheta$ being its variance. Thus, the frequency domain pre-compensation (as in Figure 27) is equivalent to precoding $\mathbf{x}(t)$, so that

$$\mathbf{x}'(t) = \mathbf{g}(t) * \mathbf{x}(t) \tag{33}$$

where $*$ denotes the convolution operation and $\mathbf{g}(t)$ is obtained as the IFFT of $\frac{1}{\mathbf{H}_{\text{FIR}\,k}}$. As proven by [64], since $\mathbf{x}'(t)$ is a linear combination of uncorrelated normally distributed random variables, it also yields a normally distributed random variable, such that $\mathbf{x}'(t) \sim \mathcal{N}(0, \vartheta')$, where $\vartheta'$ depends on coefficients of $\frac{1}{\mathbf{H}_{\text{FIR}\,k}}$. Let us remark that this is crucial in order to apply the Bussgang theorem in (20) and validate the polynomial approximation in (23) while compensating the signal. In other words, even by introducing the compensation stage and the FIR filter of the Hammerstein model, the relations assumed in (20)-(23) are still valid.

Finally, the signal $\mathbf{x}(t)$ is normalized using a root mean square (RMS) normalization, while the output signal $\mathbf{u}(t)$ is normalized according to the effects of the FIR filter, being divided by the factor

$$\upsilon = \sqrt{\sum_{f=1}^{F} \omega_f^2}. \tag{34}$$

At the receiver, we employ the DPA-LSTM-NN method. Thus, the DPA is able to learn the time and frequency characteristics of the channel and reconstruct the estimation as close as possible to the ideal channel response. Then, the LSTM structure is designed to deal with sequential data, being capable of learning the channel correlation over time and efficiently predicting future channel realizations based on previous observations. As a

consequence, the combination of the compensation step at the transmitter and the DPA-LSTM-NN scheme at the receiver results in a communication system robust to the effects of memory of the HPA.

### 5.3.2 Simulation results

We compare the LSTM-NN-DPA [17], LSTM-DPA-TA [18], and the proposed DPA-LSTM-NN estimators in terms of NMSE and BER performances in scenarios with HPA models with memory effects. A transmitted OFDM frame size of $L = 50$ symbols is taken into consideration in a scenario based on the R2V-UC [11] model to deploy the communication channel between a transmitting antenna mounted on a roadside and a receiver vehicle approaching. The analysis is performed with a speed $v = 50$ km/h, but it should be noted that the results are qualitatively similar at other mobilities.

Figure 29 presents the NMSE performance for the wireless channel affected by the impairments related to the memory HPA. The estimators' performance is almost identical at a low SNR in the scenario with QPSK modulation and IBO = 2 dB, presented in Figure 29(a). However, when the SNR is greater than 10 dB, the DPA-LSTM-NN outperforms the other methods since the DPA provides more reliable information to the LSTM layer when compared to the LS used by [17, 18]. Moreover, in the scenarios with 16-QAM modulation presented in Figures 29(b) and 29(c), we observe an advantage of the DPA-LSTM-NN estimator, that outperforms the other solutions regardless of the SNR. This highlights the gain of this estimator for the case of higher modulation orders, while the other receivers suffer from a huge estimation error.

Figure 30 presents the BER performance of the LSTM-based estimation schemes in transmission with QPSK modulation and IBO = 2 dB. Besides focusing on the memory HPA, the performance with a memoryless HPA model from previous results in Section 5.2 is also shown for comparison purposes. In addition, the effects with and without the compensation done by (32) are also put side-by-side. The comparison of Figures 30(a) and 30(b) reveals a loss of at least 6 dB to achieve a BER below $10^{-3}$. Despite this, the HPA memory compensation is shown in Figure 30(c), where the loss is reduced to less than 1 dB to achieve the same error rate, achieving a performance closer to the memory scenario for all the estimators considered. Still, for all cases considered and in agreement with the NMSE result, the DPA-LSTM-NN estimator outperforms the other solutions in high SNR scenarios.

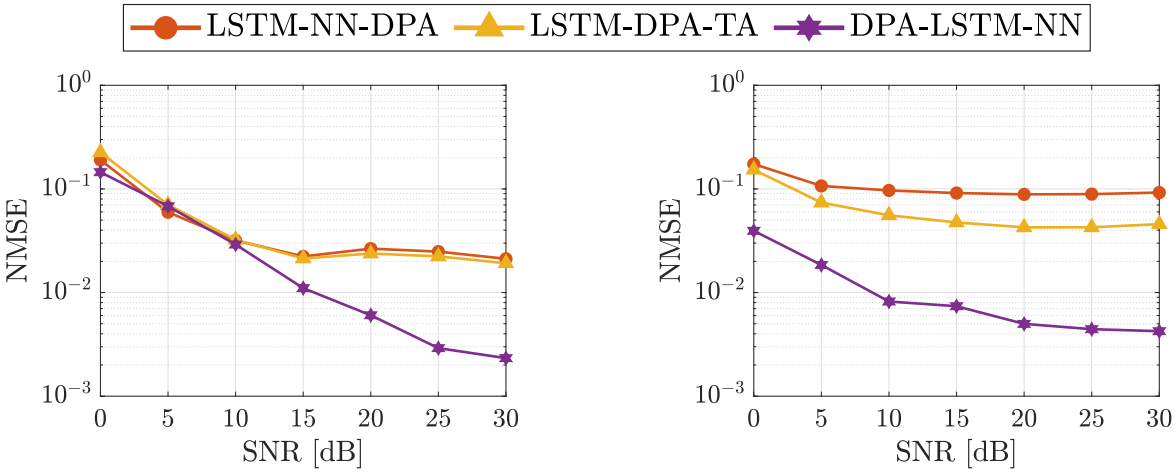


(a) QPSK and IBO = 2 dB.

(b) 16-QAM and IBO = 2 dB.

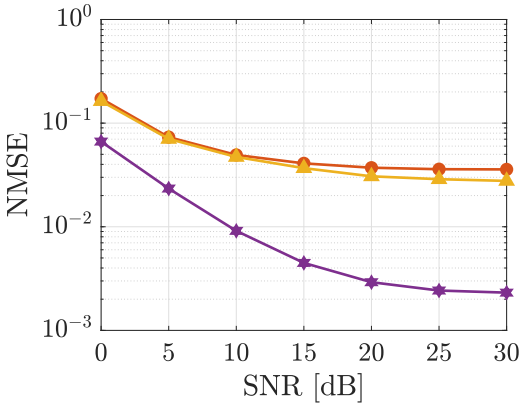


(c) 16-QAM and IBO = 4 dB.

**Figure 29 – NMSE performance in the scenario with NLD memory effects.**

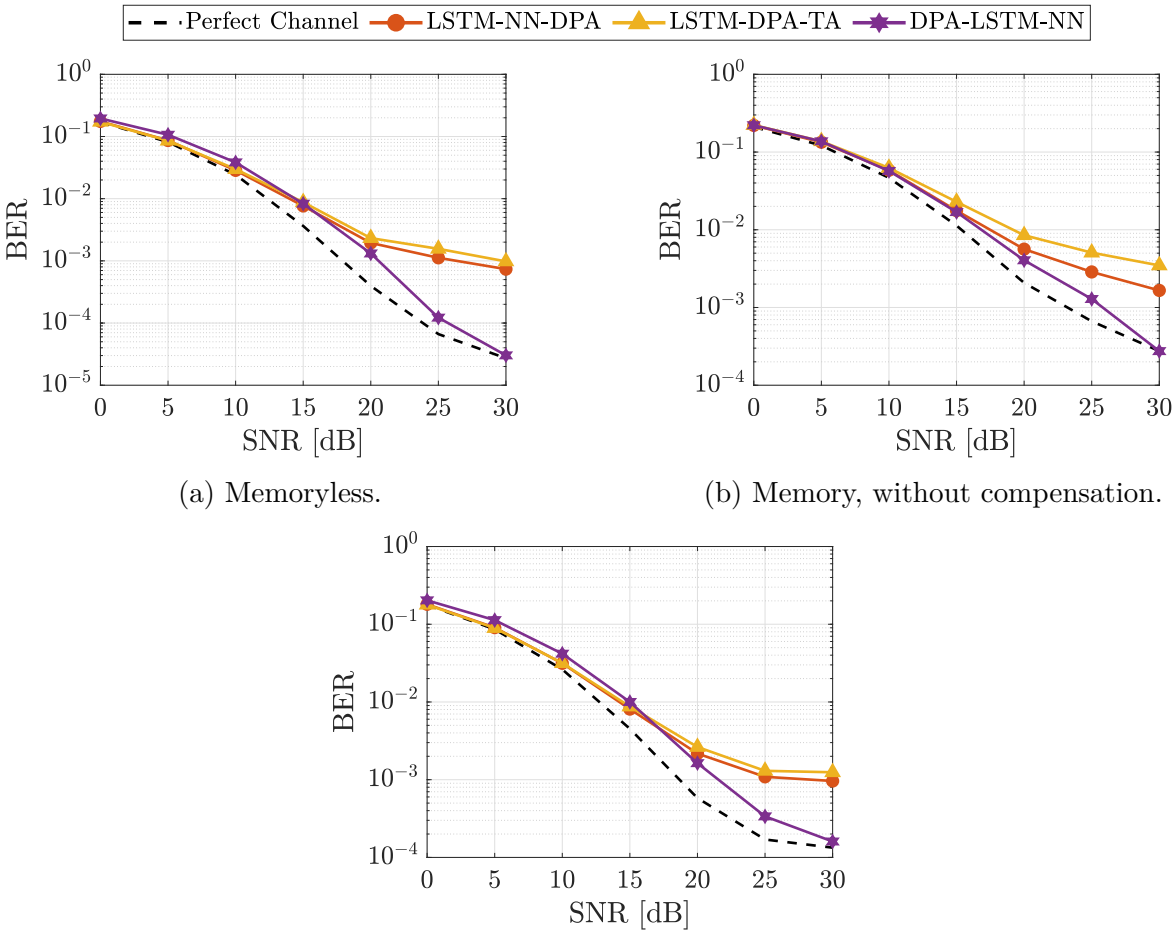


(a) Memoryless.

(b) Memory, without compensation.

(c) Memory, with compensation.

**Figure 30 – BER performance using QPSK modulation, $v = 50$ km/h and IBO = 2 dB.**

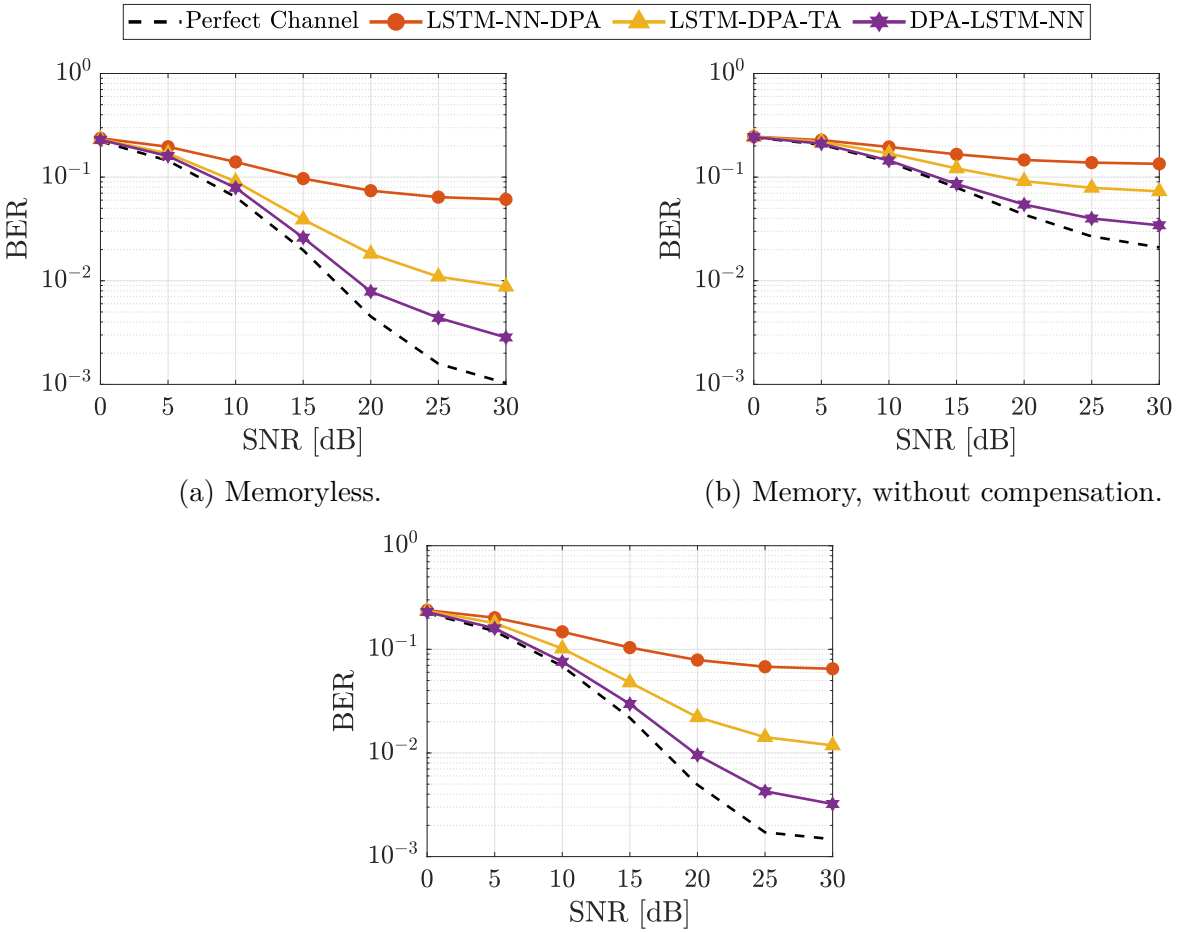


(a) Memoryless.

(b) Memory, without compensation.

(c) Memory, with compensation.

**Figure 31 – BER performance using 16-QAM modulation, $v = 50$ km/h and IBO = 2 dB.**

The effects of HPA modeling are shown in Figure 31, where memory effects severely degrade system performance with IBO = 2 dB and higher modulation order (16-QAM). Comparing Figures 31(a) and 31(b), a significant BER increase is observed due to the memory effects. By its turn, Figure 31(c) shows effective compensation using the proposed method. We remark that the compensation in (32) is practical since the FIR coefficients $\boldsymbol{\omega}$ need only to be estimated based on numerical measurements given the employed HPA, presenting a method where no high computational complexity is required on the transmitter side. Additionally, the DPA-LSTM-NN method outperforms other estimators in the presence of HPA memory effects, maintaining similar performance as shown in Figures 31(a) and 31(c). Furthermore, regardless of whether the compensation is performed in the transmitter, DPA-LSTM-NN shows an advantage over other solutions in scenarios with HPA memory effects. This indicates that the LS estimation used as the input of the LSTM layers in [17, 18] is highly degraded by the HPA NLD effects.

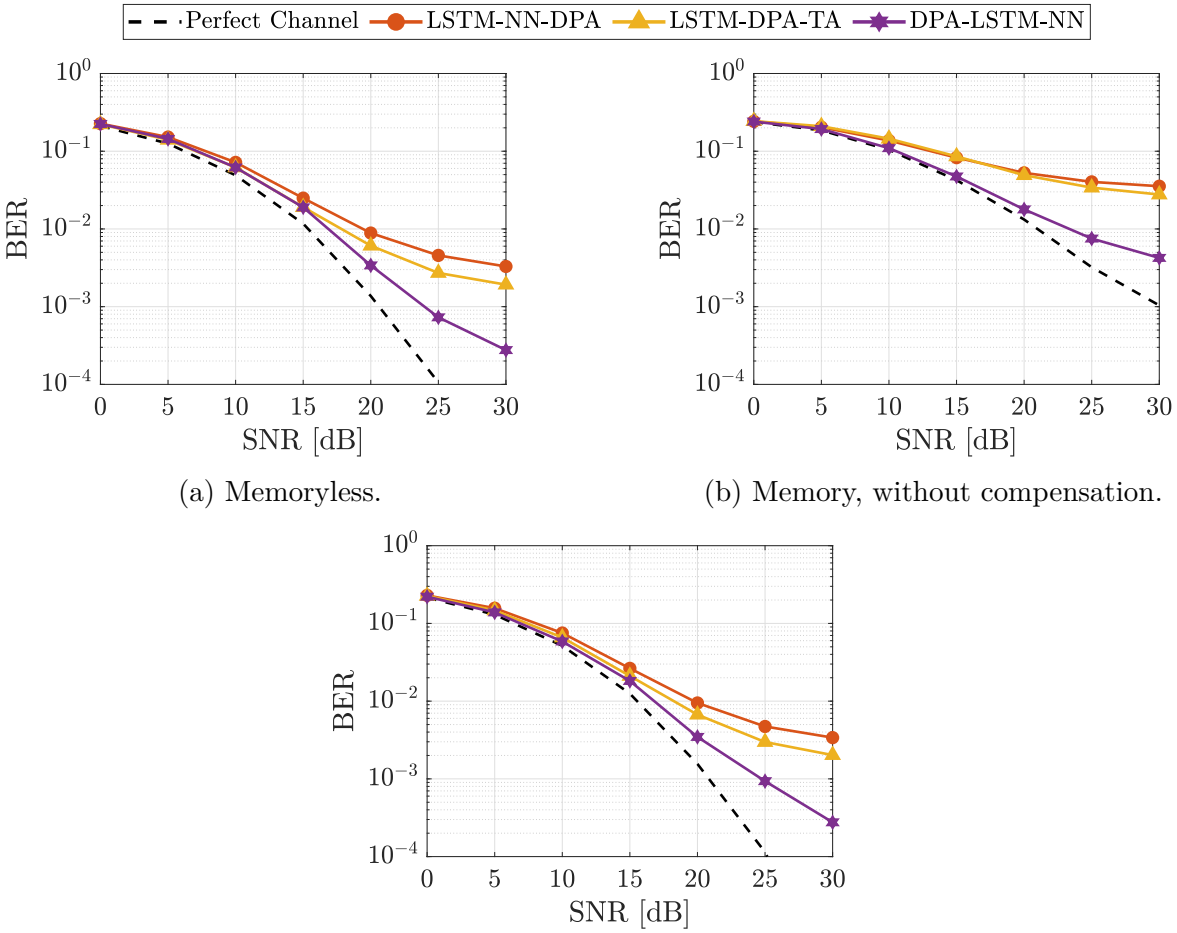


(a) Memoryless.

(b) Memory, without compensation.

(c) Memory, with compensation.

**Figure 32 – BER performance using 16-QAM modulation, $v = 50$ km/h and IBO = 4 dB.**

Finally, Figure 32 presents the BER with 16-QAM modulation and IBO = 4 dB, *i.e.*, smoother nonlinear effects. Again, the DPA-LSTM-NN performs better in minimizing the error between the perfect channel and its channel estimates, being a better choice for tracking the channel in the presence of NLD with memory. Figure 32(c) shows that the compensation done at the transmitter side significantly improves the performance for all estimators. Here, we underline the importance of this compensation step, showing that from a robust estimator, such as the proposed DPA-LSTM-NN, a compensation by means of (32) is sufficient to improve communication performance. This effect becomes evident by comparing Figure 32(b) and Figure 32(c), since a BER below $10^{-3}$ can only be obtained when the compensation stage is considered at the transmitter. In addition, when comparing the DPA-LSTM-NN estimator with [17, 18], we can observe that DPA-LSTM-NN is the sole capable of reaching a BER in the order of $10^{-3}$, while both LSTM-NN-DPA and LSTM-DPA-TA estimators present an error floor at high SNR.

## 5.4 Computational complexity analysis

In order to compare the computational complexity of the schemes, we calculate the number of real-valued operations in terms of multiplications/divisions and summations/subtractions, required to estimate the channel from a received OFDM symbol. It should be noted here that the pre-compensation required for the case of the scenario including NLD effects with memory requires only $K_{\text{on}}$ real-value operations in terms of multiplications/divisions and sums/subtractions, representing less than 2% of the overall complexity for estimating the channel from a received OFDM symbol for each of the receivers compared. Consequently, in the subsequent complexity calculations, this additional step is disregarded to maintain a comprehensive understanding of the complexity involved.

The computational complexity of the DPA-DNN estimator has been detailed in [16]. The initial DPA estimation requires $18\,K_{\text{on}}$ multiplications/divisions and $8\,K_{\text{on}}$ summations/subtractions, while the total number of multiplications and summations of the DNN depends on the number of neurons at each layer. Following [16], the number of multiplications and summations of the DNN is given by

$$C_{\text{DNN}}^{\text{Mult}} = C_{\text{DNN}}^{\text{Sum}} = \sum_{l=1}^{\iota+1} N_{l-1}^{\text{D}}\, N_{l}^{\text{D}}, \tag{35}$$

where $\iota$ is the number of hidden layers of the DNN, and $N_l^{\text{D}}$ is the number of neurons at the $l$-th hidden layer. In addition, $N_0^{\text{D}}$ denotes the number of neurons of the input layer of the DNN, while $N_{\iota+1}^{\text{D}}$ is the number of neurons of the output layer. The DPA-DNN has been designed in [15] with $\iota = 3$ hidden layers, respectively with $N_1^{\text{D}} = 40$, $N_2^{\text{D}} = 20$ and $N_3^{\text{D}} = 40$ neurons. In addition, both input and output layers depend on the number of active subcarriers multiplied by two in order to handle real and imaginary parts, so that $N_0^{\text{D}} = N_4^{\text{D}} = 2\,K_{\text{on}}$. Hence, the DPA-DNN requires $178\,K_{\text{on}} + 1600$ multiplications/divisions and $168\,K_{\text{on}} + 1600$ summations/subtractions.

The shallow NN, by its turn, has a single hidden layer, so that it computational complexity is given by

$$C_{\text{NN}}^{\text{Mult}} = C_{\text{NN}}^{\text{Sum}} = N_0\, N_1 + N_1\, N_2, \tag{36}$$

while the computational complexity of the LSTM unit has been detailed in [18], which depends on the input size of the LSTM unit $U$ and on the size of its hidden states $P$.

**Table 4 – Real-valued operations for the considered channel estimators.**

| Channel Estimator | Multiplications/Divisions | Summations/Subtractions |
|---|---|---|
| DPA-DNN | $178\,K_{\mathrm{on}} + 1600$ | $168\,K_{\mathrm{on}} + 1600$ |
| LSTM-NN-DPA | $12\,{K_{\mathrm{on}}}^2 + 81\,K_{\mathrm{on}} + 8\,K_{\mathrm{on}}\,K_{\mathrm{p}}$ | $89K_{\mathrm{on}} + 8\,K_{\mathrm{p}} - 8$ |
| LSTM-DPA-TA | $12\,{K_{\mathrm{on}}}^2 + 23\,K_{\mathrm{on}}$ | $31K_{\mathrm{on}} - 8$ |
| DPA-LSTM-NN | $3\,{K_{\mathrm{on}}}^2 + 3\,{K_{\mathrm{p}}}^2 + 6\,K_{\mathrm{on}}\,K_{\mathrm{p}} + 159/2\,K_{\mathrm{on}} + 3/2\,K_{\mathrm{p}}$ | $157/2\,K_{\mathrm{on}} + 21/2\,K_{\mathrm{p}} - 8$ |

Following [18], the overall number of real-valued operations of the LSTM unit is given by

$$C_{\mathrm{LSTM}}^{\mathrm{Mult}} = 4P^2 + 4PU + 3P, \tag{37}$$

$$C_{\mathrm{LSTM}}^{\mathrm{Sum}} = 13P + 4U - 8. \tag{38}$$

The LSTM-NN-DPA estimator considers $U = 2\,(K_{\mathrm{on}} + K_{\mathrm{p}}) = 112$ inputs for the LSTM, where the multiplication by two takes both real and imaginary parts into account, and $P = K_{\mathrm{on}} = 52$ hidden states. In addition, the input size of the NN matches the size of the LSTM output, as well as its output, that is related to the number of subcarriers, so that $N_0 = N_2 = 2\,K_{\mathrm{on}} = 104$. Also, $N_1 = 15$ has been considered for all schemes in this paper. Thus, combining the computational complexity of the LSTM, the NN and the DPA corresponds to $12\,{K_{\mathrm{on}}}^2 + 81\,K_{\mathrm{on}} + 8\,K_{\mathrm{on}}\,K_{\mathrm{p}}$ multiplications/divisions and $89K_{\mathrm{on}} + 8\,K_{\mathrm{p}} - 8$ summations/subtractions.

In addition, the LSTM unit of the LSTM-DPA-TA scheme has $U = 2K_{\mathrm{on}} = 104$ inputs and $P = K_{\mathrm{on}} = 52$ hidden states, while the TA technique requires $2\,K_{\mathrm{on}}$ multiplications/divisions and $2\,K_{\mathrm{on}}$ summations/subtractions. Thus, combining the complexity of the LSTM, DPA and TA leads to $12\,{K_{\mathrm{on}}}^2 + 23\,K_{\mathrm{on}}$ multiplications/divisions and $31K_{\mathrm{on}} - 8$ summations/subtractions.

By its turn, the proposed DPA-LSTM-NN estimator with subcarrier sampling employs the DPA initial estimation, followed by the LSTM unit with $P = \frac{K_{\mathrm{on}} + K_{\mathrm{p}}}{2} = 28$ hidden states and $U = K_{\mathrm{on}} + K_{\mathrm{p}} = 56$ inputs, with an additional NN layer with $N_0 = N_2 = 2K_{\mathrm{on}} = 104$ and $N_1 = 15$ neurons. We obtain, thus, the complexity as

$$C_{\mathrm{DPA-LSTM-NN}}^{\mathrm{Mult}} = 3\,{K_{\mathrm{on}}}^2 + 3\,{K_{\mathrm{p}}}^2 + 6\,K_{\mathrm{on}}\,K_{\mathrm{p}} + \frac{159}{2}\,K_{\mathrm{on}} + \frac{3}{2}\,K_{\mathrm{p}} \tag{39}$$

and

$$C_{\mathrm{DPA-LSTM-NN}}^{\mathrm{Sum}} = \frac{157}{2}\,K_{\mathrm{on}} + \frac{21}{2}\,K_{\mathrm{p}} - 8. \tag{40}$$

Table 4 summarizes the real-valued operations required by the channel estimation

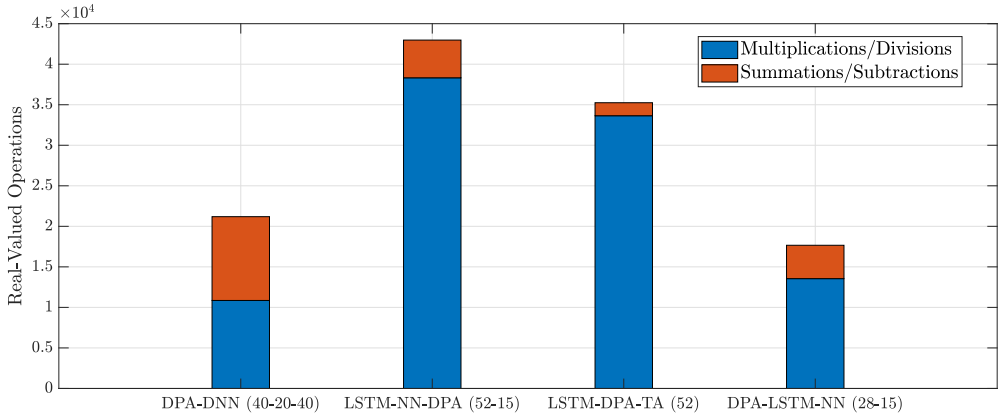


**Figure 33 – Computational complexity in terms of real-valued operations with $K_{\text{on}} = 52$ subcarriers and $K_{\text{p}} = 4$ pilots.**

schemes, as a function of the number of active subcarriers. As we observe, the proposed DPA-LSTM-NN scheme has the smallest coefficients for the most significant factors associated to $K_{\text{on}}$ in the operations of multiplications and divisions, consisting in the most impactful in the complexity of the considered estimators. This is relevant in the case, *e.g.*, of a different communication standard employing a different number of active and pilots subcarriers, so that our solution would still present a lower complexity compared to other LSTM-based solutions in the literature. In addition, Figure 33 illustrates the computational complexity of the schemes in the case of $K_{\text{on}} = 52$ subcarriers and $K_{\text{p}} = 4$ pilots. We observe that the proposed DPA-LSTM-NN estimator with subcarrier sampling has at least 49.9% less real-valued operations than other LSTM-based solutions, and 16.7% less real-valued operations than the DPA-DNN scheme, while also improving the BER at the same time.

## 5.5 Ensemble learning for vehicle channel estimation generalization

As well as other receivers present in the literature [16–18], the DPA-LSTM-NN scheme considers the training on a specific channel model, even though the channel characteristics are subject to variation and are dependent on the environment in which the vehicles are operating. The most important factors to dictate the performance of the DNN-based schemes are the channel PDP, the vehicle speed, and the modulation order used in communication. Consequently, fixing the training for a given channel will significantly degrade performance when the vehicle communicates under a different channel scenario, limiting its practical deployment.

**Algorithm 1** Ensemble Learning

**Require:** $M$ LSTM-NN models $\{m_1, m_2, \cdots, m_M\}$ trained on different subsets, with the same architecture and hyperparameters
**Require:** Input data, $X$
**Ensure:** An ensemble prediction, EL

```
function BAGGING(m_1, m_2, ..., m_M)
    Initialize empty list of predictions, P ← []
    for i = 1 to M do
        Make prediction using m_i: p_i ← m_i.predict(X)
        Append p_i to P: P ← P + p_i
    end for
    Average the predictions in P: EL ← (1/M) Σ_{i=1}^{M} p_i
    return EL
end function
```

To extend the analysis of the proposed DPA-LSTM-NN estimator, we employ the EL technique to improve the overall performance by combining the predictions from multiple models trained with datasets considering different speeds, maximum Doppler shifts, and path delays. The principle of this proposal for generalization is described by the Algorithm 1. Here, we highlight the use of the Bagging method, in which the base models are trained independently and on different subsets of data using the same algorithm configuration, and the predictions of the base models are combined using averaging with equal weight in the final prediction [65]. This choice was given the potential of the Bagging algorithm to decrease the variance of the estimate by combining multiple predictions, thus avoiding overfitting [66]. In the EL algorithm, the function "Bagging" takes $M$ LSTM-NN models $\{m_1, m_2, \cdots, m_M\}$ as input, that have been trained on different subsets with the same architecture and hyperparameters. Then, the function returns an ensemble prediction (EL) that averages predictions of the $M$ LSTM-NN models obtained.

The function initializes $\mathcal{P}$ to be an empty list of predictions. It then loops through the prediction of each input model $m_i$, from $i = 1$ to $M$, obtained using $m_i.predict(X)$. Each prediction $p_i$ is appended to $\mathcal{P}$ and then averaged to obtain the ensemble prediction EL, which is the final output of the algorithm. By using this method, the final EL prediction is able to integrate the different offline trained models, combining the strengths of multiple LSTM-NN models trained on different datasets to achieve generalized prediction performance, increasing the flexibility and robustness of the receiver against changes in the wireless channel conditions. Figure 34 presents the block diagram of the DPA-LSTM-NN channel estimator with EL.

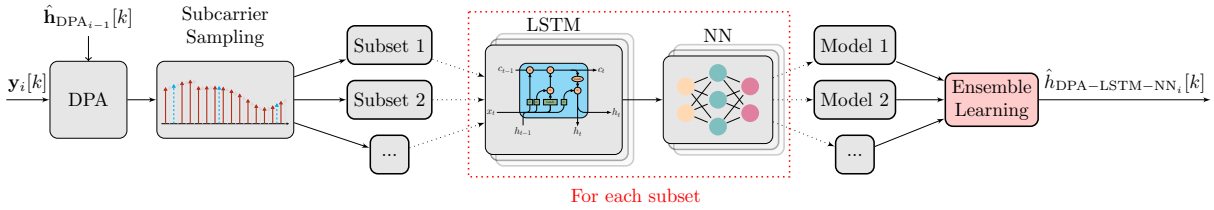


**Figure 34 – Block diagram of the DPA-LSTM-NN channel estimator with EL.**

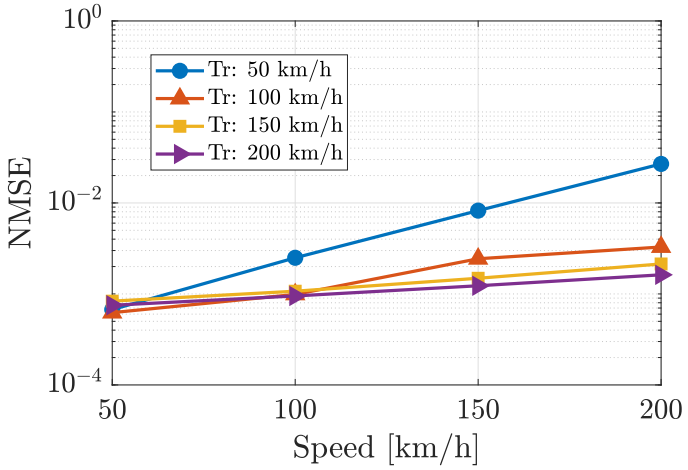


**Figure 35 – NMSE for models trained with different speeds on the R2V-UC scenario.**

### 5.5.1 Simulation results

We analyze the performance impact of employing the EL technique on the DPA-LSTM-NN estimator to generalize the solution for different scenarios. We consider single-antenna nodes, with a transmitted OFDM frame size of $L = 50$ symbols in the scenario based on the IEEE 802.11p standard.

In Figure 35, a fixed SNR = 30 dB is considered to analyze the NMSE performance of DPA-LSTM-NN models trained with different speeds for the same considered PDP, deployed as the R2V-UC scenario. The results show that models trained at higher speeds than those considered in the tested scenario exhibit certain robustness, with minimized estimation error. However, it is important to note that this robustness does not hold when different PDPs are considered during testing, requiring a model that can handle this variation. Therefore, in the subsequent analysis, we focus on the BER performance of the EL model, where $M = 4$ models are trained and combined using Algorithm 1. Specifically, our EL approach considers $m_1 = \{\text{R2V-UC}, v = 50 \text{ km/h}\}$, $m_2 = \{\text{R2V-UC}, v = 200 \text{ km/h}\}$, $m_3 = \{\text{V2V-EX}, v = 50 \text{ km/h}\}$, and $m_4 = \{\text{V2V-EX}, v = 200 \text{ km/h}\}$, given the PDP in Table 2. Then, we compare the performance of the EL model with other models trained specifically for a given PDP/speed, in different scenarios.

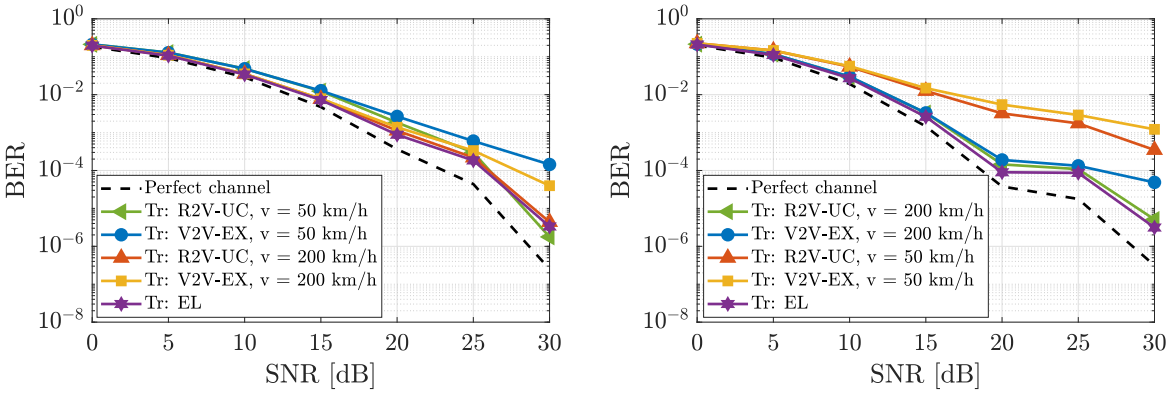


(a) $v = 50$ km/h. (b) $v = 200$ km/h.

**Figure 36 – BER for models trained with different datasets and tested on the R2V-UC dataset.**

Figure 36(a) presents the BER performance of the different models tested with a dataset deployed as the R2V-UC channel with $v = 50$ km/h. Notice that the legend of each curve indicates the scenario for which each model was trained. First, we note that the model trained with the same PDP/speed as the scenario under test is the one to achieve the best performance, while the model trained with the same PDP, but with a higher speed ($v = 200$ km/h) has almost negligible loss compared to this most effective model. Furthermore, the EL model exhibits almost negligible loss compared to the best-performing case. However, the same cannot be said when testing the models trained with a different PDP, *i.e.*, the V2V-EX channel in this case. In these cases, from 2 dB to 4 dB of performance loss is observed at the BER of $10^{-4}$.

The R2V-UC channel with $v = 200$ km/h is considered in Figure 36(b). As illustrated, there is a significant loss when moving to the high-speed scenario during the test of the models trained for a specific channel condition. In this case, it is observed that apart from the PDP considered when training the model, the choice of a dataset with speed lower than the one considered in the test phase is a crucial factor for performance loss. We observe that the EL model presents a slight performance gain in this scenario, while the models trained with the same PDP and lower speed $v = 50$ km/h or different PDP show a considerable performance loss.

Figure 37(a) shows the performance of the ensemble method for the case where the V2V-EX scenario is considered during the test phase of the models. Again, it can be noticed that for the models trained with $v = 50$ km/h, the one trained with a different PDP has a higher performance loss, which justifies the need for a combined model that generalizes the solution. Moreover, the performance loss of the EL model compared to the

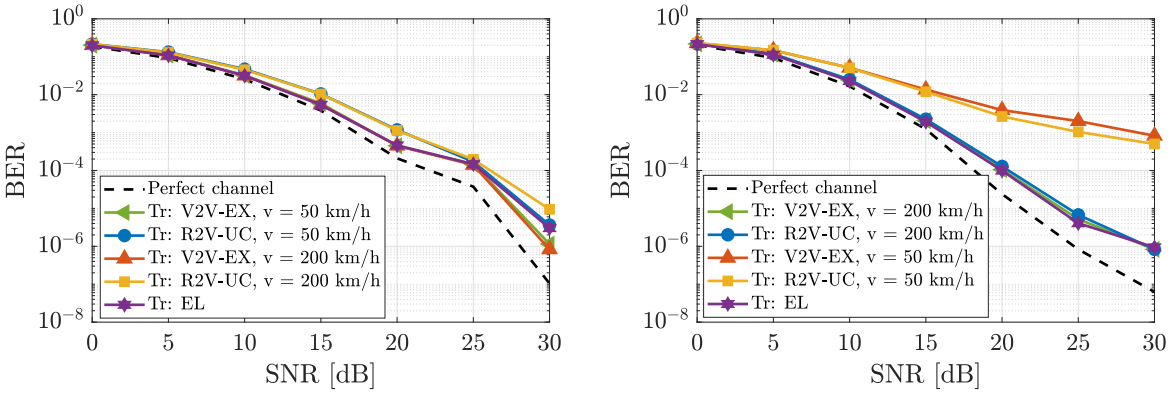


(a) $v = 50$ km/h. (b) $v = 200$ km/h.

**Figure 37 – BER for models trained with different datasets and tested on the V2V-EX dataset.**

models trained with same PDP can be understood by analyzing the path gains of the R2V-UC and V2V-EX channel models in Table 2. The fact that the V2V-EX channel model has lower average path gains compared to the R2V-UC entailed in a small performance loss for the low-speed scenario. Still, we emphasize that this loss is smaller than that presented by the models trained with different PDP, evidencing the ability of the EL model to adapt to harsh conditions.

Finally, Figure 37(b) shows that the models trained with $v = 50$ km/h are not adapted to estimate the channel with $v = 200$ km/h during the testing phase in the V2V-EX channel, presenting a loss higher than 10 dB in comparison to the EL model. This substantial loss is crucial to support that models trained for specific scenarios are insufficient to generalize the DNN-based solution for vehicular channel estimation, presenting several constraints for practical deployment. On the other hand, the EL model presents an interesting alternative by offering an estimation with considerably lower losses for different channels. Additionally, it is important to emphasize that these gains are achieved without adding computational complexity to the channel estimation, as the process of obtaining the combined EL model is done offline. Another relevant factor is related to the advantage of storage of a single model capable of estimating the channel in different scenarios, resulting in a gain compared to the storage and management of multiple models, which can be computationally expensive and can result in high storage costs, particularly when dealing with large datasets.

## 5.6 Conclusion

This chapter explores in depth the DPA-LSTM-NN estimator, a novel approach adapted to vehicular channel estimation. We begin with a comprehensive description of the method, characterized by its three fundamental components, starting with the initial DPA estimate, able to learn the time and frequency characteristics of the channel and reconstruct the estimation as close as possible to the ideal channel response. This is followed by LSTM structure, designed to deal with sequential data and capable of learning the channel correlation over time and efficiently predicting future channel realizations based on previous observations. Complementing these, the NN step is employed as an additional noise compensation step. Furthermore, the DPA-LSTM-NN method employs a subcarrier sampling approach at the input of the LSTM, strategically interpolating the subcarriers' information to effectively reduce the overall complexity of the solution when compared to the recently proposed benchmark schemes.

To begin, this estimator is validated in a scenario modeled in accordance with the IEEE 802.11p standard where it operates in the presence of a memoryless HPA. Our results confirm the superior performance of the estimator compared to state-of-the-art methods proposed in the literature. Moreover, we showcase the significant complexity reduction achieved through subcarrier sampling, demonstrating a solution with improved performance and notable complexity gain.

To extend the analysis, we also employ this proposed estimator in a scenario with more realistic NLD models, considering the effects of memory from the HPA. Our results highlight that utilizing more realistic NLD models has a substantial impact on the receivers' performances, a crucial aspect in the development of estimators for future vehicular communication applications. We further present a low-complexity method to compensate for part of the NLD memory effects on the transmitter side using only a priori known HPA information, while handling the remaining distortions along with channel estimation. The DPA-LSTM-NN estimator presents robustness face to the memory effects of the HPA. It outperforms other estimators in terms of NMSE performance and has an almost negligible error rate performance gap when comparing scenarios with memoryless and memory HPA with compensation. Furthermore, our results underline the importance of compensating the signal at the transmitter side when considering the memory effects of the HPA.

We also explore a proposal for generalizing of the method through the EL

technique, which combines models trained on different feature sets, covering various PDPs and vehicle mobilities. This approach provides robustness and general learning architecture for vehicular communication scenarios. The proposed estimator exhibits resistance to changes in the characteristics across different environments and channel models, resulting in an estimator that can work under varying conditions and leading to improved performance compared to a model trained for a specific channel condition. It is worth noting that this technique is cost-effective, with the combined model acquired offline and effectively reducing storage expenses. Therefore, the EL method offers a practical and efficient solution for accurate vehicular channel estimation in future real-world vehicular scenarios.

Motivated by the results presented, we intend to delve further into investigating the performance of LSTM-based solutions across modulation techniques other than OFDM. The aim is to explore prominent candidates for future vehicular communication scenarios and evaluate the efficiency of novel channel estimators in mitigating the NLD effects induced by HPAs, comparing them to existing methods. In this sense, OTFS modulation has emerged as a promising candidate for next-generation wireless communication systems, particularly well-suited for environments with high mobility.

# 6 LSTM-BASED CHANNEL ESTIMATION FOR OTFS SYSTEMS

This chapter proposes a novel receiver architecture for the OTFS waveform, one of the potential candidates for future communications networks in scenarios with high mobility. We first review the literature on OTFS modulation, which is followed by a presentation of the OTFS implementation considered in this chapter. Subsequently, we introduce two well-established techniques to be used as performance benchmarks for our proposed method for channel estimation in OTFS transmission subject to memoryless HPA-induced distortions. Finally, we present a comprehensive evaluation through detailed performance analysis.

It is important to point out that, in order to facilitate the understanding of this work and highlight the differences between the waveforms considered, this chapter introduces a new notation, which is not directly related to the notations considered in the previous chapters for OFDM communication.

## 6.1 Literature review

As vehicular communication scenarios continue to evolve, the demand for robust and efficient wireless communication systems becomes increasingly critical. In this context, although widely adopted, conventional multicarrier transmission schemes, such as OFDM modulation, reveal inherent limitations that may impair their effectiveness in future vehicular environments [19]. In response to this, OTFS [3, 20] has emerged as a promising modulation scheme, presenting a new approach to wireless communication. Unlike traditional modulation methods, OTFS uses the DD domain to encode and transmit information, making it robust to the doubly selective channel effects. The OTFS addresses the limitations of conventional communication systems in dynamic and highly dispersive environments. In addition, the ability of OTFS to effectively handle time-varying channels opens up new possibilities for communication technologies, being particularly suitable for high mobility scenarios and holding the promise of improved performance and extended applications in modern wireless systems.

Most of the existing techniques for channel estimation in OTFS are based on the DD domain pilot-adding method [21, 22]. A well-known approach in the literature is presented in [21], in which the authors propose a threshold-based estimation technique that considers an OTFS frame with embedded pilots, that is surrounded by a guard

band to avoid interference with the data symbols. Another work, presented in [22], also considers DD-embedded pilots along with data symbols, where a cross-correlation-based algorithm is presented to perform Doppler domain channel estimation. It is highlighted that the guard band insertion significantly degrades the spectral efficiency.

As analytically characterized by [42], although OTFS signals can exhibit lower PAPR compared to OFDM, the issue of high PAPR persists in such systems, posing a significant challenge in OTFS channel estimation. Consequently, researchers have dedicated several efforts to develop PAPR reduction techniques for OTFS [24, 67]. Nonetheless, studies that discuss the impact of high PAPR on channel estimation are still incipient in the OTFS literature and, as well as in [21,22], assume a linear communication environment. However, it is worth noting that in practical OTFS communication systems, nonlinearities in the RF interface can significantly impact the performance of channel estimation and the overall communication system [23], and addressing nonlinear effects will be crucial to developing robust and high-performance OTFS channel estimators. Furthermore, the analysis in [24, 68] highlights that adding pilot structures with high power in the DD domain can induce high PAPR and lead to these estimators becoming infeasible [23].

To avoid the problems in placing pilots and guard intervals in the DD domain, different methods for OTFS channel estimation with the pilot transmission done in the TF domain can be found, *e.g.*, in [68,69]. Although the proposal in [69] results in a significant reduction in pilot overhead and an increase in bandwidth efficiency, it comes at the cost of high computational complexity, as it considers that while pilots are transmitted in the TF domain, another OTFS frame is needed to send the data. On the other hand, in [68], the advantages of reducing interference between pilots and data are achieved through the successive interference cancellation method. However, this approach, while effective, offers less flexibility and adaptability compared to methods based on NNs, and can entail higher computational complexity.

In this chapter, we address channel estimation in OTFS systems considering HPA-induced nonlinearities. To this end, we propose a novel method based on TF domain channel estimation, reducing the PAPR while improving the capacity to detect OTFS signals. Inspired by our previous research findings, which concentrated on the OFDM channel, we show that it is possible to obtain a robust channel estimate without requiring signal linearization at the transmitter. Then, we effectively compensate for the nonlinearities along with the channel estimation. To validate the efficacy of our

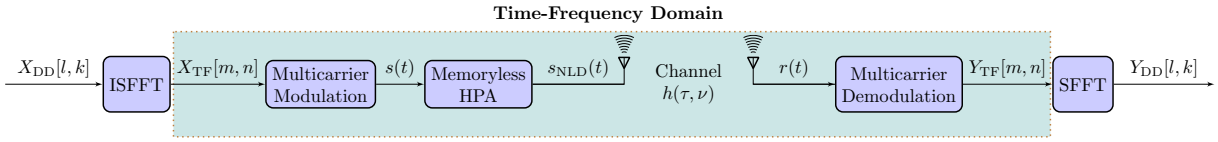


**Figure 38 – SFFT-based OTFS architecture.**

proposed estimator, we conducted a comparative analysis against the classic methods outlined in prior works [21, 22]. Our results present that this proposed method not only showcases enhanced precision in channel estimation, demonstrated through improved BER and PAPR performances, but also introduces a more efficient approach for OTFS communication systems within real-world scenarios. This is highlighted by a significant reduction in the computational complexity required for detecting the received signals compared to the benchmark methods.

## 6.2 SFFT-based OTFS

The most popular implementations for OTFS systems found in the literature use either the symplectic fast Fourier transform (SFFT) combined with a multicarrier modulation or the discrete Zak transform [39]. In this section, we first review the OTFS modulation implementation considered in this chapter, where the inverse SFFT (ISFFT) and SFFT operations are used to convert time-varying channels into invariant channels in the DD domain and vice versa, allowing us to interpret the OTFS system as pre- and post-processing blocks applied to a multicarrier signaling scheme.

### 6.2.1 OTFS modulation

Let us consider that the TF plane is sampled in time and frequency axes at intervals of $T$ (seconds) and $\Delta f$ (Hz), respectively. The multicarrier system is characterized as a block structure consisting of $N$ symbols with $M$ subcarriers each. As illustrated in Figure 38, the data symbols, denoted as $X_{\mathrm{DD}}[l,k]$, are mapped to the two-dimensional DD grid, where $l \in \{0,\ldots,M-1\}$ is the delay index and $k \in \{0,\ldots,N-1\}$ is the Doppler index. As a key component in OTFS modulation, the SFFT operation enables efficient signal mapping between DD and TF domains. Thus, the $M$-by-$N$ matrix of TF domain symbols is obtained via the ISFFT as

$$X_{\mathrm{TF}}[m,n] = \frac{1}{\sqrt{NM}} \sum_{k=0}^{N-1} \sum_{l=0}^{M-1} X_{\mathrm{DD}}[l,k] \cdot e^{j2\pi\left(\frac{nk}{N} - \frac{ml}{M}\right)}, \tag{41}$$

where the $m \in \{0, \ldots, M-1\}$ is the subcarrier index and $n \in \{0, \ldots, N-1\}$ is the symbol index.

The multicarrier modulation is performed on $X_{\mathrm{TF}}[m,n]$ to obtain the OTFS transmit signal $s(t)$ as

$$s(t) = \sum_{n=0}^{N-1} \sum_{m=0}^{M-1} X_{\mathrm{TF}}[m,n] \cdot g_{\mathrm{tx}}(t-nT) \cdot e^{j2\pi m\Delta f(t-nT)}, \tag{42}$$

where $g_{\mathrm{tx}}(t)$ is the pulse shape filter at the transmitter side. This operation is known as the Heisenberg transform, which describes a generalization of the IFFT transform, converting the TF-modulated signal into the time domain for transmission [3]. Finally, following a pattern similar to OFDM, a CP is appended at the beginning of each symbol before being transmitted.

For a more realistic characterization of wireless communication scenarios, our analysis considers that this time-domain signal is affected by HPA-induced nonlinearities, which follows the memoryless HPA model detailed in Section 3.2. This nonlinear signal, denoted as $s_{\mathrm{NLD}}(t)$, is then transmitted over a doubly selective channel being characterized by the delay-Doppler response [39]

$$h_{\mathrm{DD}}(\tau,\nu) = \sum_{k=1}^{\kappa} h_k \delta(\tau-\tau_k)\delta(\nu-\nu_k), \tag{43}$$

where $\tau$ and $\nu$ denote respectively delay and Doppler variables, $\kappa \in \mathbb{Z}$ is the number of resolvable propagation paths and $\delta(\cdot)$ is the Dirac delta function. Each path is represented by a $h_k \in \mathbb{C}$ channel coefficient and has a delay $\tau_k$ and Doppler frequency $\nu_k$. This response can be transformed to the TF domain using ISFFT as

$$\mathrm{H}_{\mathrm{TF}}[m,n] = \frac{1}{\sqrt{NM}} \sum_{\nu=0}^{N-1} \sum_{\tau=0}^{M-1} h_{\mathrm{DD}}(\tau,\nu) e^{j2\pi\left(\frac{n\nu}{N} - \frac{m\tau}{M}\right)} \tag{44}$$

Then, the signal at the OTFS receiver is given by

$$r(t) = \int\int h_{\mathrm{DD}}(\tau,\nu) e^{j2\pi\nu(t-\tau)} s_{\mathrm{NLD}}(t-\tau) d\tau d\nu + w(t), \tag{45}$$

where $w(t) \sim \mathcal{N}(0,\sigma_w^2)$ is the AWGN in the time domain.

Next, the multicarrier demodulation of the received signal $r(t)$ is performed through the Wigner transform, which presents the inverse of the Heisenberg transform. Thus, the TF domain signal is obtained as

$$Y_{\mathrm{TF}}[m,n] = \int r(t) g_{\mathrm{rx}}^{\dagger}(t-nT)\, e^{-j2\pi m\Delta f(t-nT)} dt, \tag{46}$$

where $g_{\text{rx}}^{\dagger}(t)$ represents the conjugate of the pulse shape filter at the receiver side. We consider the rectangular waveform for both $g_{\text{tx}}(t)$ and $g_{\text{rx}}(t)$ [70, 71].

By employing suitable equalization and decoding, the wireless communication channel can be effectively utilized for signal detection on the receiver side. Also, it is noted that the equalization process can be conducted in either TF or DD domains, in which the receivers in the DD domain often confers a higher degree of complexity. Referring to the details provided in [72], our system adopts the one-tap channel to derive the MMSE equalizer within the TF domain. This equalizer is mathematically represented as follows

$$\text{EQ}[m,n] = \frac{\text{H}_{\text{TF}}^{\dagger}[m,n]}{|\text{H}_{\text{TF}}[m,n]|^2 + \sigma_w^2}. \tag{47}$$

Thus, the received signal after equalization $\hat{X}_{\text{TF}}[m,n]$ can be obtained as

$$\hat{X}_{\text{TF}}[m,n] = Y_{\text{TF}}[m,n]\text{EQ}[m,n]. \tag{48}$$

## 6.3 Benchmark schemes on OTFS channel estimation

The literature related to OTFS channel estimation usually involves estimating the channel characteristics in the DD domain. In this section, we present two well-established techniques, which we will denote as threshold channel estimation (TCE) [21] and correlation channel estimation (CCE) [22], to be used as performance benchmarks for our proposed LSTM-based channel estimator.

### 6.3.1 Threshold channel estimation (TCE)

The work in [21] is a seminal work for channel estimation in OTFS systems. The authors introduced an embedded pilot scheme, in which a sufficiently large guard interval is applied around a unique pilot to improve the acquisition of delay and Doppler responses. As illustrated by Figure 39, the pilot and data symbols are allocated in the OTFS frame as

$$X_{\text{DD}}[l,k] = \begin{cases} \text{pilots} & \text{if } l = l_p, k = k_p \\ 0 & \text{if } (l_p - G_l \le l \le l_p + G_l, k_p - G_k \le k \le l_k + G_k)\,, \\ \text{data} & \text{otherwise} \end{cases} \tag{49}$$

where $G_l$ and $G_k$ present the guard band along the delay and Doppler axis, respectively. Moreover, the pilot position ($l_p$,$k_p$) is known at the receiver side. This positioning of the

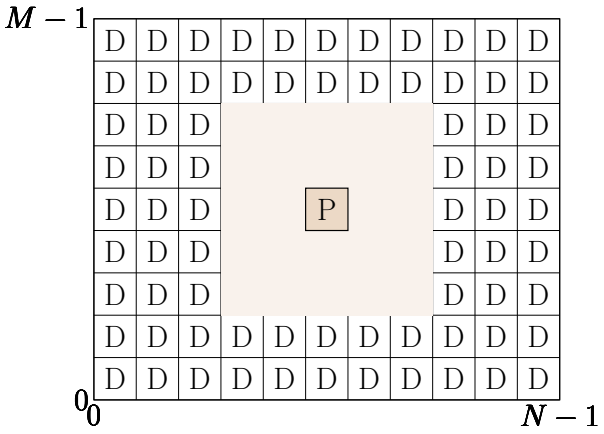


**Figure 39 – DD domain frame structure for the TCE scheme proposed by [21], where D denotes the data subcarriers and P the pilot, surrounded by the guard interval.**

pilot is strategic, allowing a simple channel estimation process by analyzing the received signal values around the DD grid of this embedded pilot. This guarantees that the receiver can segment the frame into one group comprising pilot and guard symbols, dedicated to channel estimation, and another group consisting of symbols for data detection. Such a structure ensures that received symbols designated for channel estimation do not interfere with those intended for data detection.

The channel estimation is based on the received symbols $\mathrm{Y}_{\mathrm{TCE}}[l,k]$ for the subgrid $(l_p - G_l \leq l \leq l_p + G_l, k_p - G_k \leq k \leq l_k + G_k)$. Thus, using the threshold method in which, for this grid, the estimated channel is given as

$$\widetilde{h}_{\mathrm{DD}_{\mathrm{TCE}}}[l-l_p, k-k_p] = \begin{cases} \frac{Y_{\mathrm{TCE}}[l,k]}{X_{\mathrm{DD}}[l_p,k_p]}, & \text{if } Y_{\mathrm{TCE}}[l,k] \geq \Upsilon \\ 0, & \text{otherwise} \end{cases}, \tag{50}$$

with $\Upsilon$ being the detection threshold, which is arbitrarily fixed as $\Upsilon = 3\sigma_w$. So, if there is a path, it can be seen on the receiver side as a scaled version of the pilot plus Gaussian noise [73]. Finally, the estimated channel is used for data detection.

### 6.3.2 Correlation channel estimation (CCE)

In [22], the authors propose an estimator for OTFS systems in which the cross-correlation channel matrix is acquired through estimation in the DD domain. As presented in Figure 40, they assume that the channel is invariant for more than one symbol duration, so that the pilot and information are sent at different frames. Thus, the pilot signal in

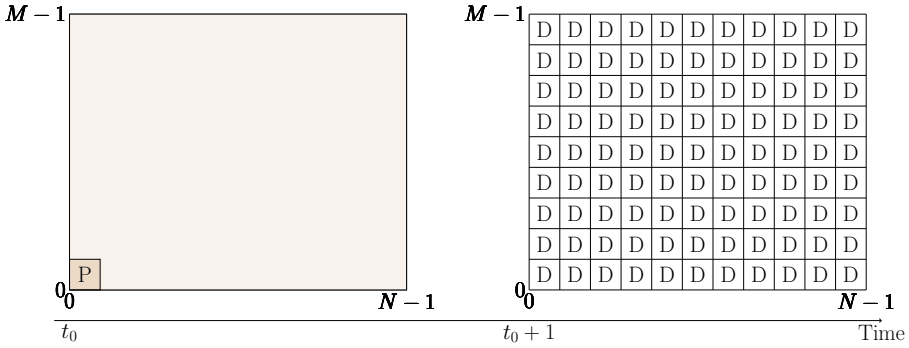


**Figure 40 – DD domain frame structure for the CCE scheme proposed by [22], where the P pilot and the D data subcarriers are sent at adjacent frames.**

the DD domain is considered as

$$X_{\mathrm{DD}}[l,k] = \begin{cases} 1 & \text{if } l = l_p, k = k_p \\ 0 & \text{otherwise} \end{cases}. \tag{51}$$

Thus, the estimated channel response in the DD domain be written as

$$\widetilde{h}_{\mathrm{DD}_{\mathrm{CCE}}}[l,k] = \sum_{p=1}^{P} h_p \delta((l-l_p)_{\mathrm{M}} - l_{\tau_p})\psi_p[l], \tag{52}$$

where $l_{\tau_p}$ is the path delay in the DD domain and $\psi_p$ is the phase shift due to the Doppler effect. Finally, this estimator is based on a cross-correlation function across Doppler delay elements, detailed in [22].

While the CCE outperforms existing approaches in the literature, it does exhibit error floors under a high SNR, which is a challenge for channel estimation in prospective OTFS applications. In addition, common to [21, 22] is that these works require a substantial guard interval to mitigate the interference of unknown data symbols in the pilots used for channel estimation. In addition, a high pilot SNR is required by the schemes proposed by [21, 22], which results in high signaling and pilot overheads to ensure accurate CSI estimation. As an important conclusion, these aspects can potentially negatively impact the PAPR of the transmitted signal, as highlighted in [23], and which can jeopardize their practical application.

## 6.4 Proposed LSTM-based channel estimation for OTFS

We propose a new channel estimation scheme for OTFS systems subject to HPA-induced distortions. Our method starts with an initial channel estimate derived from the

preamble and the frequency-domain pilots. This estimate serves as input to an LSTM layer, effectively tracking the channel's behavior. Subsequently, a shallow NN is applied to increase the denoising capability and refine the estimation accuracy. Through these steps, we can maintain low pilot overhead and attain a reliable channel estimation, especially when dealing with nonlinear and highly selective channels.

Inspired by the IEEE 802.11p standard, we consider a basic transmitted packet consisting of a preamble with a known deterministic sequence, used for primary synchronization of the channel, followed by the data field. In the data field, $M$ subcarriers are employed within each symbol, in which only $M_{\mathrm{on}}$ are active and the other are inactive subcarriers. In addition, considering the $M_{\mathrm{on}}$ subcarriers, $M_{\mathrm{p}}$ of them are allocated as pilots, while the remaining $M_{\mathrm{d}}$ subcarriers carry the data.

In our proposal, the pilots are incorporated in the TF domain and, consequently, the number of subcarriers reserved for data transmission in the DD domain is decreased, while preserving the same subcarrier spacing and bandwidth. Let us first denote the set of data subcarriers as $\mathcal{M}_{\mathrm{d}}$, so that $M_{\mathrm{d}} = |\mathcal{M}_{\mathrm{d}}|$, while the set of pilot subcarriers is $\mathcal{M}_{\mathrm{p}}$, with $M_{\mathrm{p}} = |\mathcal{M}_{\mathrm{p}}|$. Then, our configuration results in a frame with $M_{\mathrm{d}} = M - M_{\mathrm{p}}$ subcarriers dedicated to data, and we first transform $X_{\mathrm{DD}}$ to the TF domain, but only taking the data into account, obtaining the $M_{\mathrm{d}}$-by-$N$ matrix

$$X_{\mathrm{TF_d}}[m_{\mathrm{d}}, n] = \frac{1}{\sqrt{N M_{\mathrm{d}}}} \sum_{k=0}^{N-1} \sum_{l \in \mathcal{M}_{\mathrm{d}}} X_{\mathrm{DD}}[l, k] e^{j2\pi \left( \frac{nk}{N} - \frac{ml}{M_{\mathrm{d}}} \right)}, \tag{53}$$

in which $m_{\mathrm{d}} \in \mathcal{M}_{\mathrm{d}}$, and the pilot subcarriers are subsequently inserted by doing

$$X_{\mathrm{TF}}[m, n] = \begin{cases} \text{pilots} & \text{if } m \in \mathcal{M}_{\mathrm{p}} \\ X_{\mathrm{TF_d}}[m, n] & \text{if } m \in \mathcal{M}_{\mathrm{d}} \end{cases}. \tag{54}$$

Figure 41 illustrates the TF domain frame structure given in (54), in which the D represent the data subcarriers, obtained from (53), while P denotes the pilot subcarriers. In addition, the preamble is shown as PR. Importantly, this configuration ensures that there is no overlap between the pilot and data subcarriers, optimizing the use of available resources in our estimation process.

We initiate our estimation process by utilizing the LS method for the preamble and pilot information in the frequency domain. The initial channel estimation in the

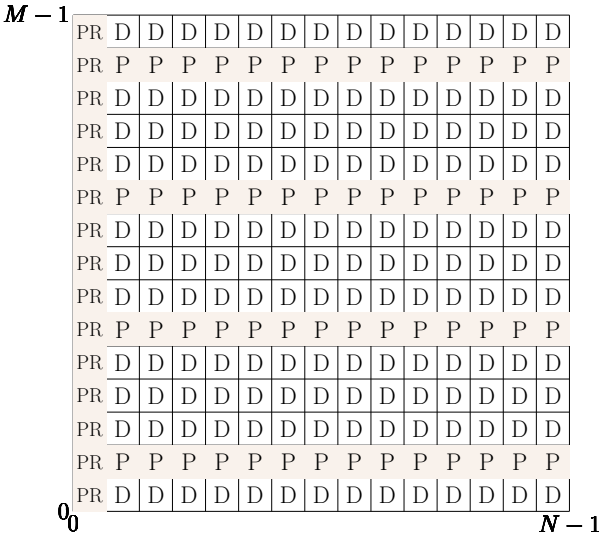


**Figure 41 – TF domain frame structure for the proposed initial channel estimation. Here we denote the pilot subcarriers as P, the preamble as PR and D as the data subcarriers.**

preamble is obtained as

$$\hat{\mathrm{H}}_{\mathrm{TF_{LS}}}[m, n_{\mathrm{pr}}] = \frac{\mathrm{Y}[m, n_{\mathrm{pr}}]}{\mathcal{P}[m]}, \quad \forall m, \tag{55}$$

where $\mathrm{Y}[m, n_{\mathrm{pr}}]$ is the frequency domain signals for each $m$-th subcarrier, obtained by the demodulation of the training sequences from the preamble at the $n_{\mathrm{pr}}$ symbol positions. Furthermore, $\mathcal{P}[m]$ represents the frequency domain predefined preamble sequence.

On the pilots' subcarriers, the initial channel estimation is obtained as

$$\hat{\mathrm{H}}_{\mathrm{TF_{LS}}}[m_{\mathrm{p}}, n] = \frac{\mathrm{Y}[m_{\mathrm{p}}, n]}{\mathrm{S}[m_{\mathrm{p}}, n]}, \quad \forall n. \tag{56}$$

Thus, for each $n$-th symbol, $\mathrm{Y}[m_{\mathrm{p}}, n]$ and $\mathrm{S}[m_{\mathrm{p}}, n]$ represent the frequency domain received and transmitted signals at the $m_{\mathrm{p}} \in \mathcal{M}_{\mathrm{p}}$ pilot positions, respectively. It should be noted here that, unlike the proposals in [21,22], the pilots have the same power as the transmitted signal. Finally, to avoid interference in the training of LSTM-NN network, which will be further explained, the information in the $M_{\mathrm{d}}$ data subcarriers is considered as null to build the initial channel estimation $\hat{\mathrm{H}}_{\mathrm{TF_{LS}}}[m, n]$. Consequently, the pilot information is used as the basis for interpolating the data carriers' information and obtain final estimation of the channel.

Taking advantage of the performance gain of the LSTM-based over traditional DNN-based receivers, as the analysis presented in Chapter 5 for the OFDM transmission. Thus, we consider the frame illustrated in Figure 41 as the initial point to perform

LSTM-based interpolation for the data positions and obtain the channel information for the entire frame. Finally, aiming to reduce the noise, the output of the LSTM layer is further processed by a shallow NN with $\omega$ neurons. The goal of the LSTM-NN network is to update the estimation initially obtained and learn to correct the estimation errors compared to the channel with perfect CSI. The NN network is trained to determine the parameter $\theta^{\star}$ that minimizes the loss function $\ell$, which measures the approximation

$$\theta^{\star} = \underset{\theta}{\operatorname{argmin}}\ \ell\left(\theta, \hat{\mathrm{H}}_{\mathrm{TF}_{\mathrm{LSTM}}}[m,n], \mathrm{H}_{\mathrm{TF}}[m,n]\right), \tag{57}$$

where $\theta$ represents the NN weight vector, $\mathrm{H}_{\mathrm{TF}}[m,n]$ is the perfect channel response obtained from the vector of training samples, used during the training stage of the proposed estimator, while $\hat{\mathrm{H}}_{\mathrm{TF}_{\mathrm{LSTM}}}[m,n]$ is the output of the LSTM.

The loss is evaluated as

$$\begin{aligned} &\ell\left(\theta, \hat{\mathrm{H}}_{\mathrm{TF}_{\mathrm{LSTM}}}[m,n], \mathrm{H}_{\mathrm{TF}}[m,n]\right) = \\ &\frac{1}{NM}\sum_{m=0}^{M-1}\sum_{n=0}^{N-1}\left|\mathrm{H}_{\mathrm{TF}}[m,n] - \hat{f}\left(\hat{\mathrm{H}}_{\mathrm{TF}_{\mathrm{LSTM}}}[m,n];\theta\right)\right|^2, \end{aligned} \tag{58}$$

where $\hat{f}\left(\hat{\mathrm{H}}_{\mathrm{TF}_{\mathrm{LSTM}}}[m,n];\theta\right)$ is the output of the NN, represented as a function of LSTM estimate $\hat{\mathrm{H}}_{\mathrm{TF}_{\mathrm{LSTM}}}$.

Notice that this process during the training stage is iterative, with the LSTM-NN network adapting $\hat{f}\left(\hat{\mathrm{H}}_{\mathrm{TF}_{\mathrm{LSTM}}}[m,n];\theta\right)$ given each training sample. Finally, the final channel estimation is obtained as

$$\hat{\mathrm{H}}_{\mathrm{LS-LSTM-NN}}[m,n] = \hat{f}\left(\hat{\mathrm{H}}_{\mathrm{TF}_{\mathrm{LSTM}}}[m,n];\theta^{\star}\right). \tag{59}$$

Figure 42 shows the block diagram of the proposed LS-LSTM-NN channel estimator for OTFS systems. Combining the initial estimate, LSTM, and NN provides robustness for estimating a channel with unknown instantaneous variation. In addition, the use of multiple pilot symbols is advantageous due to a substantial reduction in the PAPR of OTFS signals. Notably, this approach aligns with practical scenarios characterized by nonlinearities [23]. Also importantly, our analysis shows that this achievement does not compromise the spectral efficiency. In fact, our proposed solution achieves nearly optimal performance in this regard, reinforcing the effectiveness of our approach.

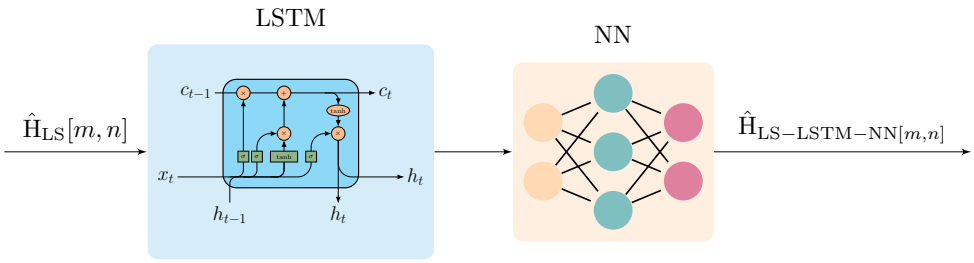


**Figure 42 – Block diagram of the proposed LS-LSTM-NN estimator.**

### 6.4.1 BER analysis

We conduct a comparative analysis to evaluate the performance of the LS-LSTM-NN receiver within a scenario affected by distortions resulting from HPA nonlinearities. The performance evaluation scheme is done in terms of BER, throughput and PAPR. We compare our proposal with the benchmark methods TCE [21] and CCE [22], in which channel estimation is done using the pilot response in the delay-Doppler domain. For both benchmark methods, the SNR for the pilots is assumed to be $\mathrm{SNR_p} = 40$ dB, as per their design.

To ensure compatibility, we also follow the physical layer specifications of the IEEE 802.11p [27] communication standard presented in Table 1. We consider a frame with $M = 64$ subcarriers and $N = 14$ symbols, which is sufficiently large to neglect the effect of fractional delay and Doppler shifts. Consequently, integer Doppler values are presumed. Furthermore, we account for turbo LTE coding with a rate of 1/2 and utilize the MMSE criterion for equalization. It is also important to note that, unlike the other estimators, our proposed method conducts the equalization process within the TF domain[1]. Our results show the performances in a scenario with the vehicles moving at speed $v = 300$ km/h and [16-QAM, QPSK] modulation orders. Furthermore, our evaluation takes into consideration the impact of HPA nonlinearities considering an $\mathrm{IBO} = 4$ dB for the highest modulation order and $\mathrm{IBO} = 2$ dB for the nonlinear effects on QPSK modulation.

Figure 43 compares the BER of the channel estimation methods in a scenario involving QPSK modulation and $\mathrm{IBO} = 2$ dB. As shown, the estimators perform similarly at low SNR. Nevertheless, as the SNR increases over 20 dB, an error floor becomes evident in the benchmark estimators. In contrast, the LS-LSTM-NN estimator is the best

[1]During our evaluations across the different scenarios, we found that conducting DD equalization within the channel estimated with our method led to detection results similar to those in the TF domain, but with increased computational complexity.

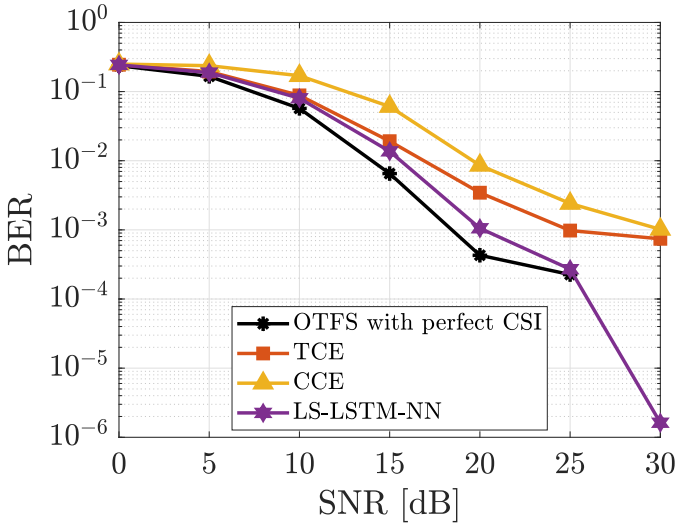


**Figure 43 – BER analysis for $v = 300$ km/h and QPSK modulation and IBO $= 2$ dB.**

performer, closely approaching the detection performance when perfect CSI is considered. Remarkably, even with an elevated SNR level of 30 dB, our estimator is the only one capable of achieving a BER below $10^{-3}$, presenting a gain of at least 5 dB for this particular error rate threshold, compared to [21, 22].

Next, Figure 44 evaluates the BER performance considering a 16-QAM modulation and IBO $= 4$ dB. Similarly to the results observed in QPSK modulation, at low SNR the considered channel estimators exhibit comparable performances. However, a notable gain is observed for the proposed method in the high SNR region. Furthermore, both estimators presented in [21] and [22] show an even more expressive error floor at high SNR for scenarios with higher modulation order. Consequently, these estimators fail to reduce the BER to a level lower than $10^{-2}$ during signal detection.

The subsequent PAPR analysis will further explore this result. Higher modulation orders yield greater variations in the amplitude of the transmitted signal, which significantly affects the detection of benchmark estimators. In this sense, we remark that the increased performance of the proposed LS-LSTM-NN is evident, as it is the only one capable of achieving an error rate of $10^{-3}$ and, therefore, is the sole one to provide reliable channel estimates in such scenarios.

### 6.4.2 Throughput analysis

Complementing the BER analysis, we now compare the channel estimators in terms of system throughput. Our proposed estimator operates within a frame structure

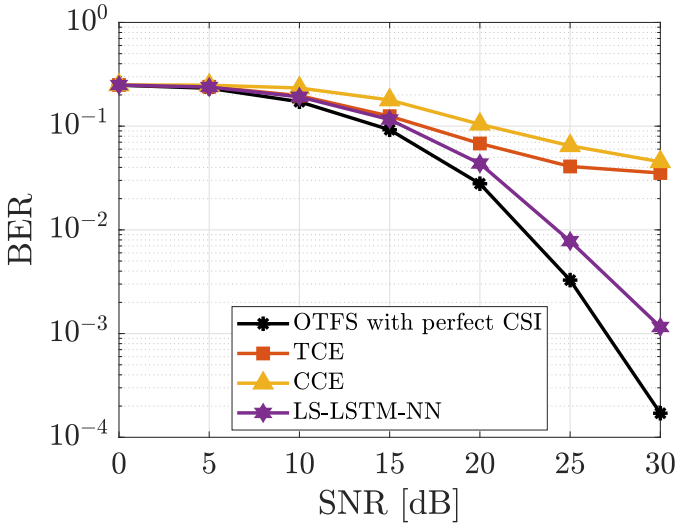


**Figure 44 – BER analysis for $v = 300$ km/h and 16-QAM modulation and IBO = 4 dB.**

where $M_{\mathrm{p}} = 8$ subcarriers are designated as pilots in the frequency domain. Meanwhile, $M_{\mathrm{d}} = 44$ subcarriers carry data, and the additional 12 subcarriers act as a guard band. Moreover, these symbols are preceded by a unique preamble. Thus, the data density of the transmitted frame can be written as

$$\eta_{\mathrm{LS-LSTM-NN}} = \frac{N \cdot M_{\mathrm{d}}}{(N+1) \cdot M} \approx 64\%. \tag{60}$$

To ensure a fair comparison, we consider that the channel estimator proposed by [21] takes into account a frame with a single pilot inserted in the DD domain that is surrounded by a guard band that achieves a data density similar to our proposal, except for the preamble. Thus,

$$\eta_{\mathrm{TCE}} = \frac{N \cdot M_{\mathrm{d}}}{N \cdot M} \approx 69\%. \tag{61}$$

In contrast, since the estimator introduced in [22] adopts an arrangement where pilot and data transmissions are transmitted in separate frames, as depicted in Figure 40, this design leads to a spectral efficiency of

$$\eta_{\mathrm{CCE}} = 50\%, \tag{62}$$

which clearly marks a reduction in the overall spectral efficiency compared to the TCE method and the proposed LS-LSTM-NN scheme. This loss can be analyzed by comparing the throughput of the transmission, calculated as

$$T_i = \eta_i \cdot B \cdot (1 - \mathrm{BER}_i), \tag{63}$$

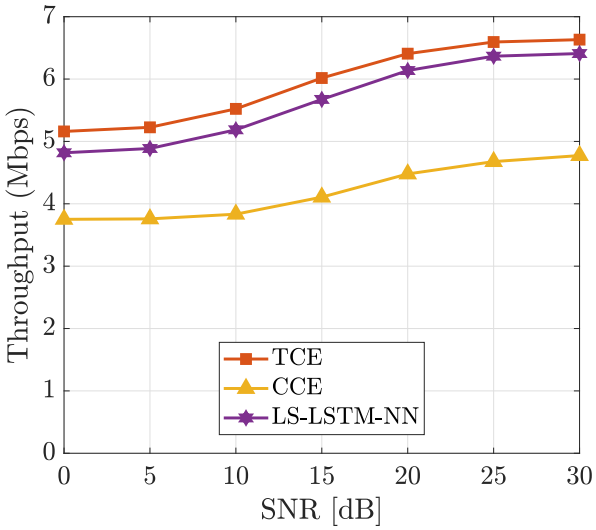


**Figure 45 – Throughput analysis for $v = 300$ km/h, 16-QAM modulation and IBO = 4 dB.**

where the index $i$ is used to differentiate the different channel estimation schemes.

Figure 45 presents the throughput comparison for the different estimators, considering $N = 14$ symbols, $v = 300$ km/h, 16-QAM modulation, and IBO $= 4$ dB. As illustrated, the estimator proposed in [21] is the one that offers the best performance in terms of throughput, which is mainly due to the choice of the guard band to define the spectral efficiency in (61). However, our proposed estimator closely approaches this benchmark while outperforming the method introduced by [22]. Moreover, it is important to highlight that the slight reduction in the throughput of our approach is counterbalanced with substantial enhancements in terms of BER, as illustrated by Figure 44. An additional investigation of the throughput in the same scenario, but with a fixed SNR of 30 dB and different frame sizes $N$, presented in Figure 46, reveals an important trend. Our proposed solution exhibits improved performance as the block size increases, which is expected due to the use of a unique preamble. For instance, when the frame size is $N \geq 30$ symbols, the proposed LS-LSTM-NN scheme outperforms [21, 22] in terms of throughput.

### 6.4.3 PAPR analysis

The PAPR analysis holds critical significance within real-world communications scenarios. In this subsection, we compare the channel estimation techniques in terms of their impact on the CCDF, defined by (10), which is often employed to assess signal PAPR distortion and provides insights into the probability of signal exceeding a given power level $\gamma$.

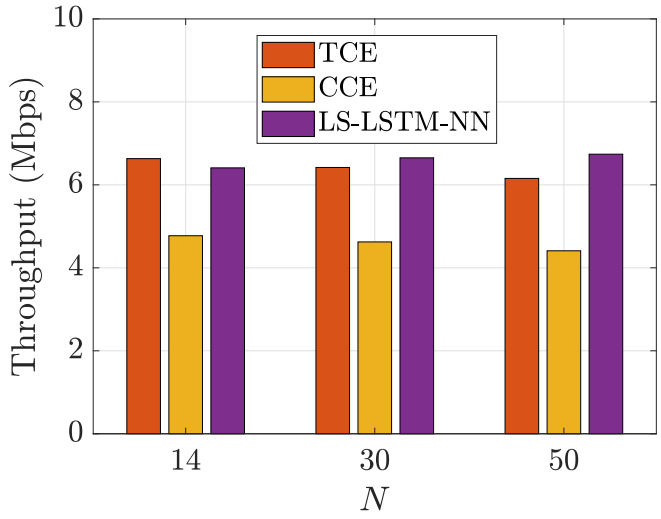


**Figure 46 – Throughput analysis for $v = 300$ km/h, 16-QAM modulation, IBO = 4 dB, and SNR = 30 dB for different frame sizes.**

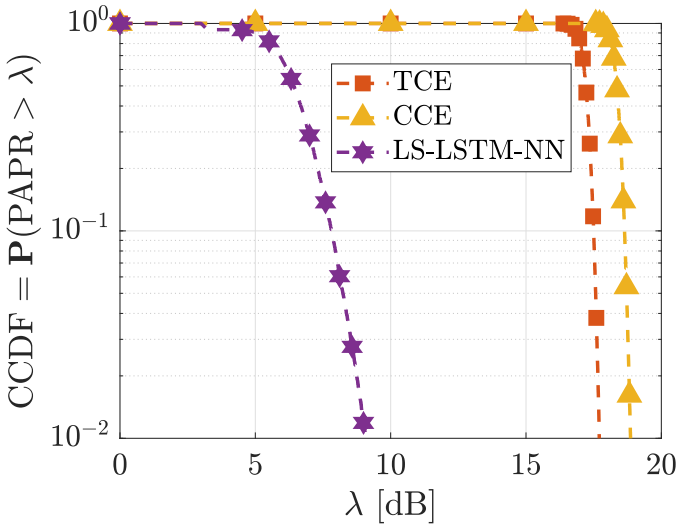


**Figure 47 – PAPR analysis.**

The CCDF analysis comparing the different estimators is illustrated in Figure 47. As we observe in the figure, the comparison between the estimators highlights the problem of allocating pilots with very high power to facilitate channel estimation in the DD domain. Specifically, the proposed LS-LSTM-NN estimator yields a PAPR threshold gain of at least 8 dB when compared with the method proposed in [21]. Moreover, this advantage is even more pronounced when compared to the estimator presented in [22].

Let us remark that determining an acceptable PAPR threshold depends on several factors, including the specific attributes of the communication system, the characteristics of the HPA, and the performance requirements of the application. Additionally, we point out that the PAPR limitation due to high power pilots in the DD domain is a factor already investigated in the existing literature [23]. Nevertheless, maintaining a lower PAPR holds paramount importance in mitigating the distortion induced by HPAs. This importance arises from the indication that the efficiency of HPA decreases with the increase of the PAPR of the input signal, as notable in (11). Indeed, it is worth noting that higher PAPR values can significantly jeopardize the quality of communication and are generally impractical in real-world scenarios [24]. In contrast, our scheme offers a practical avenue for OTFS communication.

### 6.4.4 Computational complexity analysis

To assess the computational complexity of the schemes, we quantify the complexity order of the operations needed to estimate the channel from a received symbol. The channel estimation algorithm in [21] requires comparing $N$ symbols and the maximum Doppler samples with a given threshold, which yields a complexity order of $\mathcal{O}(N\,M)$. In addition, this method depends on the equalization in the DD domain, which is significantly complex due to the need to invert the channel matrix. The complexity of the MMSE equalization in the DD domain is of order $\mathcal{O}(M_{\mathrm{d}}^3\,N^3)$ [72]. Thus, the complexity order of the TCE scheme is given by

$$\mathcal{C}_{\mathrm{TCE}} = \mathcal{O}(N\,M + M_{\mathrm{d}}^3\,N^3). \tag{64}$$

By its turn, the estimation algorithm in [22] uses the FFT for correlation operations, while equalization is also performed in the DD domain, thus having a complexity order of

$$\mathcal{C}_{\mathrm{CCE}} = \mathcal{O}(\kappa\,D\,M\,N\log N + M_{\mathrm{d}}^3\,N^3), \tag{65}$$

**Table 5 – Computational complexity.**

| Method | Computational Complexity |
|---|---|
| TCE [21] | $\mathcal{O}(MN + M_{\mathrm{d}}^3 N^3)$ |
| CCE [22] | $\mathcal{O}(\kappa MN \log N + M_{\mathrm{d}}^3 N^3)$ |
| LS-LSTM-NN | $\mathcal{O}(M_{\mathrm{on}}^2 + M_{\mathrm{p}}^2 + M_{\mathrm{on}} M_{\mathrm{p}} + M_{\mathrm{d}} N)$ |

where $D$ is the resolution of the fractional Doppler, which in the case of integer Doppler is equal to 1, while $\kappa$ is the number of paths of the vehicular channel.

The proposed LS-LSTM-NN estimator employs the LS initial estimation, with the number of operations required being

$$C_{\mathrm{LS}} = 2\, M_{\mathrm{on}}. \tag{66}$$

Such initial estimation is followed by the LSTM unit with computational complexity depending on the input size, here denoted as $U = M_{\mathrm{on}} + M_{\mathrm{p}}$, and the size of its hidden states $\chi = \frac{M_{\mathrm{on}} + M_{\mathrm{p}}}{2}$. The detail in the overall number of operations of the LSTM and NN units is given in Section 5.4, from which we can obtain the order of the computational complexity of the LS-LSTM-NN estimator as $\mathcal{O}(M_{\mathrm{on}}^2 + M_{\mathrm{p}}^2 + M_{\mathrm{on}} M_{\mathrm{p}})$.

Differently from [21, 22], the LS-LSTM-NN estimator performs equalization in the TF domain, which has a complexity of order $\mathcal{O}(M_{\mathrm{d}} N)$ [72]. Combining the above, we have that

$$\mathcal{C}_{\mathrm{LS-LSTM-NN}} = \mathcal{O}(M_{\mathrm{on}}^2 + M_{\mathrm{p}}^2 + M_{\mathrm{on}} M_{\mathrm{p}} + M_{\mathrm{d}} N). \tag{67}$$

Table 5 summarizes the complexity order required for each method compared in this work to detect the transmitted signal. In Figure 48, the order of the computational complexity is calculated over different frame sizes, clearly emphasizing the reduction in complexity achieved by the proposed LS-LSTM-NN channel estimator, independently of the chosen $N$.

## 6.5 Conclusion

This chapter is dedicated to addressing the challenge of channel estimation in OTFS communication systems while considering the nonlinear effects induced by HPAs. In this context, we introduce an alternative strategy to face the conventional methods where channel estimation relies on high-power pilot subcarriers inserted in the

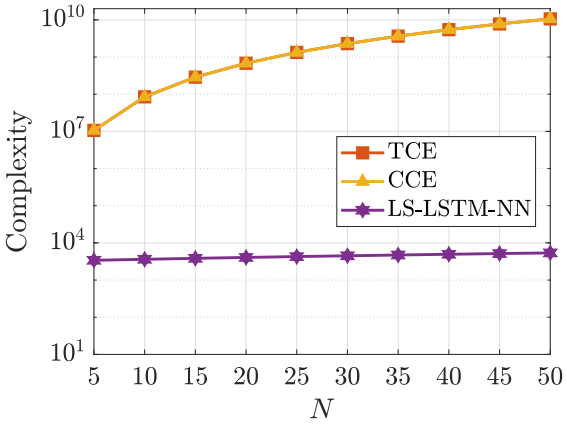


**Figure 48 – Computational complexity for different frame sizes.**

delay-Doppler domain. This conventional practice often leads to elevated PAPR levels, ultimately compromising overall system performance.

Our proposed LS-LSTM-NN estimator represents an innovative approach that combines an initial estimate, LSTM, and NN. This combination significantly enhances the robustness for estimating a channel with unknown instantaneous variation. Moreover, our approach adopts a time-frequency domain pilot insertion scheme, employing multiple pilots. This results in a substantial reduction of the PAPR in OTFS signals, a feature advantageous for practical scenarios characterized by nonlinearities. Also notably, this approach aligns with practical scenarios, since exhibits significant resistance against HPA-induced effects, as evidenced by the BER evaluations conducted under different modulation schemes and SNR conditions.

In addition, our results present that our method significantly reduces the computational complexity during signal detection, making it more suitable for future real-world applications. Finally, our analysis shows that these achievements do not compromise the spectral efficiency. In fact, our proposed solution achieves nearly optimal performance in this regard, reinforcing the effectiveness of our approach.

# 7 CONCLUSIONS AND PERSPECTIVES

This thesis addressed some of the critical challenges on vehicular channel estimation, particularly considering the effects of nonlinearities due to HPAs. First, our investigation yielded insights into the limitations of conventional methods, which often experience significant performance degradation in the presence of HPA-induced distortions. Also importantly, our research highlighted that DL techniques, particularly DNNs, show inherent robustness against these NLD effects. Consequently, this analysis encouraged further exploration and application of advanced DL-based methods for more accurate vehicular channel estimation.

The core contribution of this research consists in the introduction of novel learning-based receiver architectures explicitly tailored to accurate nonlinear vehicular channel estimation. Our emphasis is particularly on hybrid approaches, where well-known mathematical strategies are combined with learning-based methods. Initially, by considering memoryless HPA model within the IEEE 802.11p standard, our proposed DPA-LSTM-NN estimator has proven to be highly resilient against HPA-induced effects. This resilience has been substantiated through extensive BER and NMSE evaluations across varying modulation schemes, SNRs, and mobility conditions. Also importantly, combining its structure with statistical analysis of the wireless channel, this method achieves a substantial reduction in computational complexity compared to the benchmark methods.

Based on this robust receiver architecture, we extended our analysis to cover more complex scenarios that involved HPA nonlinear effects. Thus, by implementing a novel low-complexity compensation technique, we successfully validated the effectiveness of our proposed receiver in handling the intricate challenges presented by memory-affected HPAs. This marked a significant step forward in enhancing the robustness and applicability of our proposed receiver in practical communication systems.

In a subsequent study, we advanced our research presenting a proposal to generalize the method using an ensemble learning approach. This envolved combining different datasets using a characteristic learning approach, without adding online complexity to the solution. This, in turn, enabled the development of receiver architectures that are adaptive, capable of addressing a spectrum of real-world scenarios, and achieving reliable channel estimation despite variations in the scenario.

Finally, in anticipation of the forthcoming 6G wireless communication era, we also proposed an architecture for OTFS channel estimation. Thus, we propose a time-frequency domain pilot insertion scheme, significantly reducing the PAPR compared to conventional OTFS receivers, which is crucial for practical scenarios characterized by nonlinearities. The superiority of the proposal over conventional estimators in high mobility vehicular scenarios, which are expected for future vehicular communications, is presented in terms of BER performance. Also importantly, this proposed method presents a relevant reduction in the computational complexity during signal detection, enhancing its viability for real-world applications.

## 7.1 Future works

The findings of this thesis open several aspects that can be addressed in future research. In particular, we outline the perspective of future works as follows

- Multiple-Input Multiple-Output (MIMO) communication: In this study, we focused exclusively on SISO communication scenarios. Exploring MIMO channels offers an interesting extension, given the heightened complexity of the system and the potential for advanced ML tools to yield even more significant benefits.
- Explainable AI for channel estimation: The subcarrier sampling scheme proposed considers uniform selection. Recently, studies in the literature have shown the ability of AI to promote the explainability of DL-based methods, enhancing the transparency of black box models and explaining the decisions made by the trained network [74, 75]. These methods, called explainable AI (XAI), have already presented advantages in the context of channel estimation and therefore open up opportunities for future development to interpret the relevance of the subcarriers considered for training the channel estimation methods, while maintaining the primary intention of reducing the complexity of the solutions compared to those that consider all the subcarrier information as input for the post-processing of LSTM networks.
- Comparison to multicarrier waveforms candidates for 6G: This work focuses on proposing receivers for OFDM and OTFS. However, as briefly discussed in Section 2.2, various multicarrier modulation schemes are recognized in the literature as potential candidates for 6G communication. Each of these proposals offers distinct advantages adapted to specific wireless communication scenarios. Therefore,

a valuable avenue for future research would be to compare the proposed estimators, suitably adapted, when applied to different multicarrier communication waveforms. This comparative analysis would provide information on the adaptability and effectiveness of the proposed receivers in various multicarrier modulation schemes.

- Evaluation of the ability of other equalization methods to detect signals: We consider MMSE detection for the OTFS technique, which serves as a classic and effective benchmark. However, it is important to note that the literature offers alternative equalization methods aimed at reducing the complexity of detection, such as the message-passing algorithm (MPA). These alternatives present intriguing possibilities for further exploration and, since complexity optimization is paramount in future wireless communication, this presents a valuable direction for research.

- Explore joint estimation, equalization, and decoding: We aim to capitalize on the potential synergies and mutual interactions between these blocks, delving into an integrated framework. By optimizing these processes, we expect to anticipate improved efficiency, robustness, and accuracy in channel estimation, signal equalization, and subsequent decoding of transmitted information, enhancing the overall performance and reliability of wireless communication systems.

# REFERENCES


[1] I. Rahman, S. M. Razavi, O. Liberg, C. Hoymann, H. Wiemann, C. Tidestav, P. Schliwa-Bertling, P. Persson, and D. Gerstenberger, "5G evolution toward 5G advanced: An overview of 3GPP releases 17 and 18," *Ericsson Technology Review*, vol. 2021, no. 14, pp. 2–12, 2021.

[2] M. Latva-Aho and K. Leppänen, "Key drivers and research challenges for 6G ubiquitous wireless intelligence," *Oulu, Finland*, 2019.

[3] R. Hadani, S. Rakib, M. Tsatsanis, A. Monk, A. J. Goldsmith, A. F. Molisch, and R. Calderbank, "Orthogonal time frequency space modulation," in *2017 IEEE Wireless Communications and Networking Conference (WCNC)*, 2017, pp. 1–6.

[4] S. H. Han and J. H. Lee, "An overview of peak-to-average power ratio reduction techniques for multicarrier transmission," *IEEE Wireless Communications*, vol. 12, no. 2, pp. 56–65, 2005.

[5] I. Goodfellow, Y. Bengio, and A. Courville, *Deep learning*. MIT press, 2016.

[6] S. Hochreiter and J. Schmidhuber, "Long short-term memory," *Neural computation*, vol. 9, no. 8, pp. 1735–1780, 1997.

[7] J. J. Bussgang, *Crosscorrelation functions of amplitude-distorted Gaussian signals*. Res. Lab. of Electronics, MIT, Cambridge, MA., USA, Tech. Rep. 216, 1952.

[8] A. R. Belabad, S. A. Motamedi, and S. Sharifian, "An adaptive digital predistortion for compensating nonlinear distortions in RF power amplifier with memory effects," *Integration*, vol. 57, pp. 184–191, 2017.

[9] T. Wang and J. Ilow, "Compensation of nonlinear distortions with memory effects in OFDM transmitters," in *IEEE Global Telecommunications Conference.*, vol. 4, 2004, pp. 2398–2403 Vol.4.

[10] Y. Zhang, B. Li, N. Wu, Y. Ma, W. Yuan, and L. Hanzo, "Message passing-aided joint data detection and estimation of nonlinear satellite channels," *IEEE Transactions on Vehicular Technology*, vol. 72, no. 2, pp. 1763–1774, 2023.

[11] G. Acosta-Marum and M. A. Ingram, "Six time- and frequency- selective empirical channel models for vehicular wireless LANs," *IEEE Vehicular Technology Magazine*, vol. 2, no. 4, pp. 4–11, 2007.

[12] A. K. Gizzini and M. Chafii, "A survey on deep learning based channel estimation in doubly dispersive environments," *IEEE Access*, vol. 10, pp. 70 595–70 619, 2022.

[13] M. M. Awad, K. G. Seddik, and A. Elezabi, "Low-complexity semi-blind channel estimation algorithms for vehicular communications using the IEEE 802.11p

standard," *IEEE Transactions on Intelligent Transportation Systems*, vol. 20, no. 5, pp. 1739–1748, 2019.

[14] J. A. Fernandez, K. Borries, L. Cheng, B. V. K. Vijaya Kumar, D. D. Stancil, and F. Bai, "Performance of the 802.11p physical layer in vehicle-to-vehicle environments," *IEEE Transactions on Vehicular Technology*, vol. 61, no. 1, pp. 3–14, 2012.

[15] S. Han, Y. Oh, and C. Song, "A deep learning based channel estimation scheme for IEEE 802.11p systems," in *ICC 2019 - 2019 IEEE International Conference on Communications (ICC)*, 2019, pp. 1–6.

[16] A. K. Gizzini, M. Chafii, A. Nimr, and G. Fettweis, "Deep learning based channel estimation schemes for IEEE 802.11p standard," *IEEE Access*, vol. 8, pp. 113 751–113 765, 2020.

[17] J. Pan, H. Shan, R. Li, Y. Wu, W. Wu, and T. Q. Quek, "Channel estimation based on deep learning in vehicle-to-everything environments," *IEEE Communications Letters*, vol. 25, no. 6, pp. 1891–1895, 2021.

[18] A. K. Gizzini, M. Chafii, S. Ehsanfar, and R. Shubair, "Temporal averaging LSTM-based channel estimation scheme for IEEE 802.11p standard," in *IEEE GLOBECOM 2021*, 2021.

[19] Z. Wei, W. Yuan, S. Li, J. Yuan, G. Bharatula, R. Hadani, and L. Hanzo, "Orthogonal time-frequency space modulation: A promising next-generation waveform," *IEEE Wireless Communications*, vol. 28, no. 4, pp. 136–144, 2021.

[20] R. Hadani and A. Monk, "OTFS: A new generation of modulation addressing the challenges of 5G," *arXiv preprint arXiv:1802.0262*, 2018.

[21] P. Raviteja, K. T. Phan, and Y. Hong, "Embedded pilot-aided channel estimation for OTFS in delay–doppler channels," *IEEE Transactions on Vehicular Technology*, vol. 68, no. 5, pp. 4906–4917, 2019.

[22] N. Hashimoto, N. Osawa, K. Yamazaki, and S. Ibi, "Channel estimation and equalization for CP-OFDM-based OTFS in fractional doppler channels," in *2021 IEEE International Conference on Communications Workshops (ICC Workshops)*, 2021, pp. 1–7.

[23] R. Marsalek, J. Blumenstein, A. Prokes, and T. Gotthans, "Orthogonal time frequency space modulation: Pilot power allocation and nonlinear power amplifiers," in *2019 IEEE International Symposium on Signal Processing and Information Technology (ISSPIT)*, 2019, pp. 1–4.

[24] S. Gao and J. Zheng, "Peak-to-average power ratio reduction in pilot-embedded OTFS modulation through iterative clipping and filtering," *IEEE Communications Letters*, vol. 24, no. 9, pp. 2055–2059, 2020.

[25] A. Goldsmith, *Wireless Communications*, 1st ed. Cambridge University Press, 2005.

[26] M. Chafii, "Etude d'une nouvelle forme d'onde multiporteuses à PAPR réduit." Ph.D. dissertation, CentraleSupélec, 2016.

[27] IEEE Standard Association, "IEEE guide for wireless access in vehicular environments (WAVE) architecture," *IEEE Std 1609.0-2013*, pp. 1–78, 2014.

[28] D. C. Nguyen, M. Ding, P. N. Pathirana, A. Seneviratne, J. Li, D. Niyato, O. Dobre, and H. V. Poor, "6G internet of things: A comprehensive survey," *IEEE Internet of Things Journal*, vol. 9, no. 1, pp. 359–383, 2022.

[29] W. Tong and P. Zhu, *6G, the Next Horizon: From Connected People and Things to Connected Intelligence*. Cambridge University Press, 2021.

[30] Z. Zhao, X. Cheng, M. Wen, B. Jiao, and C.-X. Wang, "Channel estimation schemes for IEEE 802.11p standard," *IEEE Intelligent Transportation Systems Magazine*, vol. 5, no. 4, pp. 38–49, 2013.

[31] Y.-K. Kim, J.-M. Oh, Y.-H. Shin, and C. Mun, "Time and frequency domain channel estimation scheme for IEEE 802.11p," in *17th International IEEE Conference on Intelligent Transportation Systems (ITSC)*, 2014, pp. 1085–1090.

[32] M. A. Imran, A. F. dos Reis, G. Brante, P. V. Klaine, and R. D. Souza, "Machine learning in energy efficiency optimization," *Machine Learning for Future Wireless Communications*, pp. 105–117, 2019.

[33] F. Sandoval, G. Poitau, and F. Gagnon, "Hybrid peak-to-average power ratio reduction techniques: Review and performance comparison," *IEEE Access*, vol. 5, pp. 27 145–27 161, 2017.

[34] M. F. Haider, F. You, S. He, T. Rahkonen, and J. P. Aikio, "Predistortion-based linearization for 5G and beyond millimeter-wave transceiver systems: A comprehensive survey," *IEEE Communications Surveys  Tutorials*, vol. 24, no. 4, pp. 2029–2072, 2022.

[35] L. Cho, X. Yu, C.-Y. Hsu, and P.-H. Ho, "Mitigation of PA nonlinearity for IEEE 802.11ah power-efficient uplink via iterative subcarrier regularization," *IEEE Access*, vol. 9, pp. 15 659–15 669, 2021.

[36] A. F. dos Reis, G. Brante, R. Parisotto, R. D. Souza, P. H. V. Klaine, J. P. Battistella, and M. A. Imran, "Energy efficiency analysis of drone small cells positioning based on reinforcement learning," *Internet Technology Letters*, 2020.

[37] Y. Hong, T. Thaj, and E. Viterbo, *Delay-Doppler Communications: Principles and Applications*. Academic Press, 2022.

[38] G. Matz, H. Bolcskei, and F. Hlawatsch, "Time-frequency foundations of communications: Concepts and tools," *IEEE Signal Processing Magazine*, vol. 30, no. 6, pp. 87–96, 2013.

[39] Z. Wei, S. Li, W. Yuan, R. Schober, and G. Caire, "Orthogonal time frequency space modulation—part I: Fundamentals and challenges ahead," *IEEE Communications Letters*, vol. 27, no. 1, pp. 4–8, 2023.

[40] H. Tataria, M. Shafi, A. F. Molisch, M. Dohler, H. Sjöland, and F. Tufvesson, "6G wireless systems: Vision, requirements, challenges, insights, and opportunities," *Proceedings of the IEEE*, vol. 109, no. 7, pp. 1166–1199, 2021.

[41] A. Bemani, N. Ksairi, and M. Kountouris, "AFDM: A full diversity next generation waveform for high mobility communications," in *2021 IEEE International Conference on Communications Workshops (ICC Workshops)*, 2021, pp. 1–6.

[42] G. D. Surabhi, R. M. Augustine, and A. Chockalingam, "Peak-to-average power ratio of OTFS modulation," *IEEE Communications Letters*, vol. 23, no. 6, pp. 999–1002, 2019.

[43] I. Ajayi, Y. Medjahdi, L. Mroueh, R. Zayani, and F. Kaddour, "Secrecy energy efficiency in PAPR-aware artificial noise scheme for secure massive MIMO," in *2023 Joint European Conference on Networks and Communications 6G Summit (EuCNC/6G Summit)*, 2023, pp. 42–47.

[44] Y. Rahmatallah and S. Mohan, "Peak-to-average power ratio reduction in OFDM systems: A survey and taxonomy," *IEEE Communications Surveys Tutorials*, vol. 15, no. 4, pp. 1567–1592, 2013.

[45] X. Li and L. Cimini, "Effects of clipping and filtering on the performance of OFDM," *IEEE Communications Letters*, vol. 2, no. 5, pp. 131–133, 1998.

[46] K. Yang and S.-I. Chang, "Peak-to-average power control in OFDM using standard arrays of linear block codes," *IEEE Communications Letters*, vol. 7, no. 4, pp. 174–176, 2003.

[47] H. Chen and H. Liang, "Combined selective mapping and binary cyclic codes for PAPR reduction in OFDM systems," *IEEE Transactions on Wireless Communications*, vol. 6, no. 10, pp. 3524–3528, 2007.

[48] H. Ye, G. Y. Li, and B.-H. Juang, "Power of deep learning for channel estimation and signal detection in OFDM systems," *IEEE Wireless Communications Letters*, vol. 7, no. 1, pp. 114–117, 2018.

[49] A. Singh, S. Sharma, K. Deka, and V. Bhatia, "DL-based OTFS signal detection in presence of hardware impairments," *IEEE Wireless Communications Letters*, vol. 12, no. 9, pp. 1533–1537, 2023.

[50] F. Hussain, S. A. Hassan, R. Hussain, and E. Hossain, "Machine learning for resource management in cellular and IoT networks: Potentials, current solutions, and open challenges," *IEEE Communications Surveys Tutorials*, vol. 22, no. 2, pp. 1251–1275, 2020.

[51] H. Wang, Z. Wu, S. Ma, S. Lu, H. Zhang, G. Ding, and S. Li, "Deep learning for signal demodulation in physical layer wireless communications: Prototype platform, open dataset, and analytics," *IEEE Access*, vol. 7, pp. 30 792–30 801, 2019.

[52] J. Schmidhuber, "Deep learning in neural networks: An overview," *Neural networks*, vol. 61, pp. 85–117, 2015.

[53] H. Shaiek, R. Zayani, Y. Medjahdi, and D. Roviras, "Analytical analysis of SER for beyond 5G post-OFDM waveforms in presence of high power amplifiers," *IEEE Access*, vol. 7, pp. 29 441–29 452, 2019.

[54] P. Colantonio, F. Giannini, and E. Limiti, *High efficiency RF and microwave solid state power amplifiers*. John Wiley & Sons, 2009.

[55] D. Chowdhury, C. D. Hull, O. B. Degani, Y. Wang, and A. M. Niknejad, "A fully integrated dual-mode highly linear 2.4 GHz CMOS power amplifier for 4G WiMax applications," *IEEE Journal of Solid-State Circuits*, vol. 44, no. 12, pp. 3393–3402, 2009.

[56] D. Morgan, Z. Ma, J. Kim, M. Zierdt, and J. Pastalan, "A generalized memory polynomial model for digital predistortion of RF power amplifiers," *IEEE Transactions on Signal Processing*, vol. 54, no. 10, pp. 3852–3860, 2006.

[57] P. Gilabert, G. Montoro, and E. Bertran, "On the Wiener and Hammerstein models for power amplifier predistortion," in *2005 Asia-Pacific Microwave Conference Proceedings*, vol. 2, 2005, pp. 4 pp.–.

[58] S. Chen, "An efficient predistorter design for compensating nonlinear memory high power amplifiers," *IEEE Transactions on Broadcasting*, vol. 57, no. 4, pp. 856–865, 2011.

[59] Y. Moegiharto, A. M. Kautsar Bebyrahma, and I. Anisah, "BER performance of joint PTS PAPR reduction technique and Wiener HPA predistortion in OFDM system," in *International Electronics Symposium (IES)*, 2019, pp. 480–484.

[60] R. Zayani, R. Bouallegue, and D. Roviras, "Adaptive predistortions based on neural networks associated with Levenberg-Marquardt algorithm for satellite down links," *EURASIP Journal on Wireless Communications and Networking*, vol. 2008, pp. 1–15, 2008.

[61] X. Zhu, Z. Sheng, Y. Fang, and D. Guo, "A deep learning-aided temporal spectral channelnet for IEEE 802.11p-based channel estimation in vehicular communications," *EURASIP Journal on Wireless Communications and Networking*, vol. 2020, no. 1, pp. 1–15, 2020.

[62] A. K. Gizzini, M. Chafii, A. Nimr, R. M. Shubair, and G. Fettweis, "CNN aided weighted interpolation for channel estimation in vehicular communications," *IEEE Transactions on Vehicular Technology*, vol. 70, no. 12, pp. 12 796–12 811, 2021.

[63] A. K. Gizzini, M. Chafii, A. Nimr, and G. Fettweis, "Enhancing least square channel estimation using deep learning," in *2020 IEEE 91st Vehicular Technology Conference (VTC2020-Spring)*, 2020, pp. 1–5.

[64] B. Eisenberg and R. Sullivan, "Why is the sum of independent normal random variables normal?" *Mathematics Magazine*, vol. 81, no. 5, pp. 362–366, 2008.

[65] S. González, S. García, J. Del Ser, L. Rokach, and F. Herrera, "A practical tutorial on bagging and boosting based ensembles for machine learning: Algorithms, software tools, performance study, practical perspectives and opportunities," *Information Fusion*, vol. 64, pp. 205–237, 2020.

[66] G. Collell, D. Prelec, and K. R. Patil, "A simple plug-in bagging ensemble based on threshold-moving for classifying binary and multiclass imbalanced data," *Neurocomputing*, vol. 275, pp. 330–340, 2018.

[67] C. Naveen and V. Sudha, "Peak-to-average power ratio reduction in OTFS modulation using companding technique," in *2020 5th International Conference on Devices, Circuits and Systems (ICDCS)*, 2020, pp. 140–143.

[68] H.-T. Sheng and W.-R. Wu, "Time-frequency domain channel estimation for OTFS systems," *IEEE Transactions on Wireless Communications*, 2023, early access.

[69] S. Srivastava, R. K. Singh, A. K. Jagannatham, and L. Hanzo, "Bayesian learning aided sparse channel estimation for orthogonal time frequency space modulated systems," *IEEE Transactions on Vehicular Technology*, vol. 70, no. 8, pp. 8343–8348, 2021.

[70] P. Raviteja, K. T. Phan, Y. Hong, and E. Viterbo, "Interference cancellation and iterative detection for orthogonal time frequency space modulation," *IEEE Transactions on Wireless Communications*, vol. 17, no. 10, pp. 6501–6515, 2018.

[71] P. Raviteja, Y. Hong, E. Viterbo, and E. Biglieri, "Practical pulse-shaping waveforms for reduced-cyclic-prefix OTFS," *IEEE Transactions on Vehicular Technology*, vol. 68, no. 1, pp. 957–961, 2019.

[72] R. P. Junior, C. A. F. da Rocha, B. S. Chang, and D. Le Ruyet, "A two-dimensional FFT precoded filter bank scheme," *IEEE Transactions on Wireless Communications*, vol. 22, no. 11, pp. 8366–8377, 2023.

[73] A. Naikoti and A. Chockalingam, "Signal detection and channel estimation in OTFS," *ZTE Communications*, vol. 19, no. 4, pp. 16–33, 2021.

[74] P. Xue and Y. Zhao, "A self-learning channel modeling approach based on explainable neural network," *IEEE Wireless Communications Letters*, vol. 12, no. 7, pp. 1289–1293, 2023.

[75] A. K. Gizzini, Y. Medjahdi, A. J. Ghandour, and L. Clavier, "Towards explainable AI for channel estimation in wireless communications," *arXiv preprint arXiv:2307.00952*, 2023.